

Answer to referee #3:

We thank referee #3 for reviewing our manuscript. His/Her valuable comments and suggestions have significantly improved the quality of our manuscript.

Below, we include our detailed answers to all comments and questions.

Answers to general comments (GC):

General Comment #1:

*[...] However, the attempt to include or address so many questions in this manuscript (how important is *Phaeocystis* to carbon export; what are the spatial and temporal patterns of *Phaeocystis* and diatom biomass; what are the drivers of *Phaeocystis* and diatoms' spatio-temporal patterns) makes it feel unfocused. The structure of the paper and section headings only partly help. I am left wondering, which comparisons do the authors feel are most important, most revealing, or most surprising? Although main conclusions are stated in the conclusion section and abstract, the attention paid to each analysis step and their findings in the body does not seem to match these main points.*

[...]

*The section headings do not seem consistent with the scope of what is being assessed, particularly which PFTs are addressed. Section 3.1 includes “phytoplankton” in the heading and assessed all PFTs. In contrast, sections 3.2 and 3.3 include “phytoplankton” in the heading but only addresses *Phaeocystis* and diatoms. Likewise, section 4.2 includes “phytoplankton” in the heading but seems to only discuss *Phaeocystis*. I recommend the authors revise the headings or make the content more consistent with the headings.*

Answer to GC1:

We thank the reviewer for this important comment, highlighting the need for clarification regarding the main focus of our manuscript and a better guidance of the reader throughout. In the revised manuscript, we have adapted the section titles in the result and discussion sections to better reflect each subsection's content. The sections are now named as follows:

- 3.1 **Phytoplankton biogeography and community composition in the SO**
- 3.2 **Phytoplankton phenology and the seasonal succession of *Phaeocystis* and diatoms**
- 3.3 **Drivers of the high-latitude biogeography and seasonal succession of *Phaeocystis* and diatoms**
- 3.4 **Quantifying the importance of *Phaeocystis* for the SO carbon cycle**
- 4.1 **Drivers of phytoplankton biogeography and the competition between *Phaeocystis* and diatoms**
- 4.2 **Biogeochemical implications of high-latitude SO *Phaeocystis* biogeography**

Further, we have modified the last paragraph of the introduction to better reflect the structure of the manuscript. The paragraph now reads:

“In this study, we investigate the competition between *Phaeocystis* and diatoms and its implications for carbon cycling using a regional coupled physical-biogeochemical-ecological model configured at eddy-permitting resolution for the SO (ROMS-BEC, Nissen et al., 2018). To address the missing link between SO phytoplankton biogeography, ecosystem function, and the SO carbon cycle, we have added *Phaeocystis* colonies as an additional PFT to the model, so that it includes all major known biogeochemically relevant phytoplankton types of the SO (see e.g. Buesseler et al., 1998; DiTullio et al., 2000). Using available observations, such as satellite-derived chlorophyll concentrations, carbon biomass and pigment data, we first validate the simulated phytoplankton distributions and community structure across the SO and then particularly focus on the temporal variability of diatoms and *Phaeocystis* in the high-latitude SO. After assessing the relative importance of bottom-up and top-

down factors in controlling the contribution of *Phaeocystis* colonies and diatoms to total phytoplankton biomass over a complete annual cycle in the high-latitude SO, we show that the spatially and temporarily varying phytoplankton community composition leaves a distinct, PFT-specific imprint on upper ocean carbon cycling and POC export across the SO .”

General Comment #2:

As I read, I wonder: why is the Ross Sea singled out for evaluation, aside from other coastal areas? Also, in some manuscript sections the Ross Sea is included in the comparisons (e.g. Figure 2, section 3.3 about drivers) and other sections do not include it (e.g. Table 3, section 3.4 about carbon cycle). Why is it only considered for some of the analyses? Without an explanation, these choices make the analysis seem arbitrary. The authors should explain why the Ross Sea is being used as a special study area and why/when it is or is not being included in analyses.

Answer to GC2:

We acknowledge that some readers might be interested in the simulated dynamics in coastal regions other than the Ross Sea, but we decided on the latter as one of the focus areas in this study for several reasons: First, there is a tremendous body of literature available for the Ross Sea phytoplankton community, i.e. work discussing the competition between diatoms and *Phaeocystis*, thus making it a key focus area in the context of model evaluation. Further, we note that the simulated dynamics in ROMS-BEC in other coastal areas, e.g. the Amundsen Sea, are rather similar to those simulated in the Ross Sea (see Fig. 1 below).

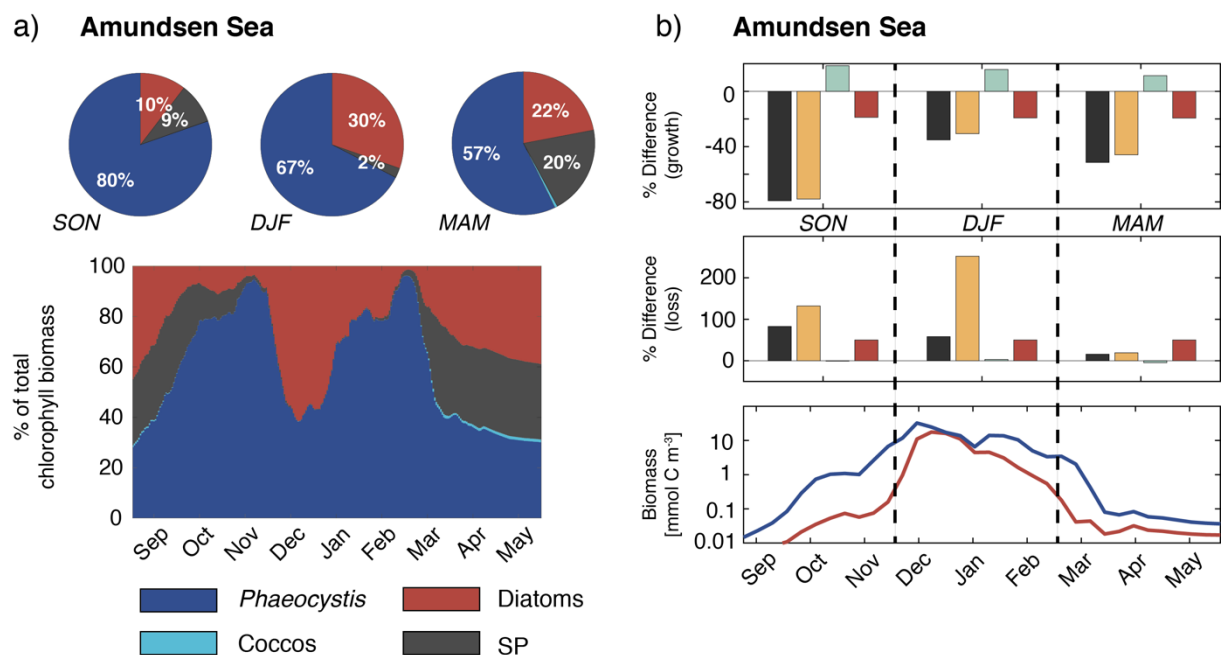


Fig. 1: Same as Fig. 2 & 5 in the manuscript, but averaged over the Amundsen Sea.

Keeping the length and readability of our manuscript in mind and given the chosen circumpolar model domain covering the whole Southern Ocean up to 24°S, we decided to contrast the phytoplankton dynamics within one coastal area to that for the basin-wide assessment, rather than presenting results for different coastal areas. Admittedly, only showing results for the larger regions 30-90°S and 60-90°S in section 3.4 (carbon cycling) and Table 3 and not for the Ross Sea might be confusing for the reader. For completeness, we have therefore added Fig. 2 below to the supplementary material of the revised version of the manuscript, which shows the cycling of carbon in the Ross Sea in ROMS-BEC. Yet, in this context, the region 60-90°S is in many aspects representative for the Ross Sea (compare Fig. 6 & 7 of the manuscript to Fig. 2 below). Any difference in total POC production and the

partitioning amongst the PFTs and pathways is small and reflects the difference in phytoplankton community structure between 60-90°S and the Ross Sea, i.e., relatively more *Phaeocystis* (especially early in the season) and hence relatively more aggregation than grazing. In the revised version of the manuscript, we have therefore added the following statement in the captions of Fig. 6 & 7 in the main text:

“Results for the Ross Sea are comparable to those between 60-90°S (see Fig. S11).”

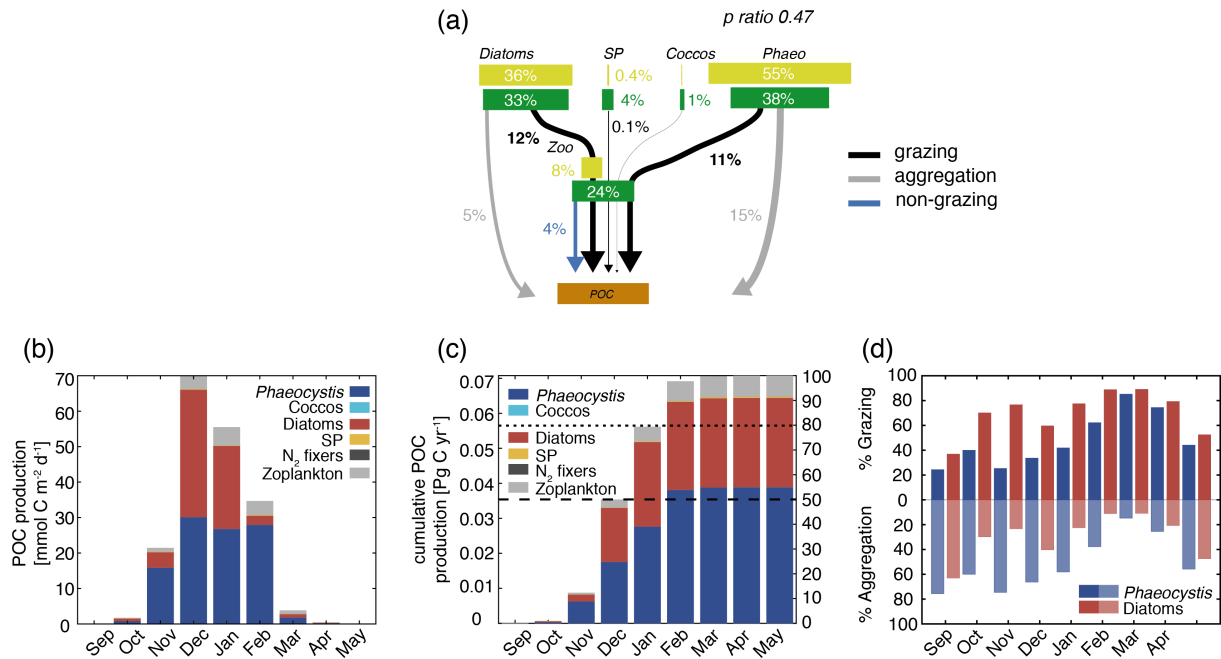


Fig. 2: Carbon cycling in the Ross Sea: The upper panel corresponds to Fig. 6 in the main text, the lower panels shows the quantities from Fig. 7 for the Ross Sea.

General Comment #3:

The differences in carbon to chlorophyll ratio may have a substantial impact on some of the conclusions, and yet it seems to have been given little consideration. I refer the authors to several additional papers discussing C:Chl ratios for *Phaeocystis* and diatoms in the Ross Sea: DiTullio and Smith (1996), Smith et al. (1998), Mathot et al. (2000), Kaufman et al. (2018). I appreciate that calibration is difficult with such a large model, however, this seems to be an important limitation not discussed. I suggest the authors consider addressing it. Moreover, If the authors did train some of the model parameters before picking the ‘best’ values for their baseline run, it should be made clear whether or not model evaluation was done using the same or different data than was used for parameter training/tuning/calibration.

Answer to GC3:

We thank the reviewer for raising this important point. In the *Baseline* setup of ROMS-BEC, the simulated monthly mean surface C:Chl ratios range from 23-103 mg C (mg chl)⁻¹ between 60-90°S, with peak ratios in summer. While this range is within the range suggested by observations (14-200 mg C (mg chl)⁻¹; DiTullio and Smith, 1996, Kaufmann et al., 2018, Mathot et al., 2000), we note that on average, in contrast to observations, ROMS-BEC currently simulates higher C:Chl ratios for *Phaeocystis* (38-103 mg C (mg chl)⁻¹) than for diatoms (23-66 mg C (mg chl)⁻¹). This model behavior is a direct result of the chosen model formulations and has implications for the presented results as outlined in the following.

In BEC, the base unit for calculations of phytoplankton biomass accumulation is carbon, and photoacclimation of phytoplankton, i.e., the amount of chlorophyll produced per unit of carbon, is then calculated following Geider et al. (1998). In this formulation, photoacclimation is calculated based on the PAR level and each PFT's specific growth rate, nitrogen uptake rate, maximum Chl:N ratio ($\theta_{N,max}$, 4.0 mg chl (mmol N)⁻¹ for diatoms, 2.5 mg chl (mmol N)⁻¹ for *Phaeocystis*), sensitivity to changes in light intensity at low light levels (α_{PI} , see Table 1 in the manuscript, $\alpha_{PI}^{phaco} > \alpha_{PI}^{diat}$ in the *Baseline* setup) and local Chl:C biomass ratio. As a result, the PFT with the higher α_{PI} and lower $\theta_{N,max}$ (*Phaeocystis* in the *Baseline* setup) has lower rates of photoacclimation than the PFT with the lower α_{PI} and higher $\theta_{N,max}$ (diatoms) for the same specific growth rate, nitrogen uptake rate, and PAR (see Fig. 3 below), resulting in lower Chl:C and thus higher C:Chl biomass ratios, explaining the higher average C:Chl ratio of *Phaeocystis* compared to that of diatoms in the *Baseline* setup of ROMS-BEC.

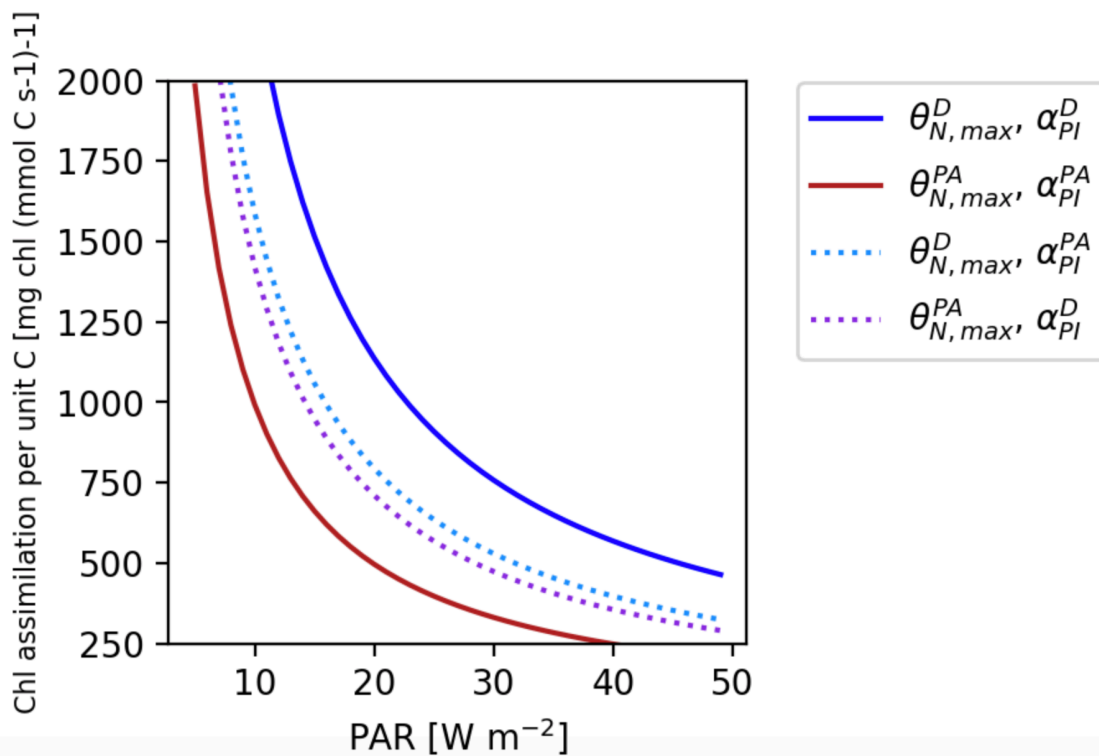


Fig. 3: Rates of chlorophyll assimilation as a function of PAR following the formulation of Geider et al. (1998). For the visualization of the functional relationship, a constant local chl:C ratio of 0.2 mg chl (mmol C)⁻¹, a nitrogen uptake rate of 1 mmol N m⁻³ s⁻¹, and a specific growth rate of 1 d⁻¹ were used. The solid lines denote the photoacclimation rates with $\theta_{N,max}$ and α_{PI} of diatoms (blue) and *Phaeocystis* (red) from the *Baseline* setup (see Table 1 of the manuscript). For the dashed lines, $\theta_{N,max}$ (purple) and α_{PI} (light blue) of diatoms was replaced by the respective value of *Phaeocystis*.

As expected, varying the parameters α_{PI} and $\theta_{N,max}$ of *Phaeocystis* will directly impact its simulated C:Chl ratios. As a response to a comment by reviewer 4, we have performed additional model experiments for the revised manuscript, in which we have, amongst others, varied these key parameters for photoacclimation by +/-50% (see Table 1 below, which was added to the revised supplementary material as Table S1). In these experiments, the simulated minimum C:Chl ratio between 60-90°S remains largely unchanged at 23-24 mg C (mg chl)⁻¹, but the maximum monthly mean ratio changes to 124 mg C (mg chl)⁻¹ ($\alpha_{PI}150$), 89 mg C (mg chl)⁻¹ ($\alpha_{PI}50$), 78 mg C (mg chl)⁻¹ ($\theta_{N,max}150$), and 183 mg C (mg chl)⁻¹ ($\theta_{N,max}50$), demonstrating the rather large sensitivity of the simulated C:Chl ratios to chosen model parameters. Yet, we note that in all these experiments, the average C:Chl biomass ratio of *Phaeocystis* remains larger than that of diatoms and that *absolute* biomass concentrations of the two PFTs change substantially as well (by more than 90% compared to the *Baseline* setup between 60-90°S, see Fig. 4 below), demonstrating the difficulty to

tune both the C:Chl ratios of Southern Ocean phytoplankton and each PFT's absolute biomass concentrations with this model formulation and a complex model like ROMS-BEC. In fact, Buitenhuis & Geider (2010) point out that for iron-limited regions such as the Southern Ocean, the parameterizations by Geider et al (1998) should be modified to include the effects of iron (rather than nitrogen as in Geider et al., 1998) on phytoplankton Fe:C and Chl:C ratios, and the effect of this modification for our model results presented here should be assessed in future work.

As biomass concentrations are the basis for the analysis presented here, our results are impacted by any bias in the C:Chl biomass ratio of *Phaeocystis* and diatoms. Specifically, any bias in photoacclimation affects the simulated carbon fields through the impact of the C:Chl ratio on the light limitation factor (Eq. B9 in appendix of manuscript). In this context, a lower C:Chl biomass ratio of *Phaeocystis*, as suggested by observations, would result in a lower light limitation factor (less light limitation, see Eq. B9 in appendix of manuscript), suggesting that we possibly underestimate *Phaeocystis* carbon biomass and its relative importance in the phytoplankton community. Furthermore, a decrease in the light limitation of *Phaeocystis* growth would impact its simulated seasonality and the succession patterns of PFTs, with the lower light limitation being especially critical early in the growth season in the Ross Sea, where/when our model suggests differences in light limitation between *Phaeocystis* and diatoms to be an important driver for the simulated succession from *Phaeocystis* to diatoms throughout the season (see Fig. 5 in the manuscript).

In summary, we acknowledge the sensitivity of our model results to biases in the simulated C:Chl biomass ratios of *Phaeocystis*. In particular, recent advances in our understanding of differences in the adaptation between *Phaeocystis* and diatoms to low levels of light, iron, and temperature warrant a reassessment of model parametrizations and a closer assessment of the simulated Chl:C ratios in future work (see e.g. Strzepek et al., 2019). We have added a statement along these lines in the caveat section:

“As iron-light interactions are key for the simulated Fe:C and Chl:C ratios of SO phytoplankton (Buitenhuis and Geider, 2010) and in light of more recent advances regarding our understanding of the adaptation of SO phytoplankton to persisting low levels of light, iron, and temperature (Strzepek et al., 2019), a reassessment of model parametrizations describing phytoplankton growth and photoacclimation is advisable in future work.”

Furthermore, the description and assessment of the new parameter sensitivity experiments is included as section S2 in the revised supplementary material of the manuscript:

Table 1: Overview of parameter sensitivity simulations, varying parameters by +/- 50%. PA=Phaeocystis, D=diatoms. See also Table 1 in the submitted manuscript.

Run Name	Description	
Topt150	Increase T_{opt}^{PA} by 50%	} Param_Topt
Topt50	Decrease T_{opt}^{PA} by 50%	
kFe150	Increase k_{Fe}^{PA} by 50%	} Param_kFe
kFe50	Decrease k_{Fe}^{PA} by 50%	
alphaPI150	Increase α_{PI}^{PA} by 50%	} Param_alphaPI
alphaPI50	Decrease α_{PI}^{PA} by 50%	
mortality150	Increase $\gamma_{m,0}^{PA}$ by 50%	} Param_mortality
mortality50	Decrease $\gamma_{m,0}^{PA}$ by 50%	
aggregation150	Increase $\gamma_{a,0}^{PA}$ by 50%	} Param_aggregation
aggregation50	Decrease $\gamma_{a,0}^{PA}$ by 50%	
grazing150	Increase $\gamma_{g,max}^{PA}$ by 50%	} Param_grazing
grazing50	Decrease $\gamma_{g,max}^{PA}$ by 50%	
thetaNmax50	Increase $\theta_{chl:N,max}^{PA}$ by 50%	} Param_thetaNmax
thetaNmax50	Decrease $\theta_{chl:N,max}^{PA}$ by 50%	

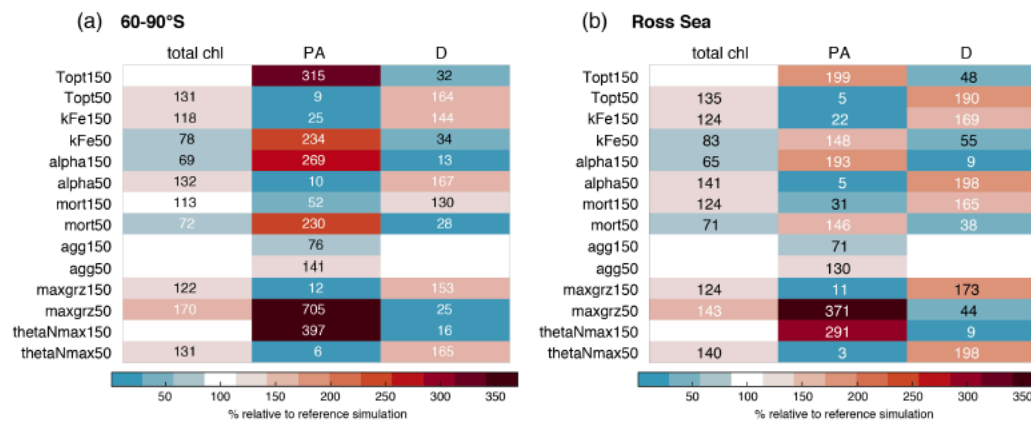


Fig. 4: Annual mean surface chlorophyll concentrations of all phytoplankton (Chl), *Phaeocystis* (PA), and diatoms (D) in the parameter sensitivity simulations (see Table 1 above) relative to the *Baseline* simulation. The model output is averaged over a) 60-90°S and b) the Ross Sea.

With regard to the reviewer’s comment on the model tuning, we note that the goal of the tuning of BEC model parameters was to identify that set of phytoplankton growth and loss parameters within the range of observational uncertainty (see Table 1 in the manuscript) that yielded the best agreement in the simulated spatio-temporal variability in phytoplankton community composition between ROMS-BEC and available observational data of carbon biomass concentrations and community structure (e.g., Vogt et al., 2012, Swan et al., 2016). Due to the scarcity in observational data in the Southern Ocean, the complete set of carbon biomass concentrations and community composition was used in the tuning exercise. In the revised manuscript, we have clarified the text in section 2.1 as follows:

“Generally, model parameters for *Phaeocystis* in the *Baseline* setup are chosen to represent the colonial form of *Phaeocystis* whenever information is available in the literature (see e.g. review by Schoemann et al., 2005), and model parameters were tuned to maximize the model-data agreement in the spatio-temporal variability of the phytoplankton community structure between ROMS- BEC and all available observations (see also section 2.3.1).”

Answers to specific comments (SC):

SC1: The last paragraph of the introduction does not accurately reflect the organization of the paper. This seems like a great place for the authors to more coherently state the purpose of the analyses.

Please see our answer to GC1. We have revised the last paragraph of the introduction.

SC2: Line 95: Perhaps it is just me, but I am confused by this sentence. Also, the implication that the model provides “a correct representation of SO phytoplankton biogeography” (emphasis added) seems very presumptuous.

We have rephrased the last sentence of the introduction as follows in the revised version of the manuscript: “[...] we show that the spatially and temporarily varying phytoplankton community composition leaves a distinct imprint on upper ocean carbon cycling and POC export across the SO.”

SC3: In section 2.1, the authors refer to a “baseline” simulation before it is described. It would be helpful for the authors to refrain from referencing baseline before it is defined.

As the description of the *Phaeocystis* PFT in section 2.1 and the presented parameter choices refer to the *Baseline* setup of ROMS-BEC, we have introduced the “*Baseline*” setup earlier in the revised version of the manuscript to clarify this for the reader. The respective part of section 2.1 now reads:

“Generally, model parameters for *Phaeocystis* in the *Baseline* setup are chosen to represent the colonial form of *Phaeocystis* whenever information is available in the literature (see e.g. review by Schoemann et al., 2005).”

SC4: Sect. 2.3: I wonder what the authors mean by “analysis framework” in the section title? To me, growth rate ratios are not an analysis framework, but rather simply a diagnostic variable.

We agree with the reviewer that the growth ratios are diagnostic tools. To avoid confusion, we have renamed section 2.3 to “Data and diagnostics used in the model assessment” in the revised manuscript.

SC5: Sect. 2.3.2: The authors should define Betas in the text.

We have added a definition of the “betas” in the revised version of the manuscript. It now reads:

“Further, β_T , β_N , and β_I describe the logarithmic ratio of the limitation by temperature, nutrients, and light of growth by diatoms and *Phaeocystis*. Thereby, these terms denote the log-normalized contribution of each environmental factor to the simulated relative growth ratio. At high-latitudes south of 60° S, the ratio of the nutrient limitation of growth β_N corresponds to that of the iron limitation β_{Fe} in our model (Fig. S1).»

SC6: Line 279, and elsewhere: I think “N” is being used to represent both diazotrophs and nutrients. The authors should restrict its meaning to only one or the other.

We thank the reviewer for this comment. In the revised manuscript, we now use “DZ” to denote diazotrophs in Table 1 and keep “N” for nutrients throughout the text.

SC7: Lines 318-323: I think the bias could also be due to poor calibration, especially of the newly introduced *Phaeocystis* group.

The positive chlorophyll bias at high latitudes was already simulated in the 4-PFT setup of ROMS-BEC (similar in magnitude, see Nissen et al., 2018), suggesting that the implementation of *Phaeocystis* is not the reason for this model behavior. In fact, while a fraction of this bias might be due to parameter choices of the different phytoplankton groups (not only *Phaeocystis*, see e.g. also the overestimated temperature-limited growth rate of diatoms at low temperatures in the model, see Fig. A1 of the manuscript), extensive testing with the 4-PFT setup in Nissen et al. (2018) has suggested that missing model complexity in the zooplankton compartment might drive this bias, as the implementation of more zooplankton functional types has been shown to substantially alter the phytoplankton-zooplankton coupling and hence the simulated chlorophyll concentrations in ecosystem models (Le Quéré et al., 2016).

SC8: Line 331: “compared to the 4-PFT”

Changed as suggested.

SC9: Line 361-362: “Our model suggests that *Phaeocystis* is an important member of the high-latitude phytoplankton community.” -- I question whether the authors claim that their model suggests something new here is actually in regard to something already known. Furthermore, this is already evidenced by the fact that the authors saw *Phaeocystis* as important enough to include in the model and write a manuscript about.

We thank the reviewer for this comment. We admit that the chosen formulation does not reflect the state of knowledge before our work. The sentence now reads:

“Overall, our model agrees with observational data that *Phaeocystis* is an important member of the high-latitude phytoplankton community.”

SC10: Figure 6: I believe the “p ratio” should be defined in the caption or removed.

We have adapted the figure caption in the revised manuscript, and it now reads:

“**Figure 6.** Pathways of particulate organic carbon (POC) formation in the *Baseline* simulation of ROMS-BEC averaged annually over a) 30-90° S and b) 60-90° S. The green and yellow boxes show the relative contribution (%) of *Phaeocystis*, diatoms, coccolithophores, small phytoplankton (SP), and zooplankton (Zoo) to the combined phytoplankton and zooplankton biomass (green) and total POC production (yellow) in the top 100 m, respectively. The arrows denote the relative contribution of the different POC production pathways associated with each PFT (black = grazing by zooplankton, grey = aggregation, blue = non-grazing mortality), given as % of total NPP in the top 100 m. Numbers are printed if $\geq 0.1\%$ and rounded to the nearest integer if $> 1\%$. The sum of all arrows gives the POC production efficiency, i.e., the fraction of NPP which is converted into sinking POC upon biomass loss (p ratio). Note that diazotrophs are not included in this figure due to their minor contribution to NPP in the model domain. «

Cited literature

- Buesseler, K. O. (1998). The decoupling of production and particulate export in the surface ocean. *Global Biogeochemical Cycles*, *12*(2), 297–310. <https://doi.org/10.1029/97GB03366>
- Buitenhuis, E. T., & Geider, R. J. (2010). A model of phytoplankton acclimation to iron-light colimitation. *Limnology and Oceanography*, *55*(2), 714–724. <https://doi.org/10.4319/lo.2009.55.2.0714>
- DiTullio, G. R., & Smith, W. O. (1996). Spatial patterns in phytoplankton biomass and pigment distributions in the Ross Sea. *Journal of Geophysical Research: Oceans*, *101*(C8), 18467–18477. <https://doi.org/10.1029/96JC00034>
- DiTullio, G. R., Grebmeier, J. M., Arrigo, K. R., Lizotte, M. P., Robinson, D. H., Leventer, A., Barry, J. P., VanWoert, M. L., & Dunbar, R. B. (2000). Rapid and early export of *Phaeocystis* antarctica blooms in the Ross Sea, Antarctica. *Nature*, *404*(6778), 595–598. <https://doi.org/10.1038/35007061>
- Geider, R. J., MacIntyre, H. L., & Kana, T. M. (1998). A dynamic regulatory model of phytoplanktonic acclimation to light, nutrients, and temperature. *Limnology and Oceanography*, *43*(4), 679–694. <https://doi.org/10.4319/lo.1998.43.4.0679>
- Kaufman, D. E., Friedrichs, M. A. M., Hemmings, J. C. P., & Smith Jr., W. O. (2018). Assimilating bio-optical glider data during a phytoplankton bloom in the southern Ross Sea. *Biogeosciences*, *15*(1), 73–90. <https://doi.org/10.5194/bg-15-73-2018>
- Le Quéré, C., Buitenhuis, E. T., Moriarty, R., Alvain, S., Aumont, O., Bopp, L., ... Vallina, S. M. (2016). Role of zooplankton dynamics for Southern Ocean phytoplankton biomass and global biogeochemical cycles. *Biogeosciences*, *13*(14), 4111–4133. <https://doi.org/10.5194/bg-13-4111-2016>
- Mathot, S., Smith, W. O., Carlson, C. A., Garrison, D. L., Gowing, M. M., & Vickers, C. L. (2000). Carbon partitioning within *Phaeocystis* Antarctica (Prymnesiophyceae) colonies in the Ross Sea, Antarctica. *Journal of Phycology*, *36*(6), 1049–1056. <https://doi.org/10.1046/j.1529-8817.2000.99078.x>
- Nissen, C., Vogt, M., Münnich, M., Gruber, N., & Haumann, F. A. (2018). Factors controlling coccolithophore biogeography in the Southern Ocean. *Biogeosciences*, *15*(22), 6997–7024. <https://doi.org/10.5194/bg-15-6997-2018>

- Schoemann, V., Becquevort, S., Stefels, J., Rousseau, V., & Lancelot, C. (2005). Phaeocystis blooms in the global ocean and their controlling mechanisms: a review. *Journal of Sea Research*, 53(1–2), 43–66. <https://doi.org/10.1016/j.seares.2004.01.008>
- Smith, W. O., Carlson, C., Ducklow, H., & Hansell, D. (1998). Growth dynamics of Phaeocystis antarctica-dominated plankton assemblages from the Ross Sea. *Marine Ecology Progress Series*, 168, 229–244. <https://doi.org/10.3354/meps168229>
- Strzepek, R. F., Boyd, P. W., & Sunda, W. G. (2019). Photosynthetic adaptation to low iron, light, and temperature in Southern Ocean phytoplankton. *Proceedings of the National Academy of Sciences*, 116(10), 4388–4393. <https://doi.org/10.1073/pnas.1810886116>
- Swan, C. M., Vogt, M., Gruber, N., & Laufkoetter, C. (2016). A global seasonal surface ocean climatology of phytoplankton types based on CHEMTAX analysis of HPLC pigments. *Deep Sea Research Part I: Oceanographic Research Papers*, 109, 137–156. <https://doi.org/10.1016/j.dsr.2015.12.002>
- Vogt, M., O'Brien, C., Peloquin, J., Schoemann, V., Breton, E., Estrada, M., Gibson, J., Karentz, D., Van Leeuwe, M. A., Stefels, J., Widdicombe, C., & Peperzak, L. (2012). Global marine plankton functional type biomass distributions: *Phaeocystis* spp. *Earth System Science Data*, 4(1), 107–120. <https://doi.org/10.5194/essd-4-107-2012>

Answer to referee #4:

We thank referee #4 for reviewing our manuscript in such great detail. His/Her valuable comments and suggestions have significantly improved the quality of our manuscript.

Below, we include our detailed answers to all comments and questions.

Answers to general comments (GC):

General Comment #1:

My main concern with the paper is that given that the outcome is highly sensitive to the model parameterization, the authors should place a very high priority on reporting uncertainties throughout. In its current form uncertainties are seldom reported. I also recommend that the authors conduct more sensitivity tests that examine how the model output changes when more than one parameter is perturbed. The model framework constructed by the authors would be ideal for a thorough exploration of how NPP and export vary with changing parameters, and presents an excellent opportunity to isolate the environmental conditions where model uncertainty is greatest. Additionally, cellular Fe:C ratios should be included in these sensitivity experiments. As Fe:C will make a very large difference to the POC calculated, and is central to the paper title, it is necessary that the authors investigate how Fe:C, which is sensitive to both light and iron, can change the model outcome. I believe that this paper will be much more useful to biogeochemists if error bars can be placed on the model estimates during major revisions, with particular consideration of parameter sensitivity to light and iron limitation.

Answer to GC1:

We thank the reviewer for this comment, which regards the broader topics of “model uncertainty” and “iron cycling” in ROMS-BEC, which we will separately address in the following.

Reporting uncertainties in an ecosystem model:

We agree with the reviewer that any quantitative information provided in our manuscript, such as the simulated distribution of chlorophyll, the integrated net primary production (NPP) and the contribution of the different phytoplankton functional types (PFTs) to NPP or the export of particulate organic carbon (POC), is associated with an uncertainty which should ideally be quantified. However, we believe it is important to distinguish between model uncertainty and model sensitivity in the current case.

In any biogeochemical model, the *model uncertainty* of any of the above biogeochemical quantities is defined as the variability of the respective quantity across *equally plausible realizations* of the model. Such an uncertainty results from several sources, namely the sensitivity of e.g. the chlorophyll fields to 1) the underlying physical fields (here simulated by ROMS), 2) the chosen structural complexity of the biogeochemical model (here BEC), and 3) the chosen model parameters describing e.g. the growth and loss of phytoplankton biomass in the biogeochemical model (BEC). To the best of our knowledge, there is currently no methodology available in the literature to *computationally efficiently* quantify the combined uncertainty of biogeochemical quantities due to these three factors in numerical ocean biogeochemical models with the complexity of ROMS-BEC, and this quantification is therefore currently not common practice in the biogeochemical modeling community. In the field of climate sciences, *equally plausible* model realizations are often achieved by perturbing the initial conditions, by perturbing certain parameters of a given model, or by comparing a number of different models with different structural complexity and/or model parameters in Monte-Carlo type analysis frameworks (see e.g. IPCC or the CMIP efforts, e.g. Bopp et al., 2013), but the total uncertainty of biogeochemical quantities like NPP is typically not systematically quantified for individual model studies using a single model. Given the complexity of our biogeochemical model, including hundreds of model parameters, and the comparatively high resolution used here, which results in hundreds of cores needed for one single simulation, an assessment of the total model uncertainty is computationally both

beyond the scope of the current work and beyond the limited computational resources available for this work.

However, we argue that the current set-up is suitable for the assessment of the *model sensitivity* of the above-mentioned bulk properties to the input parameters of the biogeochemical model, which is what we believe the reviewer had in mind in his/her comment. Hence, we describe how we have 1) quantified the *spatio-temporal variability* of the contribution of the PFTs to NPP and POC export in the model and 2) more systematically quantified the *sensitivity* of the simulated biomass distributions in ROMS-BEC to chosen *Phaeocystis* model parameters in the revised version of the manuscript.

In our study, the results of our *Baseline* setup represent the “*best*” model solution in terms of its agreement with the spatio-temporal distribution and variability of PFTs with available observations (i.e., *Baseline* has the lowest model-data-misfit), with all model parameters chosen within the ranges reported in the literature (see method section of the manuscript for references), and tuned to fit observational evidence. As a means to quantify the spatial variability in the contributions of different PFTs to the seasonally averaged chlorophyll distributions and annually integrated NPP and POC export, we add the area-weighted standard deviation of these quantities to the respective reported means in the abstract, in Table 3, and throughout the result section in the revised version of the manuscript:

Abstract:

all biogeochemically relevant Southern Ocean phytoplankton types. We find that *Phaeocystis* contribute $46 \pm 21\%$ (1σ in space) and $40 \pm 20\%$ to annual NPP and POC export south of 60° S, respectively, making them an important contributor to high-latitude carbon cycling. In our simulation, the relative importance of *Phaeocystis* and diatoms is mainly controlled by spatio-

Table 3:

Table 3. Comparison of ROMS-BEC based phytoplankton biomass, production, and export estimates with available observations (given in parentheses). Data sources are given below the Table. The reported uncertainty of the contribution of the PFTs to the simulated integrated NPP corresponds to the area-weighted spatial variability of each PFT’s contribution to annual NPP (1σ).

		ROMS-BEC (Data)	
		30-90° S	60-90° S
Surface chlorophyll biomass	total, annual mean [Gg chl]	40.8 (34.5 ^a)	17.1 (9.5 ^a)
Diatom carbon biomass	0-200m, annual mean [Pg C]	0.059 (global ^b : 0.10-0.94)	0.015
<i>Phaeocystis</i> carbon biomass	0-200m, annual mean [Pg C]	0.019 (global ^b : 0.11-0.71)	0.010
Coccolithophore carbon biomass	0-200m, annual mean [Pg C]	0.012 (global ^b : 0.001-0.03)	0.001
NPP	Pg C yr ⁻¹	17.2 (12.1-12.5 ^c)	3.0 (0.68-1.7 ^c)
	Diatoms [%]	52.0 (± 26.2)	49.1 (± 19.9)
	<i>Phaeocystis</i> [%]	15.3 (± 24.5)	45.8 (± 20.7)
	Coccolithophores [%]	14.6 (± 15.3)	0.7 (± 1.0)
POC export at 100m	SP [%]	17.2 (± 16.1)	4.5 (± 1.9)
	Pg C yr ⁻¹	3.1 (2.3-2.96 ^d)	0.62 (0.21-0.24 ^d)

^a Monthly climatology from MODIS Aqua (2002-2016, NASA-OBPG, 2014a), SO algorithm (Johnson et al., 2013)

^b The reported estimates from the MAREDAT data base in Buitenhuis et al. (2013) are global estimates of phytoplankton biomass.

^c Monthly climatology from MODIS Aqua VGPM (2002-2016, Behrenfeld and Falkowski, 1997; O’Malley, last access: 16 May 2016), NPP climatology from Buitenhuis et al. (2013, 2002-2016)

^d Monthly output from a biogeochemical inverse model (Schlitzer, 2004) and a data-assimilated model (DeVries and Weber, 2017).

Section 3.1:

dinal trend (see Fig. 2b-d and section 2.3.1, Swan et al., 2016). Averaged over 30-90° S (60-90° S), the simulated relative contributions of *Phaeocystis*, diatoms, and coccolithophores to total chlorophyll in summer are 20±28% (33±34%; subarea mean as shown in Fig. 2b & c ±1σ in space), 68±33% (64±33%), and 5±17% (<1±2%), respectively, in good agreement with the CHEMTAX climatology (28% (27%), 46% (48%), and 3% (1%), respectively). Acknowledging the uncertainty in the attribution of the group "Other" in the CHEMTAX data to a model PFT ("Other" includes dinoflagellates, cryptophytes, and chlorophytes here, see section 2.3.1), the model also captures the seasonal evolution of the relative importance of *Phaeocystis* and diatoms reasonably well, both averaged over 30-90° S (Fig. 2b) and at high SO latitudes (Fig. 2c-d). The model overestimates the contribution of *Phaeocystis* in fall (39±14% as compared to 24% in CHEMTAX) and spring (51±22% as compared to 28%) between 60-90° S and in the Ross Sea, respectively (Fig. 2c-d), but the limited number of data points available in the CHEMTAX climatology in this area and the uncertainty in the attribution of pigments in CHEMTAX to the *Phaeocystis* PFT in ROMS-BEC have to be noted (see section 2.3.1).

Section 3.4:

Phaeocystis is an important member of the SO phytoplankton community in our model, particularly south of 60°S, where it contributes 46±21% and 40±20% to total annual NPP and POC formation, respectively (Table 3 & Fig. 6). Even when considering the entire region south of 30°S, the contribution of *Phaeocystis* to NPP (15±24%) and POC production (16±22%) is sizeable. The simulated spatial differences in phytoplankton community structure have direct implications for the fate of

Additionally, we have performed a second set of model parameter sensitivity experiments in order to more systematically quantify the *sensitivity* of the simulated distributions of *Phaeocystis* and diatoms and integrated estimates of NPP and POC export in ROMS-BEC to *Phaeocystis* model parameter choices (section S2 of the revised supplementary material). To this end, we have systematically increased/decreased all key *Phaeocystis* parameters by 50%, allowing for an objective ranking of model sensitivities. We varied the following seven parameters of *Phaeocystis* (resulting in a total of 14 new simulations, see Table 1 below): the temperature optimum T_{opt} , the half-saturation constant of iron k_{Fe} , the maximum chl:N ratio $\theta_{chl:N, max}$, alphaPI, the linear mortality rate, the quadratic mortality rate (aggregation), and the maximum grazing rate of zooplankton on *Phaeocystis*. We note, however, that this systematic assessment does not result in equally plausible realizations of ROMS-BEC, as some of these changes will result in unrealistic biomass distributions of *Phaeocystis* and diatoms when compared to available observations. Therefore, we refer to these experiments as an assessment of *sensitivity* rather than *uncertainty*.

Table 1 (included in the revised manuscript as table S1): Overview of parameter sensitivity simulations, varying parameters by +/- 50%. PA=Phaeocystis, D=diatoms. See also Table 1 in the submitted manuscript.

Run Name	Description	
Topt150	Increase T_{opt}^{PA} by 50%	} Param_Topt
Topt50	Decrease T_{opt}^{PA} by 50%	
kFe150	Increase k_{Fe}^{PA} by 50%	} Param_kFe
kFe50	Decrease k_{Fe}^{PA} by 50%	
alphaPI150	Increase α_{PI}^{PA} by 50%	} Param_alphaPI
alphaPI50	Decrease α_{PI}^{PA} by 50%	
mortality150	Increase $\gamma_{m,0}^{PA}$ by 50%	} Param_mortality
mortality50	Decrease $\gamma_{m,0}^{PA}$ by 50%	
aggregation150	Increase $\gamma_{a,0}^{PA}$ by 50%	} Param_aggregation
aggregation50	Decrease $\gamma_{a,0}^{PA}$ by 50%	
grazing150	Increase $\gamma_{g,max}^{PA}$ by 50%	} Param_grazing
grazing50	Decrease $\gamma_{g,max}^{PA}$ by 50%	
thetaNmax50	Increase $\theta_{chl:N, max}^{PA}$ by 50%	} Param_thetaNmax
thetaNmax50	Decrease $\theta_{chl:N, max}^{PA}$ by 50%	

We quantify the sensitivity S of any target variable A (here A being one of the following targets: total phytoplankton, *Phaeocystis*, and diatom chlorophyll concentrations, total NPP, and POC export across 100m) to changes in the parameter X as follows, allowing for a ranking of the seven sets of simulations by the magnitude of the sensitivity (see Table 2 below, note that the resulting ranking of model experiments with regard to chlorophyll distributions is insensitive to the choice of chlorophyll rather than carbon here, as the simulated changes in carbon biomass fields of the PFTs are qualitatively similar to those in chlorophyll; not shown):

$$S_X^A = 100 \cdot \frac{A_{X150} - A_{X50}}{A_{XBaseline}} \quad (1)$$

As expected (see also Nissen et al., 2018), we find that both total chlorophyll concentrations and chlorophyll levels of *Phaeocystis* and diatoms are highly sensitive to parameters describing the growth and loss of *Phaeocystis* biomass, with increases of up to 700% (grazing50) and declines of up to >90% (Topt50, thetaNmax50) in *Phaeocystis* biomass between 60-90°S for a 50% change in the associated parameters (see Fig. 1 below). In general, any decline/increase in *Phaeocystis* chlorophyll biomass is associated with an increase/decline in diatom chlorophyll biomass, pointing to the direct competition for resources of these two phytoplankton types at high SO latitudes. Yet, the biomass compensation is not always complete due to non-linearities in the model system (e.g. food web feedbacks), resulting in changes of up to 70% (grazing150) in total chlorophyll levels upon changes in *Phaeocystis* parameters. The ranking of model sensitivities between 60-90°S reveals the highest sensitivity of *Phaeocystis* and diatom chlorophyll concentrations to the maximum grazing rate, the maximum chl:N ratio, the initial slope of the photosynthesis-irradiance curve, and the temperature optimum of *Phaeocystis* growth (Param_grazing, Param_thetaNmax, Param_alphaPI, Param_Topt in Table 1 above and Table 2 below). In comparison, the opposed changes in *Phaeocystis* and diatom chlorophyll levels (see Fig. 1 below) result in lower sensitivities of total chlorophyll levels to changes in *Phaeocystis* parameters in general and a lower ranking of the temperature optimum and thetaNmax experiments in particular (Param_Topt and Param_thetaNmax in Table 2 below).

Table 2 (included in the revised manuscript as table S2): Ranking of the parameter sensitivity experiments by the absolute sensitivity of annual mean total surface chlorophyll ($|S_X^{Chl}|$), *Phaeocystis* chlorophyll ($|S_X^{ChlPA}|$), and diatom chlorophyll ($|S_X^{ChlD}|$) to a +/-50% change in the model parameter X relative to the Baseline setup of ROMS-BEC between 60-90°S and in the Ross Sea, respectively. The sensitivity S (%) is quantified using Eq. 1.

See Table 1 above for details on the experimental setup and Fig. S12 for details on the resulting chlorophyll fields in ROMS-BEC in each experiment. Note that the simulated changes in carbon biomass fields are qualitatively similar to those of chlorophyll (not shown) and that the ranking shown here is therefore insensitive to the choice of chlorophyll in the analysis.

	Ranking ($ S_X^{Chl} $ in %)	Ranking ($ S_X^{ChlPA} $ in %)	Ranking ($ S_X^{ChlD} $ in %)
60-90°S	1. Param_alphaPI (63.6)	1. Param_grazing (693.1)	1. Param_alphaPI (153.4)
	2. Param_grazing (48.3)	2. Param_thetaNmax (390.9)	2. Param_thetaNmax (149.6)
	3. Param_mortality (40.6)	3. Param_Topt (306.8)	3. Param_Topt (132.7)
	4. Param_kFe (39.8)	4. Param_alphaPI (259.4)	4. Param_grazing (128.3)
	5. Param_Topt (37.5)	5. Param_kFe (209.1)	5. Param_kFe (109.6)
	6. Param_thetaNmax (33.0)	6. Param_mortality (178.0)	6. Param_mortality (101.8)
	7. Param_aggregation (6.4)	7. Param_aggregation (65.1)	7. Param_aggregation (10.2)
Ross Sea	1. Param_alphaPI (76.3)	1. Param_grazing (360.3)	1. Param_thetaNmax (189.1)
	2. Param_mortality (53.3)	2. Param_thetaNmax (288.9)	2. Param_alphaPI (189.1)
	3. Param_thetaNmax (46.4)	3. Param_Topt (194.2)	3. Param_Topt (142.1)
	4. Param_Topt (41.6)	4. Param_alphaPI (188.3)	4. Param_grazing (129.8)
	5. Param_kFe (41.3)	5. Param_kFe (126.2)	5. Param_mortality (126.7)
	6. Param_grazing (19.2)	6. Param_mortality (114.8)	6. Param_kFe (114.3)
	7. Param_aggregation (12.3)	7. Param_aggregation (59.5)	7. Param_aggregation (9.0)

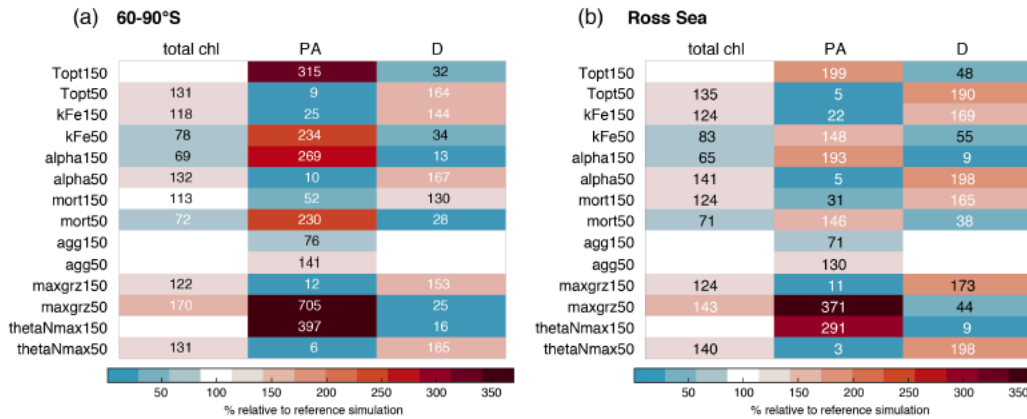


Fig. 1 (included in the revised manuscript as Fig. S13): Annual mean surface chlorophyll concentrations of all phytoplankton (Chl), *Phaeocystis* (PA), and diatoms (D) in the parameter sensitivity simulations (see Table 1 above) relative to the *Baseline* simulation. The model output is averaged over a) 60-90°S and b) the Ross Sea.

In comparison to the ranking of model experiments for total chlorophyll, the model sensitivities for NPP and POC export across 100 m are similar in magnitude both between 60-90°S and in the Ross Sea (20-90%, compare Table 2 above & Table 3 below). Additionally, the ranking of model experiments for NPP and POC export reveals only small differences to the ranking of model sensitivities for total chlorophyll: While the experiments *Param_alphaPI* and *Param_grazing* consistently rank amongst the top two most sensitive experiments for NPP and POC export and between 60-90°S for total chlorophyll concentrations, the experiments *Param_mortality/Param_Topt* are less/more important for NPP and POC than for total chlorophyll levels in ROMS-BEC (compare Table 2 & 3). In summary, this demonstrates the large model sensitivity of bulk biogeochemical quantities to parameter choices describing the temperature and light dependence of *Phaeocystis* growth and zooplankton grazing.

Table 3 (included in the revised manuscript as Table S3): Ranking of the parameter sensitivity experiments by the absolute sensitivity of annually integrated NPP ($|S_X^{NPP}|$) and POC export across 100 m ($|S_X^{POC100m}|$) to a +/-50% change in the model parameter X relative to the Baseline setup of ROMS-BEC between 60-90°S and in the Ross Sea, respectively. The sensitivity S (%) is quantified using Eq. 1. See Table 1 above for details on the experimental setup.

	Ranking ($ S_X^{NPP} $ in %)	Ranking ($ S_X^{POC100m} $ in %)
60-90°S	1. <i>Param_grazing</i> (68.4)	1. <i>Param_grazing</i> (86.4)
	2. <i>Param_alphaPI</i> (46.7)	2. <i>Param_alphaPI</i> (35.4)
	3. <i>Param_Topt</i> (43.6)	3. <i>Param_Topt</i> (26.7)
	4. <i>Param_kFe</i> (23.6)	4. <i>Param_mortality</i> (12.9)
	5. <i>Param_thetaNmax</i> (23.4)	5. <i>Param_kFe</i> (11.6)
	6. <i>Param_mortality</i> (11.6)	6. <i>Param_thetaNmax</i> (10.7)
	7. <i>Param_aggregation</i> (7.6)	7. <i>Param_aggregation</i> (1.4)
Ross Sea	1. <i>Param_grazing</i> (55.6)	1. <i>Param_grazing</i> (71.9)
	2. <i>Param_alphaPI</i> (48.5)	2. <i>Param_alphaPI</i> (39.0)
	3. <i>Param_Topt</i> (44.0)	3. <i>Param_Topt</i> (26.9)
	4. <i>Param_thetaNmax</i> (24.7)	4. <i>Param_thetaNmax</i> (11.9)
	5. <i>Param_kFe</i> (20.4)	5. <i>Param_kFe</i> (10.5)
	6. <i>Param_aggregation</i> (11.6)	6. <i>Param_mortality</i> (10.2)
	7. <i>Param_mortality</i> (8.3)	7. <i>Param_aggregation</i> (2.6)

Given computational constraints, we focused on *Phaeocystis* parameters here, but acknowledge that the simulated biomass distributions, NPP, and POC export are equally sensitive to parameters of the other PFTs and that the quantitative results might change when varying multiple parameters at once. We agree with the reviewer that this type of sensitivity experiments would ideally be performed in addition to the single-parameter perturbations, but given the number of available parameters in ROMS-BEC, the systematic assessment of these co-variation landscapes is beyond the scope of this study. We have added the above Tables and Figure as Tables S1, S2 & S3 and Fig. S13 to the revised supplementary information, together with the motivation of the experiments and the description of the main findings discussed above. Furthermore, we have added the new simulations to Table 2 and section 2.2 in the main text, as well as added small revisions to the appendix of the revised manuscript:

Table 2. Overview of sensitivity experiments aiming to 1) assess the sensitivity of the simulated *Phaeocystis*-diatom competition to chosen parameter values and parameterizations of *Phaeocystis* (competition experiments, runs 1-8) and 2) assess the sensitivity of the simulated biomass distributions to chosen *Phaeocystis* parameter values (parameter sensitivity experiments, runs 9-22). The results of the parameter sensitivity experiments are discussed in the supplementary material. See Table 1 and section 2.1 for parameter values and parameterizations of *Phaeocystis* in the reference simulation. PA=*Phaeocystis*, D=diatoms.

Competition	Run Name	Description
1	TEMPERATURE	Use μ_{\max}^D , Q_{10}^D , and $\mu_T^{PA} = \mu_{\max}^D \cdot Q_{10}^D \cdot \frac{T - T_{ref}}{10^{\frac{T - T_{ref}}{C}}}$ to compute the temperature-limited growth rate of <i>Phaeocystis</i> instead of Eq. 1
2	ALPHA _{PI}	Set α_{PI}^{PA} to α_{PI}^D
3	IRON	Set k_{Fe}^{PA} to k_{Fe}^D
4	GRAZING	Set $\gamma_{g,\max}^{PA}$ to $\gamma_{g,\max}^D$
5	AGGREGATION	Set $\gamma_{a,0}^{PA}$ to $\gamma_{a,0}^D$
6	MORTALITY	Set $\gamma_{m,0}^{PA}$ to $\gamma_{m,0}^D$
7	THETA_N_MAX	Set $\theta_{chl:N,\max}^{PA}$ to $\theta_{chl:N,\max}^D$
8	VARYING_kFE	Use $k_{Fe}^{PA}(I) = 2.776 \cdot 10^{-5} \cdot (I + 20)^2 - 0.00683 \cdot (I + 20) + 0.46$ (with the irradiance I in $W\ m^{-2}$) instead of a constant k_{Fe}^{PA}
Parameter sensitivity	Run Name	Description
9	Topt150	Increase T_{opt}^{PA} by 50%
10	Topt50	Decrease T_{opt}^{PA} by 50%
11	kFe150	Increase k_{Fe}^{PA} by 50%
12	kFe50	Decrease k_{Fe}^{PA} by 50%
13	alphaPI150	Increase α_{PI}^{PA} by 50%
14	alphaPI50	Decrease α_{PI}^{PA} by 50%
15	mortality150	Increase $\gamma_{m,0}^{PA}$ by 50%
16	mortality50	Decrease $\gamma_{m,0}^{PA}$ by 50%
17	aggregation150	Increase $\gamma_{a,0}^{PA}$ by 50%
18	aggregation50	Decrease $\gamma_{a,0}^{PA}$ by 50%
19	grazing150	Increase $\gamma_{g,\max}^{PA}$ by 50%
20	grazing50	Decrease $\gamma_{g,\max}^{PA}$ by 50%
21	thetaNmax150	Increase $\theta_{chl:N,\max}^{PA}$ by 50%
22	thetaNmax50	Decrease $\theta_{chl:N,\max}^{PA}$ by 50%

Section 2.2:

Furthermore, we perform two sets of sensitivity experiments (22 simulations in total), in order to 1) assess the sensitivity of the simulated *Phaeocystis* biogeography and the competition of *Phaeocystis* and diatoms to chosen parameters and parameterizations (competition experiments, runs 1-8 in Table 2) and 2) systematically assess the sensitivity of the simulated biomass distributions to chosen *Phaeocystis* parameter values (parameter experiments, runs 9-22). For the former set, we set the parameters and parameterizations of *Phaeocystis* to those used for diatoms in ROMS-BEC (runs 1-8 in Table 2). Generally, the differences in parameters between *Phaeocystis* and diatoms affect either the simulated biomass accumulation rates (runs TEMPERATURE, ALPHA_{PI}, IRON, and THETA_N_MAX) or loss rates (runs GRAZING, AGGREGATION, and MORTALITY). By successively eradicating the differences between *Phaeocystis* and diatoms, these simulations allow us to directly quantify the impact of parameter differences on the simulated relative importance of *Phaeocystis* for total phytoplankton biomass. To assess the impact of iron-light interactions on the competitive success of *Phaeocystis* at high SO latitudes, we ultimately run a simulation in which the half-saturation constant of iron (k_{Fe}) of *Phaeocystis* is a function of the light intensity, following a polynomial fit of available laboratory data (VARYING_kFE, Fig. A1b; Garcia et al., 2009). For the second set of experiments, we systematically vary *Phaeocystis* growth and loss parameters by $\pm 50\%$, and the results of these experiments are discussed in detail in section S2 of the supplementary material. All sensitivity experiments use the same physical and biogeochemical spin-up as the *Baseline* simulation and start from the end of year 10 of the coupled ROMS-BEC spin-up. Each simulation is then run for an additional 10 years, of which the average over the last 5 full seasonal cycles is analyzed in this study.

Appendix:

A1 Sensitivity of *Phaeocystis* biogeography to chosen parameter differences between *Phaeocystis* and diatoms

We assess the sensitivity of the simulated annual mean *Phaeocystis* biogeography to parameter choices by performing a set of sensitivity experiments (competition experiments, runs 1-8 in Table 2). Overall, the simulated surface *Phaeocystis* biomass concentrations change by $\gtrsim \pm 50\%$ for each of the experiments in the high-latitude SO (Fig. A2). Between 60-90° S and in the Ross Sea, the largest increases in *Phaeocystis* biomass concentrations are simulated for THETA_N_MAX (+332% and +217%, respectively, Fig. A2b & c) and AGGREGATION (+112% and +96%, respectively, Fig. A2b & c), whereas the strongest decline is simulated for ALPHA_{PI} (-76% and -87%, respectively, Fig. A2b & c). As a response to changes in *Phaeocystis* parameters, diatom biomass changes overall more than that of SP on a basin scale, suggesting *Phaeocystis* is indeed mostly competing with diatoms for resources in the high-latitude SO. Between 60-90° S, the magnitude of change is similar for the experiments TEMPERATURE (-73%), ALPHA_{PI} (-76%), and IRON (+70%), while in the Ross Sea, the response in IRON is substantially smaller (+17%) than that for the other two experiments (-82% and -87% for TEMPERATURE and ALPHA_{PI}, respectively; Fig. A2b & c). This supports our findings from section 3.3, namely that the difference in light sensitivity between *Phaeocystis* and diatoms is more important in coastal areas than on a basin scale in controlling the relative importance of *Phaeocystis* for total phytoplankton biomass.

Iron cycling in BEC:

We thank the reviewer for raising this important point. In the following, we will describe how Fe:C uptake ratios of diatoms and *Phaeocystis* are parametrized in the model and how these choices impact the simulated biomass distributions in ROMS-BEC. For more details on other aspects of the cycling of iron in BEC (e.g. scavenging, external sources), we kindly refer the reviewer to our answer to SC59 below.

In BEC, all of the dissolved iron (Fe) pool is assumed to be bioavailable to phytoplankton, whose Fe:C uptake stoichiometry for a given carbon uptake during photosynthesis varies from 3-20 $\mu\text{mol mol}^{-1}$ for all PFTs except diazotrophs (12-60 $\mu\text{mol mol}^{-1}$). In BEC, the Fe:C uptake ratio depends on surrounding Fe concentrations and the half-saturation constants of iron of the respective PFT (k_{Fe} , see Fig. 2 below for diatoms and *Phaeocystis*). Generally, when seawater Fe concentrations fall below a critical level (specific to the PFT's half-saturation constant), the PFT reduces its cellular Fe:C requirements. As a result, diatoms generally have higher intracellular Fe:C ratios than *Phaeocystis* colonies in ROMS-BEC, and Fe:C ratios of all phytoplankton are highest in winter and lowest in summer, in concert with the seasonal evolution of upper ocean Fe levels (see Fig. 3 below). Photoacclimation affects the photosynthetic carbon uptake of phytoplankton (see model equations in

the appendix of the submitted manuscript) and thereby further modifies the intracellular Fe:C ratio of each PFT (not shown here).

As the Fe uptake per unit of C of phytoplankton is regulated by each PFT's k_{Fe} in ROMS-BEC, these differences between *Phaeocystis* and diatoms are eliminated in the simulation IRON, in which the k_{Fe} of *Phaeocystis* is set to the value of diatoms (see method section 2.2 of the manuscript). In general, any simulated changes in the biomass distributions in this experiment relative to the *Baseline* setup result from the interaction of two factors: First, the lower k_{Fe} of *Phaeocystis* in the IRON experiment (see Table 2 of the manuscript) leads to a lower Fe limitation of photosynthetic growth and hence more C uptake of *Phaeocystis* in the model, facilitating a higher buildup of biomass. Second, the higher Fe uptake per unit of C of *Phaeocystis* in the IRON experiment leads to a quicker Fe depletion, which ultimately drives *Phaeocystis* back into severe Fe limitation, slowing down the accumulation of carbon biomass.

In ROMS-BEC, the annual mean surface *Phaeocystis* biomass between 60-90°S in the IRON experiment increases to 170% of the concentration simulated in the *Baseline* setup, while the simulated average diatom biomass concentration declines to 65% of its *Baseline* value (see Fig. A2 in manuscript; note that the values in Fig. A2 refer to each PFT's chlorophyll biomass, but that the relative change in carbon biomass are comparable in magnitude). As expected, in the experiments $k_{Fe}150/k_{Fe}50$, the simulated changes are larger (25%/234% and 144%/34% for *Phaeocystis* and diatoms, respectively, see Fig. 1 above), resulting directly from the larger perturbation of k_{Fe} compared to the experiment IRON. Overall, this suggests that changes in the iron uptake, through changes in both iron limitation in photosynthesis and the Fe:C uptake ratio, significantly alter the relative abundance of *Phaeocystis* and diatoms in the high-latitude Southern Ocean. Yet, as a result of the at least partially compensating changes of *Phaeocystis* and diatom biomass for the simulated total phytoplankton biomass, the simulated changes in POC export between 60-90°S are rather small compared to the changes in community composition in ROMS-BEC upon changes in iron uptake dynamics (103.8%/94.8%/106.5% of *Baseline* in the experiments IRON/ $k_{Fe}150/k_{Fe}50$). While this suggests a rather small sensitivity of bulk properties like POC export or total phytoplankton biomass to the phytoplankton Fe:C uptake ratios, the large simulated changes in the phytoplankton community structure imply a large sensitivity of the exact pathways of carbon from its uptake to its export to the chosen Fe uptake parameters in ROMS-BEC. Further, we acknowledge that the current parametrization of Fe:C uptake ratios in BEC neglects more direct impacts of light availability (see e.g. Strzepek et al., 2019), the effect of which on the competition of *Phaeocystis* and diatoms and carbon export fluxes we can currently not assess.

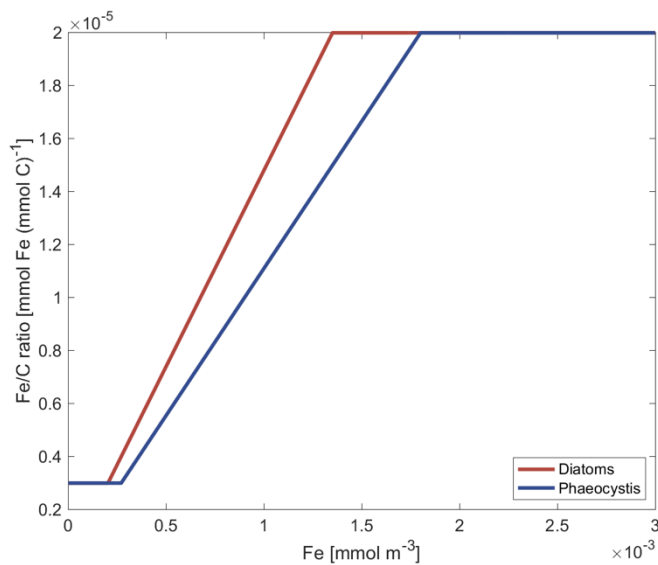


Fig. 2: The Fe:C uptake ratio of diatoms (red) and *Phaeocystis* (blue) in ROMS-BEC as a function of Fe levels.

In the revised version of the manuscript, we have added information on the Fe:C uptake ratios of phytoplankton to the method section. It reads:

“In ROMS-BEC, phytoplankton Fe uptake relative to the uptake of C varies as a function of seawater Fe levels and decreases linearly below a critical concentration which is specific to each PFT’s k_{Fe} (see Eq. B11). In concert with the seasonal evolution of upper ocean Fe levels, the Fe:C ratios of all PFTs are highest in winter and lowest in summer (not shown). As a result of their higher k_{Fe} in the model, *Phaeocystis* generally have lower Fe:C uptake ratios than diatoms.”

Furthermore, we have added the model equations to the appendix in the revised manuscript:

In BEC, the Fe:C ratio $\theta_{Fe:C}^i$ [$\mu\text{mol mol}^{-3}$] of growth by phytoplankton i varies between the maximum Fe:C ratio $\theta_{Fe:C,max}^i$ at high seawater Fe concentrations and the minimum Fe:C ratio $\theta_{Fe:C,min}^i$ at very low Fe concentrations. Below a critical surrounding Fe concentration, which depends on each PFT’s half-saturation constant of iron k_{Fe}^i (see Table 1), the ratio is reduced from the maximum Fe:C ratio following:

$$\theta_{Fe:C}^i = \theta_{Fe:C,max}^i \quad (B11)$$

$$\theta_{Fe:C}^i = \max\left(\theta_{Fe:C}^i \cdot \frac{[Fe]}{9 \cdot k_{Fe}^i}, \theta_{Fe:C,min}^i\right) \quad \text{where } [Fe] < 9 \cdot k_{Fe}^i \quad (B12)$$

For this study, $\theta_{Fe:C,max}^i$ is 60 for diazotrophs and 20 for all other PFTs, and $\theta_{Fe:C,min}^i$ is 12 for diazotrophs and 3 for all other PFTs.

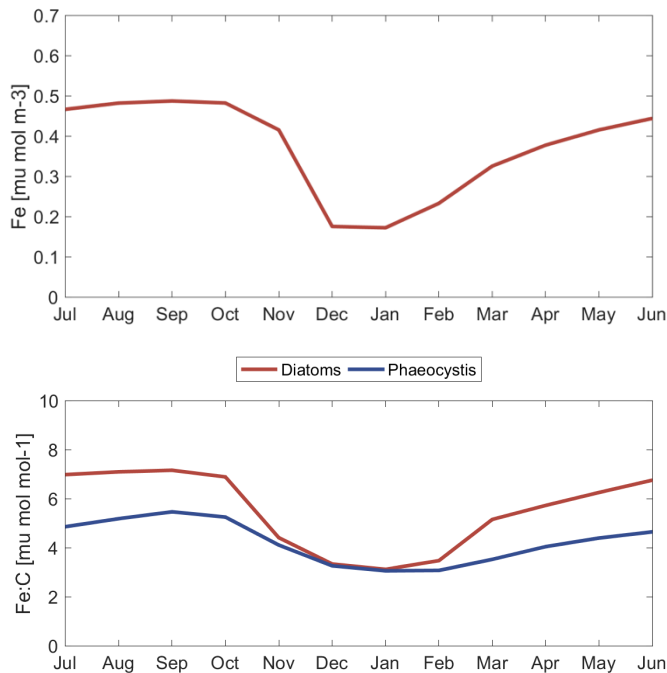


Fig. 3: Top: Monthly averaged surface iron concentrations in the Ross Sea. Bottom: The intracellular Fe:C ratio of diatoms (red) and *Phaeocystis* (blue). Both panels show output from the *Baseline* simulation of ROMS-BEC.

Answers to specific comments (SC):

SC1: Line 5: “improved” instead of “extended”

We have changed the sentence as follows:

“We improved ROMS-BEC by adding an explicit parameterization of *Phaeocystis* colonies, so that the model, together with the previous addition of an explicit coccolithophore type, now includes all biogeochemically relevant Southern Ocean phytoplankton types.”

SC2: Line 7: This implies solitary *Phaeocystis* are not biogeochemically relevant, when commonly used to understand succession in the Ross sea

We kindly refer the reviewer to our answer to SC15 & SC18.

SC3: Line 7: Please report uncertainties

As described in more detail in our answer to GC1, we quantify the spatial variability of the contribution of *Phaeocystis* to integrated annual NPP and POC export as the area-weighted standard deviation of the reported averages in the revised manuscript. The abstract now reads:

“We find that *Phaeocystis* contribute $46\pm 21\%$ (1σ in space) and $40\pm 20\%$ to annual NPP and POC export south of 60° S, respectively, making them an important contributor to high-latitude carbon cycling.”

SC4: Line 9: Saying “temporal variability” here implies spatial variability is not a considerable factor, when in the following line you say that there is a difference at the coast

In order to clarify, we have rephrased this part of the abstract as follows:

“In our simulation, the relative importance of *Phaeocystis* and diatoms is mainly controlled by spatio-temporal variability in temperature and iron availability. In addition, in more coastal areas, such as the Ross Sea, the higher light sensitivity of *Phaeocystis* at low irradiances promotes the succession from *Phaeocystis* to diatoms. “

SC5: Line 11: Remove “Still,” from this sentence, it’s unclear how this sentence follows from the previous

Changed as suggested in the revised version of the manuscript

SC6: Line 24-25: There is no previous statement that there is observed succession, just that the other groups contribute to biomass. Please include such a statement and provide references.

In the revised version of the manuscript, to link spatial and temporal variability of phytoplankton community structure and its importance for biogeochemical cycles, we have changed the respective sentence to also state *when* coccolithophores and *Phaeocystis* contribute substantially to biomass. It now reads:

“However, calcifying coccolithophores and dimethylsulfide (DMS) producing *Phaeocystis* have been found to contribute in a significant way to total phytoplankton biomass in summer/fall at subantarctic (Balch et al., 2016; Nissen et al., 2018) and in spring/summer at high latitudes, respectively (Smith and Gordon, 1997; Arrigo et al., 1999; DiTullio et al., 2000; Poulton et al., 2007; Arrigo et al., 2017), thus suggesting that the succession and competition of different plankton groups governs biogeochemical cycles at the (sub)regional scale.”

SC7: Line 32: Since there are few and not zero estimates, please briefly reference them here.

In the revised manuscript, we have added references that quantify the contributions of different members of the high-latitude phytoplankton community to Southern Ocean NPP and POC export:

“While a number of recent studies have elucidated the importance of coccolithophores for subantarctic carbon cycling (e.g. Rosengard et al., 2015; Balch et al., 2016; Nissen et al., 2018; Rigual Hernández

et al., 2020), few estimates quantify the role of present and future high-latitude SO phytoplankton community structure for ecosystem services such as NPP and carbon export (e.g. Wang and Moore, 2011; Yager et al., 2016).”

SC8: Line 48: This is unclear. Do you mean that grazing would not be as significant of a loss as aggregation?

Yes, this is what we mean. Since *Phaeocystis* colonies are more likely to form aggregates than single cells and since they are additionally less likely to be grazed than single cells (both purely based on size assumptions), the observed dominance of colonies over solitary cells in summer (see e.g. Smith et al., 2003) likely leads to relatively more important aggregation than grazing for total *Phaeocystis* biomass loss. We have rephrased the respective sentence to clarify:

“Its alternation between solitary cells of a few μm in diameter and gelatinous colonies of several mm to cm in diameter (e.g. Rousseau et al., 1994; Peperzak, 2000; Chen et al., 2002; Bender et al., 2018) directly impacts community biomass partitioning and the relative importance of aggregation, viral lysis, and grazing for *Phaeocystis* biomass losses, its susceptibility to zooplankton grazing relative to that of diatoms (Granéli et al., 1993; Smith et al., 2003), and ultimately the export of particulate organic carbon (POC; Schoemann et al., 2005). With *Phaeocystis* colonies typically dominating over solitary cells during the SO growing season (Smith et al., 2003) and with larger cells being more likely to form aggregates and less likely to be grazed by microzooplankton (Granéli et al., 1993; Caron et al., 2000; Schoemann et al., 2005; Nejtgaard et al., 2007), *Phaeocystis* biomass loss via aggregation possibly increases in relative importance at the expense of grazing as more colonies are formed and colony size increases (Tang et al., 2008).”

SC9: Line 52: “expensive” instead of “difficult”
Changed as suggested in the revised version of the manuscript

SC10: Line 66: Reference Yager et al., 2016
We have added the reference as suggested. See also SC12.

SC11: Line 67: Zooplankton grazing rates on *Phaeocystis* are low (Yang et al., 2016)
We have added the reference as suggested. See also SC12.

SC12: Line 68: There are also arguments that the hydrography results in the resurfacing of any sunken *Phaeocystis*-associated POC (Lee et al., 2017)
We thank the reviewer for the additional references which we were not aware of. We have changed this sentence of the introduction, which now reads:

“While some have found blooms of *Phaeocystis* to be important vectors of carbon transfer to depth through the formation of aggregates (Asper and Smith, 1999; DiTullio et al., 2000; Ducklow et al., 2015; Yager et al., 2016; Asper and Smith, 2019), others suggest their biomass losses to be efficiently retained in the upper ocean by local circulation (Lee et al., 2017) and degraded in the upper water column through bacterial and zooplankton activity (Gowing et al., 2001; Accornero et al., 2003; Reigstad and Wassmann, 2007; Yang et al., 2016), making *Phaeocystis* a minor contributor to SO POC export.

SC13: Line 79: State how the referenced models parameterize *Phaeocystis* differently, and the possible consequences on the model outcome
We have added a statement addressing this comment in the introduction of the revised version of the manuscript:

“In this context, whether the model explicitly represents both *Phaeocystis* life stages (Pasquer et al., 2005; Kaufman et al., 2017; Losa et al., 2019) or only the colonial stage (Wang and Moore, 2011; Le Quéré et al., 2016) is key, as single cells are known to have lower iron requirements than *Phaeocystis* colonies (Veldhuis et al., 1991).”

SC14: Line 88: The introduction is missing a description of observed succession in SO sectors outside of the Ross Sea

We thank the reviewer for this comment, but would like to clarify. In the introduction of the submitted manuscript, three of the six cited papers on Southern Ocean phytoplankton succession include a discussion from regions outside of the Ross Sea, namely from the Western Antarctic Peninsula (Arrigo et al., 2017) and from the circumpolar Southern Ocean (Green et al., 2006; Alvain et al., 2008), and all cited studies describe a succession from *Phaeocystis* to diatoms throughout spring and summer. Furthermore, as the Ross Sea is one of the key areas for the competition of *Phaeocystis* and diatoms in the Southern Ocean and was therefore chosen as one of the focus regions in our manuscript, the cited papers on phytoplankton succession in the introduction reflect past research efforts, which, as far as we are aware of, focused more heavily on the Ross Sea than on other sectors.

SC15: Line 93: Why did you not include solitary *Phaeocystis* when it's been used in other successful models (such as those published by Kaufman)?

We fully agree with the reviewer that better constraining the role of life cycle transitions of *Phaeocystis* for Southern Ocean carbon cycling is of high interest. Yet, for this study, we decided to focus on the colonial stage of *Phaeocystis* for two reasons. To the best of our knowledge, colonial *Phaeocystis* is dominant over solitary cells in terms of total *Phaeocystis* biomass during late spring and summer (e.g. Smith et al., 2003) and likely dominates for downward carbon fluxes (e.g. DiTullio et al., 2000; Yang et al., 2016), making the colonial stage the more relevant *Phaeocystis* life stage for our study. Furthermore, there is currently only 390 *Phaeocystis* biomass data points in the whole Southern Ocean, and the distinction between colonial and solitary *Phaeocystis* is often difficult (Vogt et al. 2012), impeding the basin-wide model evaluation of both *Phaeocystis* life stages, especially on a seasonal scale (see also section 4.3 of the manuscript). We note that single-celled *Phaeocystis* are implicitly included in the small phytoplankton group in ROMS-BEC (see method section 2.1). Thereby, while not being able to distinguish single-celled *Phaeocystis* from other nanophytoplankton cells in the model, the contribution of this *Phaeocystis* life stage to total phytoplankton biomass is contained in the estimate for the small phytoplankton group.

SC16: Line 95: Please give a brief statement here on how the model was validated.

In the revised manuscript, we have added a statement describing the model validation to this paragraph:

“Using available observations, such as satellite-derived chlorophyll concentrations, carbon biomass and pigment data, we first validate the simulated phytoplankton distributions and community structure across the SO and then particularly focus on the temporal variability of diatoms and *Phaeocystis* in the high-latitude SO.”

As a response to a comment by referee #3, we have further modified the last paragraph to better reflect the structure of the manuscript. The whole paragraph now reads:

“In this study, we investigate the competition between *Phaeocystis* and diatoms and its implications for carbon cycling using a regional coupled physical-biogeochemical-ecological model configured at eddy-permitting resolution for the SO (ROMS-BEC, Nissen et al., 2018). To address the missing link between SO phytoplankton biogeography, ecosystem function, and the SO carbon cycle, we have added *Phaeocystis* colonies as an additional PFT to the model, so that it includes all major known biogeochemically relevant phytoplankton types of the SO (see e.g. Buesseler et al., 1998; DiTullio et al., 2000). Using available observations, such as satellite-derived chlorophyll concentrations, carbon biomass and pigment data, we first validate the simulated phytoplankton distributions and community structure across the SO and then particularly focus on the temporal variability of diatoms and *Phaeocystis* in the high-latitude SO. After assessing the relative importance of bottom-up and top-down factors in controlling the contribution of *Phaeocystis* colonies and diatoms to total phytoplankton biomass over a complete annual cycle in the high-latitude SO, we show that the spatially and temporarily varying phytoplankton community composition leaves a distinct, PFT-specific imprint on upper ocean carbon cycling and POC export across the SO .”

SC17: Line 102: does the addition of the new PFT affect the validation metrics done in Nissen et al. 2018?

In comparison to the 4-PFT setup of ROMS-BEC in Nissen et al. (2018), the model performance has improved in the 5-PFT setup of this study, as described in section 3.1 and seen in Fig. 2 & S7 of the manuscript. In summary, general trends like the too high chlorophyll biomass and NPP at high latitudes and the associated too low macronutrient concentrations remain also in the 5-PFT setup presented in this study, but the existing biases in these biogeochemical tracers are reduced upon the implementation of *Phaeocystis* into the model.

SC18: Line 107: isn't solitary *Phaeocystis* also important in the SO?

We agree with the reviewer that solitary cells can temporarily be more important for total *Phaeocystis* biomass than its colonial life form, but to the best of our knowledge, at the bloom peak, the colonial form typically dominates over solitary cells in the Southern Ocean (late spring/summer, e.g. Smith et al., 2003). In the revised version of the manuscript, we have rephrased the respective sentence to read:

“Here, we extend the version of Nissen et al. (2018) to include an explicit parameterization of colonial *Phaeocystis antarctica*, which is the only bloom-forming species of *Phaeocystis* occurring in the SO (Schoemann et al., 2005) and which typically dominates over solitary cells when SO *Phaeocystis* biomass levels are highest (Smith et al., 2003).”

Furthermore, as stated in our response to SC15 above, single-celled *Phaeocystis* are implicitly included in the small phytoplankton group in ROMS-BEC.

SC19: Line 110: Wouldn't you need to assume a minimum cell concentration for this to be valid?

Here, we assume enough cells to be available at any time in the small phytoplankton functional type of ROMS-BEC, in the same way it was previously done by Wang & Moore (2011). As model parameters for *Phaeocystis* growth are chosen to reflect the colonial life stage in ROMS-BEC and as biomass accumulation of this phytoplankton type thus only accelerates when environmental conditions are favorable for *Phaeocystis* colonies, we only expect a small sensitivity of the simulated *Phaeocystis* seasonality to the explicit inclusion of a minimum cell concentration for colony formation.

SC20: Line 114: Please give your rationale for using this function instead of Eppley

As indicated in the manuscript (section 2.1), the new phytoplankton functional type *Phaeocystis* represents a single species (*Phaeocystis Antarctica*) rather than a multitude of species as e.g. in the case of diatoms. As individual phytoplankton species typically show an optimum temperature for growth in laboratory experiments, above and below which its growth is slowed down (see Fig. 4 below), this justifies the choice to use an optimum curve to describe temperature-dependent growth of the *Phaeocystis* functional type in ROMS-BEC. In contrast, within the model PFT “diatoms”, we do not model a specific species of diatoms, but the whole diatom community (typical PFT approach; Le Quéré et al., 2005), and the use of a so-called Q10-function (Eppley 1972) can hence be interpreted as the overlap of numerous optimum curves of numerous individual species.

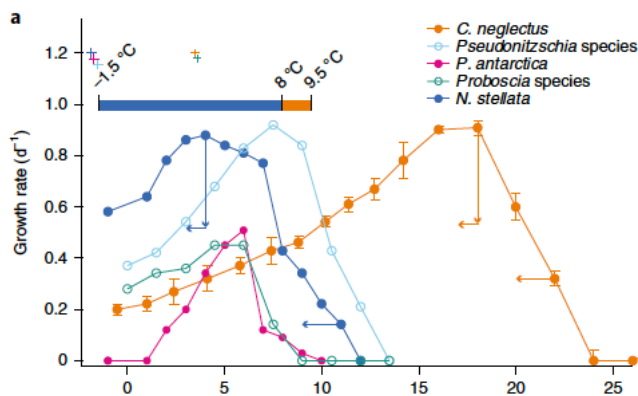


Fig. 4: Growth rates as a function of temperature for example high-latitude SO species of diatoms and *Phaeocystis* (Boyd 2019).

SC21: Table 1: Why did you choose a slightly different grazing rate for diatoms and *Phaeocystis*? This choice is motivated based on size-mismatch assumptions between diatoms and *Phaeocystis* colonies and the single zooplankton grazer in ROMS-BEC (see section 2.1 of the manuscript).

SC22: Line 149: shouldn't alpha be sensitive to the iron concentration? (Strzepek et al., 2019)
 We thank the reviewer for pointing us to the paper by Strzepek et al. (2019). In ROMS-BEC, the sensitivity of phytoplankton to changes in light intensity at low light, i.e., alpha PI, is set as a constant for each phytoplankton functional type (see Table 1 of the manuscript). However, the light limitation formulation also accounts for effects of photoacclimation (see appendix of the manuscript; Geider et al., 1998), thereby allowing for interactions between light and nutrient availability (iron availability in the case of the high SO latitudes; see Fig. 5 below). We note that while the respective curves for diatoms and *Phaeocystis* look rather similar in Fig. 5 below (compare e.g. the two solid lines), differences in the model simulation are larger at any location and any given point in time due to differences in their temperature growth limitation function, which further modifies the light limitation factor (not considered in Fig. 5 below, but see Eq. B9 of the manuscript), their iron half-saturation constants and the resulting differences in their nutrient limitation factor. Still, we acknowledge that this parametrization should be re-assessed in the light of recent advances (such as the study by Strzepek et al.) in future work.

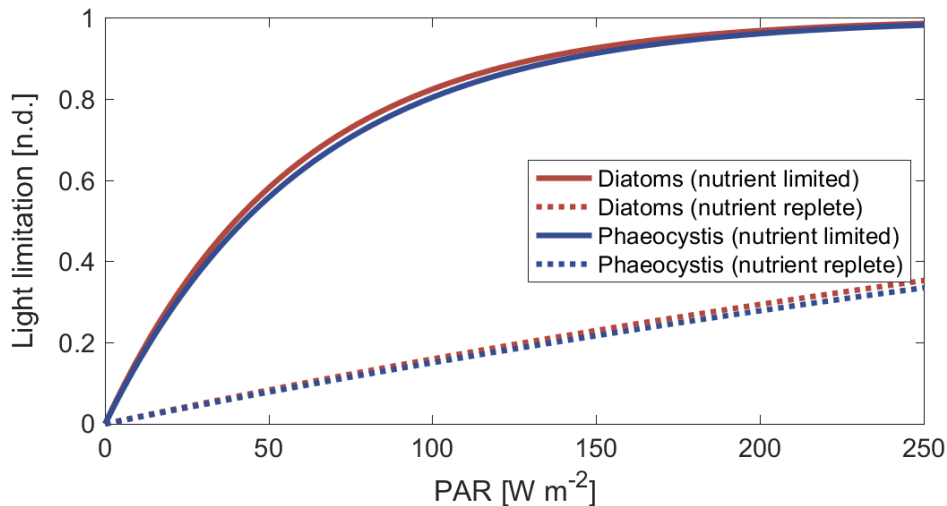


Fig. 5: Light limitation [n.d.] as a function of light intensity (PAR, W m^{-2}) in ROMS-BEC for growth by diatoms (red) and *Phaeocystis* (blue). A light limitation factor of 1 denotes no light limitation of phytoplankton growth. The dashed line represents a nutrient limited case, the dotted line a nutrient replete case. For the computation, the annual mean surface C:Chl ratio of diatoms ($54.8 \text{ mg C (mg chl)}^{-1}$) and *Phaeocystis* ($83.7 \text{ mg C (mg chl)}^{-1}$) between $60\text{-}90^\circ\text{S}$ is used. Note that in the model, in addition to nutrient limitation, temperature stress further modifies this ratio, see Eq. B9 of the manuscript. Consequently, while the respective curves for diatoms and *Phaeocystis* look rather similar here (compare e.g. the two solid lines), differences in the model simulation are larger at any location and any given point in time due to differences in their temperature growth limitation function, their iron half-saturation constants, and the resulting differences in their nutrient limitation factor.

SC23: Line 162: this is a very small difference, what is the net sensitivity of the output to this parameter?

Admittedly, the difference in the maximum grazing rate between grazing on diatoms (3.8 d^{-1}) and grazing on *Phaeocystis* (3.6 d^{-1}) appears rather small. Yet, high-latitude biomass distributions in ROMS-BEC are rather sensitive to this difference. In fact, in the experiment GRAZING, in which we set the maximum grazing rate on *Phaeocystis* to the value of diatoms, i.e., we increase the grazing pressure on *Phaeocystis* (see section 2.2 and Table 2 of the manuscript), annual mean *Phaeocystis* biomass concentrations decrease to 52% and even 38% of the levels in the *Baseline* simulation between $60\text{-}90^\circ\text{S}$ and in the Ross Sea, respectively (see Fig. A2 of the manuscript). At the same time, biomass levels of diatoms increase to 121% and 149% of the levels in the *Baseline* simulation,

demonstrating the rather large sensitivities to this parameter. We note, however, that by choosing the same grazing rate on diatoms and *Phaeocystis*, the resulting phytoplankton community structure at high SO latitudes shows a larger discrepancy to the observed community structure (compare e.g. Fig. A2 to Fig. 2 in the manuscript), suggesting that the choice of a higher maximum grazing rate on diatoms than on *Phaeocystis* in our model setup is justified as it results in a more ecologically sound ecosystem structure.

SC24: Line 190: what day of year are you initializing with?

All model simulations are started on January, 1 of the respective year. Please see also our answer to SC25 for a discussion of the sensitivity of the results to the chosen initial conditions of the phytoplankton community composition.

SC25: Line 194: what is the sensitivity of the model outcome to your initial community composition?

The simulated phytoplankton biomass concentrations assessed in this manuscript are averaged over the last five full annual cycles of a 20-year long simulation (see section 2.2 of the manuscript). In fact, the simulated phytoplankton biomass distributions for this analysis period are controlled more by chosen model parameters than by the chosen initial biomass distributions. Initial chlorophyll fields of each PFT are derived using satellite-derived total chlorophyll concentrations and a fixed partitioning onto the model PFTs. For our simulations, the chosen partitioning (90% small phytoplankton, 4% diatoms and coccolithophores, 1% diazotrophs and *Phaeocystis*, see method section 2.2) is admittedly motivated by the phytoplankton community composition at the open northern boundary at 24°S, i.e., in the middle of the subtropical gyre, where small phytoplankton (e.g. *Prochlorococcus* and *Synechococcus*) dominate. In contrast, at high SO latitudes, large phytoplankton types, such as diatoms and *Phaeocystis* dominate (e.g. Swan et al., 2016). Nevertheless, phytoplankton distributions at high latitudes are quickly in steady state, as biomass levels of all phytoplankton types decrease to very low levels in the high-latitude winter months (due to the absence of light), resulting in a phytoplankton community close to equilibrium already in the 2nd growth season. Therefore, by analyzing the years 15-20 of each model simulation, our results are independent of the chosen initial community composition.

SC26: Line 212: diatom and phaeo cellular Fe:C ratios should also be informed by light and iron limitation (Strzepek et al., 2011)

As described in more detail in our answer to GC1, the Fe:C uptake ratios of phytoplankton are a function of the surrounding Fe concentrations in the version of ROMS-EBC used for this study. In addition, photoacclimation affects the cellular Fe:C content of phytoplankton by impacting the light limitation factor (see Eq. B9 in the manuscript), which is used to calculate the photosynthetic carbon uptake in the model.

SC27: Line 240: Top 50 m is not deep enough for analyzing export.

We agree with the reviewer on this statement. This is why, for the analysis of export fluxes, the top 100m are assessed (see Fig. 6 and Table 3 of the manuscript), but we note that in our model, at high latitudes, ~80% of total biomass can be found in the top 50m. The reason for choosing the top 50m for the analysis of the spatial distribution of the PFTs in ROMS-BEC was thus twofold. First, we decided on this depth level for Fig. 1 and the niche analysis for an easy comparison with the plots from the 4-PFT setup of ROMS-BEC presented in Nissen et al. (2018). Second, most of the available phytoplankton carbon biomass validation data are from the top 50m of the water column.

SC28: Line 246: References to supplemental figures are not in order

We thank the reviewer for pointing this out. We have corrected the order in the revised manuscript.

SC29: Line 250: What does the outcome look like with an attempt at a quantitative comparison? This would at least be useful to see in the supplemental material.

The study by Brun et al. (2015) is based on all available observations in the MAREDAT database (e.g. for *Phaeocystis*, see Vogt et al., 2012), but environmental niche centers and widths for each phytoplankton functional type are presented for the whole year only, as data coverage is generally low and skewed towards the summer season, especially in the Southern Ocean. Therefore, we believe that

constructing monthly niche centers based on the few available observations would not be meaningful at the moment. Since monthly niche centers are therefore not provided by Brun et al. (2015), we decided to compare the provided niche centers to December-March averages in ROMS-BEC and to thereby focus the quantitative comparison on the seasonal scale (see section 3.3 of the manuscript).

SC30: Line 263: This doesn't seem like an insurmountable problem; satellite chlorophyll data should be employed for model validation. Binning and temporal averaging are potential workarounds for the issues presented.

Data coverage of satellite-chlorophyll in the focus area of this study, i.e., the Southern Ocean south of 60°S, is low, already at monthly temporal resolution, but especially at daily resolution (see Fig. S4 in the supplement). As correctly pointed out by the reviewer, this problem can be surmounted by aggregating data in time. For this reason, we use satellite-derived chlorophyll concentrations to validate the simulated summer average chlorophyll field of ROMS-BEC (Fig. 1 of the manuscript). Yet, the assessment of phytoplankton bloom metrics requires a higher temporal frequency in the chlorophyll time series than monthly (ideally daily). As satellite data coverage is highest in the summer months (December-March), especially south of 60°S (Fig. S4 in the supplement), which coincides with peak phytoplankton biomass levels, we have decided to focus the discussion of bloom phenology on the bloom peak in this manuscript, instead of focusing on bloom initiation (typically in spring, see also our answer to SC32). Furthermore, regarding the seasonality of phytoplankton functional types, the cited literature discussing diatoms and *Phaeocystis* phenology often refers to the bloom peak of these two (see e.g. Peloquin & Smith 2007, Smith et al., 2011), thereby facilitating a direct comparison with our model output.

SC31: Line 263: if you are using timing from the literature, why not use bloom initiation from the literature as well?

Please see our answer to SC30.

SC32: Line 265: I recommend you also validate using bloom initiation as well.

Defining the bloom start as the day at which total chlorophyll levels first surpass 105% of the annual median chlorophyll concentrations (see Nissen et al., 2018), the total chlorophyll bloom south of 60°S starts in late September in ROMS-BEC (week 11, calendar starts in July), at least 2 months earlier than suggested by satellite-derived chlorophyll data (see e.g. Thomalla et al., 2011). This is consistent with the difference in the timing of the bloom peak discussed in the manuscript (section 3.2). In the revised manuscript, we have added a statement along these lines in section 3.2:

“Maximum total chlorophyll concentrations are simulated for the first half of December across latitudes in ROMS-BEC (solid blue line in Fig. 3a), and at high SO latitudes south of 60° S, total chlorophyll blooms start already in late September in the model (not shown). Thereby, the model-derived timing of total chlorophyll bloom start and peak is 2-3 and 1-2 months earlier, respectively, than satellite-derived estimates (for bloom peak, see black line in Fig. 3a, for bloom start, see e.g. Thomalla et al., 2011).”

SC33: Line 314: Could the overestimate have to do with modeled Fe:Chl ratios?

The recent study by Strzepek et al. (2019) suggests that Southern Ocean phytoplankton have higher photosynthetic rates at low iron, light, and temperature than temperate phytoplankton, suggesting that the formulations describing photoacclimation used here are possibly not applicable globally (see Geider et al., 1998) and should be reassessed in ROMS-BEC in future work. Yet, the overestimation is also seen in the carbon biomass distributions (see Fig. 1 & S5 in the manuscript), suggesting that factors describing the carbon uptake and/or loss are dominantly driving the high biomass bias. Please also see our answer to GC34.

SC34: Line 315: Please state the reason why Chl was overestimated in Nissen et al., 2018

Biases in simulated chlorophyll levels in ocean biogeochemistry models can be caused by a bias either in physics (temperature, mixed layer depth, thus impacting light availability) or in biology (growth or loss rates). Generally, in ROMS-BEC, temperature is biased high and the mixed layer is biased shallow, i.e., light availability is biased high, both favoring the accumulation in phytoplankton

biomass (Nissen et al., 2018). In Nissen et al. (2018), we have tested the effect of the biases in the physical fields by correcting the temperature and light field only in the BEC-subroutine (i.e., not affecting ocean dynamics). In conclusion, the simulated biases in temperature and light availability are not large enough to explain the simulated bias in chlorophyll concentration (~80-90% remained unexplained, see Nissen et al., 2018).

Hence, biological factors must be the reason for the bias. While biases in the chosen maximum growth rates of phytoplankton functional groups certainly contribute to the simulated chlorophyll bias at high SO latitudes (see e.g. Fig. A1 of the manuscript for the positive bias in the temperature-limited growth rate of diatoms at low temperatures compared to available laboratory data), correcting this unavoidably leads to a negative chlorophyll bias at subantarctic latitudes in the model, demonstrating the difficulty of simulating the whole diatom community with a single model functional type (see also discussion in Losa et al., 2019). The study by Le Quéré et al. (2016) demonstrates how adding additional complexity in the zooplankton compartment can reduce high-latitude chlorophyll biases by directly affecting total grazing rates on phytoplankton and the coupling of phytoplankton and zooplankton in the model.

Since ROMS-BEC currently only includes a single zooplankton functional type and given that we have tested the impact of all other potential factors causing the simulated bias in total chlorophyll levels at high SO latitudes in ROMS-BEC, this is the most likely reason for the positive chlorophyll bias at high latitudes, which yet needs to be tested in our model.

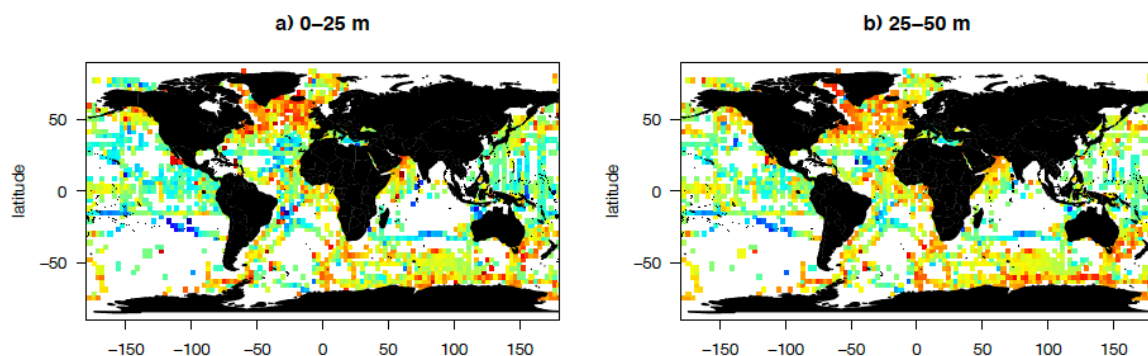
We kindly refer the reviewer to L. 320-323 in the manuscript, where we write:

“[...] the bias is likely due to a combination of underestimated high-latitude chlorophyll concentrations in satellite-derived products (Johnson et al., 2013) and the missing complexity in the zooplankton compartment in ROMS-BEC, as biases in the simulated physical fields (temperature, light) have been shown to only explain a minor fraction of the simulated high-latitude biomass overestimation (Nissen et al., 2018).”

SC35: Figure 1: The model is not capturing spatial variability in chlorophyll concentration- if it's truly due to a latitudinal bias in the ocean color product, please validate against data from shipboard CTDS. As explained in more detail in our answer to SC34 above, missing complexity in the zooplankton compartment is currently our leading hypothesis for causing the positive chlorophyll bias at high SO latitudes in ROMS-BEC. While Johnsen et al. (2013) show that at chlorophyll concentrations $>2\text{mg chl m}^{-3}$, their satellite-derived chlorophyll fields are typically 20-30% lower than in-situ chlorophyll concentrations (based on HPLC data), this underestimation is, however, not enough to fully account for the positive bias simulated by ROMS-BEC. Please see also our answer to SC 36 below.

SC36: Line 320: How does modeled Chl compare to measurements from CTDs, gliders, BGC Argo floats, etc. from the region? Then you can determine if it's a satellite underestimate issue.

Fluorescence-based chlorophyll observations (ship-based, floats etc.) reveal concentrations of up to 10 mg chl m^{-3} in the high-latitude SO (see Fig. 6 below), in agreement with the total chlorophyll distribution simulated by ROMS-BEC (Fig. 1 of the manuscript). However, while acknowledging the data scarcity in the in situ data (see Fig. 6 below), the very high chlorophyll concentrations ($>2\text{ mg chl m}^{-3}$) appear to be too wide-spread in ROMS-BEC when comparing to Fig. 6 below, which also shows areas with concentrations $<2\text{ mg chl m}^{-3}$ at latitudes $>60^\circ\text{S}$.



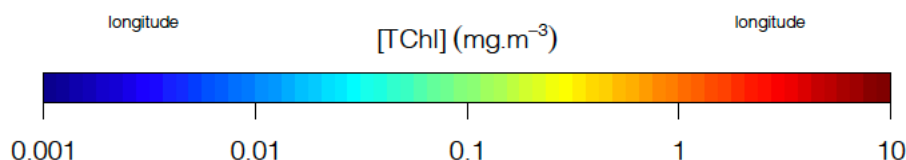


Fig. 6: Median total chlorophyll a concentration from fluorescence-based chlorophyll observations (ship-based, floats etc.; mg chl m⁻³) scaled to a 3° spatial resolution for a) 0-25m and b) 25-50m (Sauzède et al., 2015). Data are from all months, but data availability is skewed to the summer months (see Sauzède et al., 2015).

SC37: Line 324: “distinct” instead of “distinctly different”
 Changed as suggested.

SC38: Table 3: Please include confidence intervals on ROMS-BEC values
 Please see our answer to GC1 for details. We revised Table 3 as follows:

Table 3. Comparison of ROMS-BEC based phytoplankton biomass, production, and export estimates with available observations (given in parentheses). Data sources are given below the Table. The reported uncertainty of the contribution of the PFTs to the simulated integrated NPP corresponds to the area-weighted spatial variability of each PFT’s contribution to annual NPP (1 σ in space).

		ROMS-BEC (Data)	
		30-90° S	60-90° S
Surface chlorophyll biomass	total, annual mean [Gg chl]	40.8 (34.5 ^a)	17.1 (9.5 ^a)
Diatom carbon biomass	0-200m, annual mean [Pg C]	0.059 (global ^b : 0.10-0.94)	0.015
<i>Phaeocystis</i> carbon biomass	0-200m, annual mean [Pg C]	0.019 (global ^b : 0.11-0.71)	0.010
Coccolithophore carbon biomass	0-200m, annual mean [Pg C]	0.012 (global ^b : 0.001-0.03)	0.001
NPP	Pg C yr ⁻¹	17.2 (12.1-12.5 ^c)	3.0 (0.68-1.7 ^c)
	Diatoms [%]	52.0 (\pm 26.2)	49.1 (\pm 19.9)
	<i>Phaeocystis</i> [%]	15.3 (\pm 24.5)	45.8 (\pm 20.7)
	Coccolithophores [%]	14.6 (\pm 15.3)	0.7 (\pm 1.0)
	SP [%]	17.2 (\pm 16.1)	4.5 (\pm 1.9)
POC export at 100m	Pg C yr ⁻¹	3.1 (2.3-2.96 ^d)	0.62 (0.21-0.24 ^d)

^a Monthly climatology from MODIS Aqua (2002-2016, NASA-OBPG, 2014a), SO algorithm (Johnson et al., 2013)

^b The reported estimates from the MAREDAT data base in Buitenhuis et al. (2013) are global estimates of phytoplankton biomass.

^c Monthly climatology from MODIS Aqua VGPM (2002-2016, Behrenfeld and Falkowski, 1997; O’Malley, last access: 16 May 2016), NPP climatology from Buitenhuis et al. (2013, 2002-2016)

^d Monthly output from a biogeochemical inverse model (Schlitzer, 2004) and a data-assimilated model (DeVries and Weber, 2017).

SC39: Table 3: Why do you use a 100 m depth horizon for export? The 0.1% light depth horizon is more biogeochemically relevant (Buesseler et al., 2020)

We thank the reviewer for this comment. Unsurprisingly, the simulated POC export between 30-90°S and 60-90°S are lower when using the depth at which PAR corresponds to 0.1% of the incoming PAR at the surface (1.9 and 0.4 Pg C yr⁻¹, respectively, based on monthly averages) than when using a fixed depth of 100 m (3.1 and 0.62 Pg C yr⁻¹), as the former is often at depths greater than 100 m in the focus area of this study (at around 110-120 m, see Buesseler et al., 2020). Yet, we note that our estimates of the contribution of diatoms and *Phaeocystis* to POC export is largely unaffected by this difference, as virtually all POC in ROMS-BEC is produced above 100 m (not shown) and as the model currently only includes one class of POC, meaning that the remineralization of POC with depth is identical for POC originating from diatoms and *Phaeocystis* and thereby conserving the contribution of different functional types to POC production with depth. Further, we decided to report the export fluxes of POC at 100 m because this is still the norm in the field of biogeochemical modeling (see e.g. Bopp et al., 2013, Laufkötter et al., 2016)

SC40: Line 338: It would increase model confidence to include whether coccolithophore biomass corresponds to positioning of the great calcite belt.

We thank the reviewer for this comment. Indeed, the distribution of coccolithophore biomass in ROMS-BEC agrees well with the location of the “Great Calcite Belt” at subantarctic latitudes (Balch et al., 2011; Nissen et al., 2018). We have added this information in the revised version of the manuscript:

“In contrast to both *Phaeocystis* and diatoms, the simulated biomass levels of coccolithophores are highest in the subantarctic (highest concentrations of 3 mmol C m⁻³ on the Patagonian Shelf, Fig. 1e & S3d). Overall, their simulated SO biogeography agrees well with the position of the "Great Calcite Belt" (Balch et al., 2011, 2016) and remains largely unchanged compared to the 4-PFT setup (Nissen et al., 2018).”

SC41: Line 342: Please include standard deviations on these percentages.

Following our answer to GC1, we have included the spatial variability of each PFT’s relative contribution to the seasonally averaged total chlorophyll levels in the revised manuscript, expressed as one standard deviation within the respective subarea. The sentence now reads:

“Averaged over 30-90°S (60-90°S), the simulated relative contributions of *Phaeocystis*, diatoms, and coccolithophores to total chlorophyll in summer are 20±28% (33±34%; subarea mean as shown in Fig. 2b & c ±1σ in space), 68±33% (64±33%), and 5±17% (<1±2%), respectively, in good agreement with the CHEMTAX climatology (28% (27%), 46% (48%), and 3% (1%), respectively).”

SC42: Figure 2: Please use box-and-whisker plots instead of pie charts to display categorical data and the associated error.

In the revised manuscript, we have reported the standard deviation as an estimate of the spatial variability of the contribution of the PFTs to seasonally averaged chlorophyll (see SC41 above & SC43 below). Given that the focus of the manuscript is on the simulated average community composition in key areas, we have decided to keep the Figure as is.

SC43: Line 347: Again, please include error on your reported percentages.

We have adapted the respective sentence to now include a quantification of the spatial variability (see also GC1 and S41 above):

“The model overestimates the contribution of *Phaeocystis* in fall (39±14% as compared to 24% in CHEMTAX) and spring (51±22% as compared to 28%) between 60-90° S and in the Ross Sea, respectively (Fig. 2c-d), but the limited number of data points available in the CHEMTAX climatology in this area and the uncertainty in the attribution of pigments in CHEMTAX to the *Phaeocystis* PFT in ROMS-BEC have to be noted (see section 2.3.1).”

SC44: Line 361: “agrees” instead of “suggests”

Changed as suggested in the revised version of the manuscript

SC45: Line 370: Please also include a comparison to bloom initiation.

Please see our comment to SC32 above.

SC46: Line 374: This doesn’t seem right. *Phaeocystis* are often associated with bloom peaks in coastal polynyas.

We thank the reviewer for this valuable comment and have corrected the text to reflect this imprecision. In fact, analyzing the model output in more detail revealed that our statement only holds for the broad spatial averages presented in Figure 2 & 3. In fact, when looking at the contribution of *Phaeocystis* to total phytoplankton chlorophyll biomass at the day of the total chlorophyll bloom peak in ROMS-BEC, we see that besides in parts of the open ocean, *Phaeocystis* dominate many coastal regions at bloom peak, e.g. in the Ross Sea and in the Amundsen polynya (see Fig. 7 below), in agreement with observations (see e.g. Yager et al., 2016). The respective sentence in the revised manuscript now reads:

”As diatoms dominate the phytoplankton community at peak total chlorophyll concentrations for all latitudinal averages in the model domain (compare their bloom timing in Fig. 3c to Fig. 3a and to the simulated community composition in Fig. 2b-d, but note that *Phaeocystis* often dominate in coastal areas, not shown), the mismatch in timing is likely related to the representation of this PFT in the model, and is possibly at least partly caused by their comparatively high growth rates at low temperatures (see Fig. A1a).”

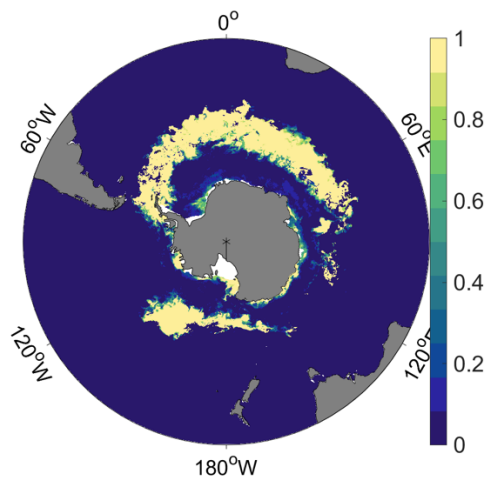


Fig. 7: Relative contribution of *Phaeocystis* to total chlorophyll at the day of the annually maximum chlorophyll concentration in the *Baseline* setup of ROMS-BEC.

SC47: Figure 3: Why don't *Phaeocystis* concentrations reach values much higher than 3 $\mu\text{g/L}$? Much higher concentrations have been observed.

Figure 3b of the manuscript shows the simulated zonally averaged daily surface chlorophyll concentrations of *Phaeocystis*. When plotting the annual maximum of daily averaged *Phaeocystis* chlorophyll concentrations at each grid cell in the *Baseline* setup of ROMS-BEC, the simulated concentrations exceed 10 mg chl m^{-3} locally (especially in coastal areas, see Figure 8 below), thus significantly higher than the zonal average suggests and in agreement with observed *Phaeocystis* chlorophyll concentrations. We have added this information to section 3.2 of the revised manuscript:

”In contrast to diatoms, maximum zonally averaged chlorophyll concentrations of *Phaeocystis* are simulated for late November or early December across most latitudes in the model (only around 70°S a peak in late January is simulated, Fig. 3b; note that locally, maximum *Phaeocystis* chlorophyll concentrations exceed 10 mg chl m^{-3} , not shown here).”

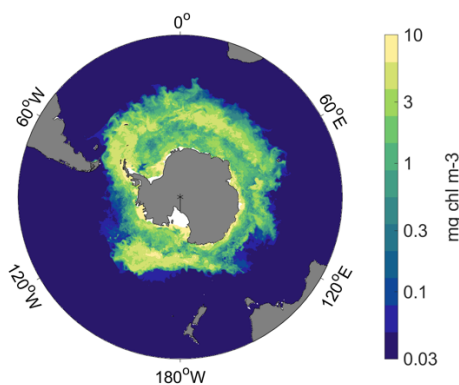


Fig. 8: Annual maximum of daily averaged *Phaeocystis* chlorophyll concentration [mg chl m^{-3}] in the *Baseline* setup of ROMS-BEC.

SC48: Line 382: How specifically does the diatom parameterization drive this bias?

In general, total chlorophyll concentrations peak too early in ROMS-BEC, especially at high latitudes. As the phytoplankton community is mainly composed of diatoms and *Phaeocystis* in this area, biases in the chlorophyll seasonality of either of the two could contribute to this bias. Since the chlorophyll seasonality of *Phaeocystis* is in broad agreement with the reported seasonality of DMS concentrations in the high SO latitudes, we have concluded that diatoms mainly control this bias in total chlorophyll concentrations. Any too quick accumulation of diatom biomass (and hence chlorophyll) early in the

season is caused by an imbalance of their growth and loss rates at those times. In particular, if their growth rates were biased high in the model (e.g. due to a too high maximum growth rate in this area, see Fig. A1 of the manuscript), whereas e.g. zooplankton grazing were lagging behind and were biased low, this would result in a decoupling of diatoms and zooplankton, allowing for the build-up of high diatom biomass levels early in the growth season.

We have adapted the manuscript as follows:

“This further corroborates the hypothesis that the bias in the timing of maximum total chlorophyll levels in ROMS-BEC is likely caused by how diatoms are parameterized in the model (see e.g. the rather high temperature-limited growth rate of diatoms at low temperatures compared to available laboratory data, see Fig. A1). “

SC49: Line 405: Wouldn't the lower cell density associated with deeper MLD bias this assessment? It is known that *Phaeocystis* thrive under lower light conditions than diatoms, so this doesn't seem right. We agree with the reviewer, that based on available laboratory and in situ studies, it is known that *Phaeocystis* colonies cope better with low light environments than diatoms (see introduction and method section of the manuscript). However, we are not sure we understand how this relates to the topic discussed in this part of the manuscript. Here, assuming that *Phaeocystis surface* chlorophyll concentrations are most representative for air-sea fluxes of DMSP & DMS, we compare the timing of the simulated maximum *surface* chlorophyll concentrations of *Phaeocystis* in ROMS-BEC to the reported timing of peak DMSP & DMS concentrations in the atmosphere. Since we find a good agreement between the two, we conclude that biases in *Phaeocystis* phenology are possibly small and that the bias in total phytoplankton chlorophyll phenology must be driven by biases in the seasonal evolution of diatom chlorophyll.

SC50: Line 408: It is important to note here that much of the SO is light limited, in particular the canyons near the WAP (Carvalho et al., 2016).

We fully agree with the reviewer and apologize for any confusion. In L. 408 of the manuscript, we refer to iron as being the most limiting amongst all *nutrients* for phytoplankton growth in ROMS-BEC (Fig. S1). In the revised version of the manuscript, we have changed the respective sentence to make this clearer, and it now reads:

“With regard to iron, the two PFTs do not occupy distinct ecological niches in ROMS-BEC (niche centers at $0.32 \mu\text{mol m}^{-3}$ for both PFTs, see Fig. S9). Yet, *as all simulated phytoplankton growth is most limited by iron availability in the high-latitude SO compared to the availability of other nutrients* (Fig. S1), this suggests that the spatio-temporal averaging applied for the niche analysis here potentially precludes the assessment of the role of iron in the competition between *Phaeocystis* and diatoms, especially on a sub-seasonal scale.”

SC51: Line 414: If this analysis is not useful for the scientific questions proposed, it should be either removed or moved to the supplemental information.

We thank the reviewer for this comment and apologize for the confusion. The analysis of environmental niches of phytoplankton in ROMS-BEC and the comparison of these niches with those reported for individual phytoplankton taxa. Here, in agreement with observations, our analysis reveals a separation of diatoms and *Phaeocystis* in NO₃ and temperature space. However, maybe surprisingly, this analysis does not reveal any difference in the niche regarding MLPAR and iron, likely due to model biases (MLPAR) and the temporal averaging (iron; due to observational data scarcity, see also SC29 above). As this analysis serves as a link between the evaluation of the simulated distributions of diatoms and *Phaeocystis* and the analysis of the factors controlling these distributions, we have decided to keep it in the main text.

SC52: Line 422: If this is the case, why do *Phaeocystis* never dominate at the bloom peak in the model?

We thank the reviewer for this comment. In fact, the analysis of the bottom-up factors only partly informs about the realized biomass distributions, as these are a result of bottom-up and top-down factors at any given time and location (see Fig. 5 and Lines 446ff of the manuscript). Thus, if it was

only bottom-up factors controlling which phytoplankton type was the dominant one, *Phaeocystis* should outcompete diatoms over much of the Southern Ocean in ROMS-BEC. Therefore, in our model, bottom-up factors only *promote the accumulation* of *Phaeocystis* biomass relative to that of diatoms, whereas top-down factors achieve the opposite. As a result, *Phaeocystis* only successfully outcompete diatoms in terms of their contribution to total biomass at certain locations and at certain times of the year (see Fig. 5i & j, but see also Fig. 7 above).

SC53: Figure 4: The temperature range covered here is very large- where are water column temperatures getting so hot in the model? This may be killing off the *Phaeocystis*. Figure 4 in the manuscript is shown for the area south of 40°S. As shown in the Figure 9 below, top 50m and DJFM average temperatures close to 40°S reach 20°C, in agreement with observed temperatures (Locarnini et al., 2013). We note, however, that the temperature between 60-90°S, where *Phaeocystis Antarctica* is a key player of the phytoplankton community, ranges from ~-2-8°C in the model (see red bars next to the temperature axes in Fig. 4 of the manuscript), resulting in zero growth of *Phaeocystis* north of ~60°S in ROMS-BEC (see temperature function in Fig. A1 of the manuscript), in agreement with laboratory studies (Buma et al., 1991) and observations (Schoemann et al., 2005).

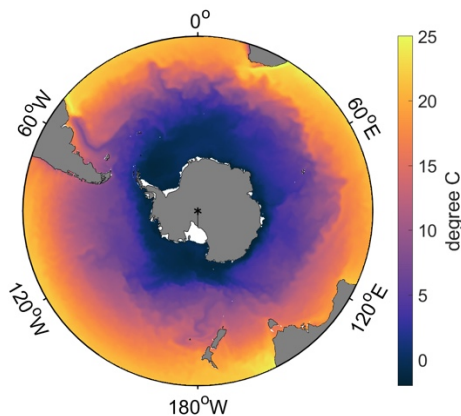


Fig. 9: Top 50 m and DJFM average temperature [°C] in ROMS-BEC (30-90°S).

SC54: Line 430: It would be useful to see how photoacclimation effects on the Fe:C ratio would affect the outcome.

Please see our answer to SC26 and GC1. As stated there, photoacclimation only impacts the Fe:C ratio of phytoplankton through its impact on the light limitation factor and hence photosynthetic carbon uptake. Thereby, the effects of photoacclimation are included in the assessment of the differences in the light limitation factor in Fig. 5 of the manuscript.

SC55: Figure 5: Iron is green here, not blue.

In fact, it is shown in blue.

SC56: Line 442: It would also be good to see Pine Island Polynya and the Amundsen Sea Polynya to compare with the Ross Sea.

Overall, the seasonal evolution of the contribution of each PFT to total phytoplankton biomass concentrations in the Amundsen Sea (averaged over the whole coastal area south of 71°S and between 240-260°W) is very similar to those in the Ross Sea, with *Phaeocystis* generally being more important for total phytoplankton biomass in the Amundsen Sea than in the Ross Sea (compare Fig. 2 in the manuscript to Fig. 10a below). Furthermore, the factors controlling the biomass distributions in the Amundsen Sea are overall similar to those in the Ross Sea, with advantages in light limitation of *Phaeocystis* relative to diatoms being larger than in the Ross Sea (compare Fig. 5 in the manuscript to Fig. 10b below), explaining the higher relative importance of *Phaeocystis* in the Amundsen Sea.

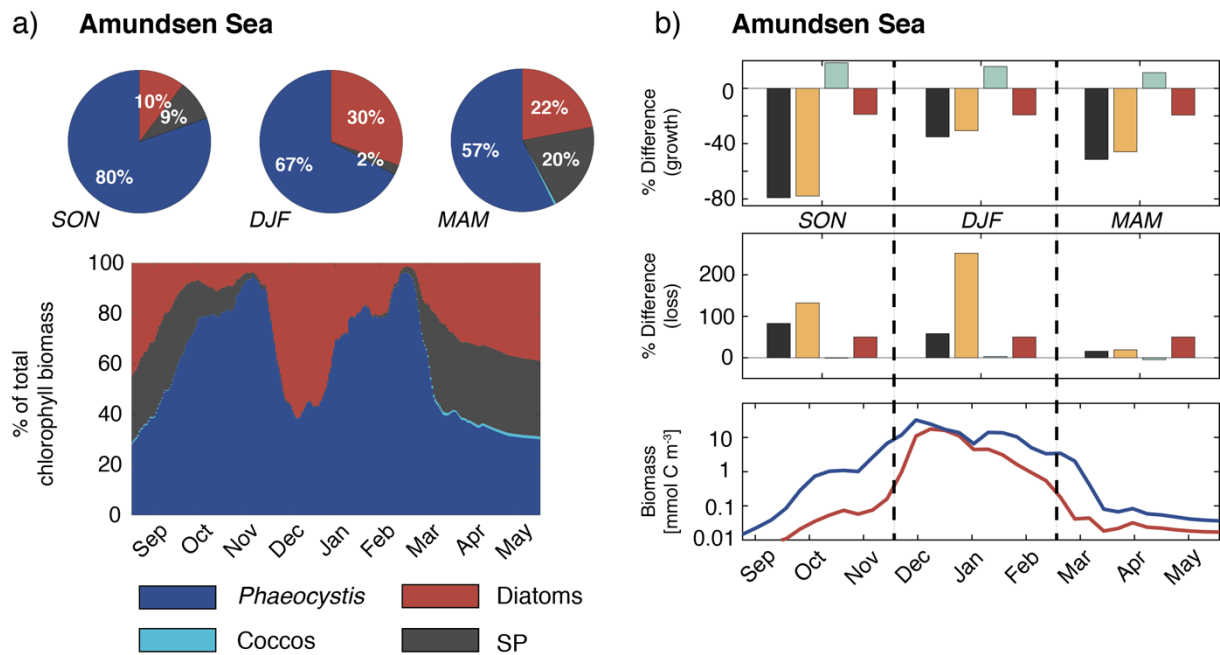


Fig. 10: Same as Fig. 2 & 5 in the manuscript, but averaged over the Amundsen Sea.

SC57: Line 445: In the model they should be considered, but what is your confidence in the model when it cannot reproduce a Chl max in *Phaeocystis*?

As shown in Fig. 8 above, the model simulates maximum daily chlorophyll concentrations of >10 mg chl m^{-3} locally for *Phaeocystis*, in agreement with observations, which are not visible due to the broad spatial averaging in Fig. 3 of the manuscript. We are therefore confident in the simulated interplay of bottom-up and top-down factors in controlling the high-latitude competition between diatoms and *Phaeocystis* in our model. We also refer the reviewer to our answer to SC47 & SC52.

SC58: Line 457: It is necessary to know how sensitive the model is to the range of these parameters to determine how likely this result is to mirror reality.

As shown in Fig. A2 of the submitted manuscript, the simulated high-latitude chlorophyll fields of *Phaeocystis* and diatoms are highly sensitive to the chosen model parameters for *Phaeocystis* biomass loss rates (experiments GRAZING, AGGREGATION, and MORTALITY). The magnitude of change in the chlorophyll fields is largest when neglecting parameter differences between *Phaeocystis* and diatoms for aggregation (followed in decreasing order by mortality and grazing), which is in agreement with the analysis shown in Fig. 5 and discussed in section 3.3 of the manuscript.

Yet, the additionally performed parameter sensitivity experiments in this round of revisions revealed a different picture regarding the ranking of the experiments, with the largest simulated change in *Phaeocystis* and diatom chlorophyll concentrations when varying the maximum zooplankton grazing rate on *Phaeocystis* by $\pm 50\%$, followed by the response when varying the mortality and aggregation rates (see GC1 and supplementary material of the revised manuscript). However, we note that the relative change in the model parameters was different for the experiments shown in Fig. A2, explaining the differences in the simulated response and making the two sets of experiments not directly comparable.

Given that the model parameters in the *Baseline* simulation of ROMS-BEC are chosen to best reflect the observed high-latitude phytoplankton community structure throughout the year, we are more confident in the qualitative dynamics simulated by the model than in the quantitative results, i.e. the relative importance of bottom-up and top-down factors, due to the large parameter uncertainty demonstrated in our sensitivity experiments (and with uncertainty resulting from interactions of multiple parameters not having been assessed here) and the scarcity of the observational data used to constrain the model.

SC59: Line 467: It would be great to include some necessary information in this manuscript about the way iron is cycled in ROMS-BEC. How are organic ligands parameterized? How about scavenging processes? Is the relief from iron limitation in the Ross Sea driven by wind-driven sediment resuspension (McGillicuddy et al., 2015)?

Besides uptake by phytoplankton (please see also our answer to GC1 for details on the model parametrizations of the Fe:C uptake ratios of phytoplankton in ROMS-BEC), particle scavenging is the second loss pathway of dissolved iron (Fe). Scavenging rates of Fe are a function of surrounding Fe concentrations (to crudely account for the effect of iron-binding ligands, which are not explicitly included in BEC) and available sinking particles (particulate organic carbon, as well as the ballast materials calcite, opal, and dust). Overall, the higher the concentrations of Fe and particles, the higher is the loss of Fe through scavenging. For more details, the reviewer is kindly referred to Moore & Braucher 2008 and Lima et al. (2014), which thoroughly describe and discuss the cycling of iron and treatment of particles in BEC.

In the version of ROMS-BEC used here, sediments (and hence wind/circulation-driven sediment resuspension) are not explicitly modeled, and all particles are immediately buried, i.e., lost from the system, or remineralized when reaching the ocean floor. In the model, fluxes of iron from the sediments are supplied to the bottom model layer and parametrized as a function of the particle flux to the sediment and bottom water oxygen concentrations following Dale et al. (2015). As a consequence, even though sediment resuspension is not explicitly modeled, wind-driven mixing of the water column is a key process in supplying the upper water column with dissolved iron released from the sediments. This is especially true at high SO latitudes, where atmospheric deposition is low (Mahowald et al., 2009). Here, any seasonal change in the supply of iron to the mixed layer is the result of entrainment of higher iron concentrations from below, which result from the remineralization of sinking particulate organic matter.

SC60: Line 475: Please include error bars on these estimates. Propagate the error using the sensitivity analyses, and the standard deviation across the domain.

Following our answer to GC1, we have included the spatial variability of each PFT's relative contribution to the NPP and POC export in the revised manuscript, expressed as one standard deviation within the respective subarea. The sentence now reads:

“*Phaeocystis* is an important member of the SO phytoplankton community in our model, particularly south of 60°S, where it contributes $46\pm 21\%$ and $40\pm 20\%$ to total annual NPP and POC formation, respectively (Table 3 & Fig. 6). Even when considering the entire region south of 30°S, the contribution of *Phaeocystis* to NPP ($15\pm 24\%$) and POC production ($16\pm 22\%$) is sizeable.”

SC61: Figure 6: Please report uncertainty on the numbers in this figure

A thorough assessment of the uncertainty of all fluxes presented in Fig. 6 to describe the routing of carbon through the phytoplankton and zooplankton compartments in ROMS-BEC would be computationally expensive and is beyond the scope of this study. Please see also our answer to GC1.

SC62: Line 492: It would be helpful to see a breakdown of these fluxes in comparison to other modeled and observed export in the SO.

We appreciate this comment. While there is a number of observational studies assessing individual pathways of carbon through the system (see e.g. reviews for diatoms and *Phaeocystis* by Sarthou et al., 2005 and Reigstad et al., 2007, respectively), there is, to the best of our knowledge, no observation-based study available which holistically quantifies the relative importance of aggregation, grazing, and non-grazing mortality (e.g. viral lysis) for the biomass losses of different PFTs in the Southern Ocean. Yet, assumptions made in ROMS-BEC when choosing model parameters are motivated by available in situ or laboratory based studies which focused on individual aspects of the routing of carbon through the system (see method section of the manuscript). With regards to biogeochemical models, Laufkötter et al. (2016) present a detailed comparison of the routing of carbon through the high-latitude ecosystem in state-of-the-art ocean biogeochemistry models (see Figure 11 below). In summary, the importance of different pathways, namely grazing, aggregation, or mortality, for POC production at high latitudes varies widely, with some models suggesting diatom aggregation to be the most important pathway (REcoM and BEC), whereas others point to the big importance of zooplankton

mortality. Overall, acknowledging that all of these models only include two phytoplankton functional types, making a direct quantitative comparison with the results in ROMS-BEC difficult, this points to the uncertainty surrounding the representation of particle treatment in state-of-the-art ocean biogeochemistry models and highlights the need for more observational/laboratory studies to guide modelers in improving these parametrizations. In this context, on-going projects like EXPORTS (<https://oceanexports.org/about.html>) are an important contribution in the field, shedding light on how carbon is routed through the upper ocean.

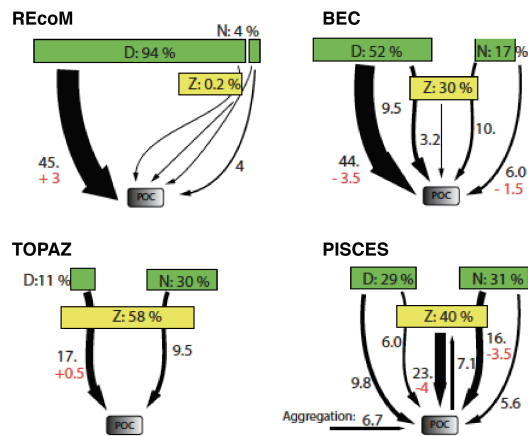


Fig. 11: Routing of carbon through the ecosystem in the high latitudes south/north of 60°S/N in REcoM, BEC (CESM version), TOPAZ, and PISCES. Adapted from Laufkötter et al. (2016). The boxes denote the relative contribution of each functional type to total biomass (green) and particle production (yellow), respectively. The arrows show, from left to right, diatom aggregation, diatom grazing by zooplankton, zooplankton mortality, nanophytoplankton grazing by zooplankton, and nanophytoplankton aggregation.

SC63: Figure 7: Since there is a wide potential range of aggregation rates, how would this figure change when testing using that range?

As expected, changing the quadratic loss rate in aggregation in ROMS-BEC leads to a shift in the relative importance of grazing and aggregation for total phytoplankton biomass loss. Based on size assumptions, generally higher aggregation rates are assumed for *Phaeocystis* colonies than for diatoms in ROMS-BEC (see method section of the submitted manuscript). In fact, the difference in the quadratic loss rate parameter between *Phaeocystis* and diatoms (see Table 1 of the manuscript) is one of the reasons why the model simulates the differences in aggregation vs grazing for these two phytoplankton types (Fig. 7 of the manuscript). However, we note that in ROMS-BEC, the simulated aggregation rate for a given phytoplankton PFT at any point in time is additionally a function of the quadratic biomass at the given location (see model equations in the appendix of the manuscript), meaning that ROMS-BEC simulates substantial spatio-temporal variability in phytoplankton biomass aggregation rates as a direct result of the simulated spatio-temporal variability in carbon biomass concentrations.

SC64: Line 497: Why is the peak in *Phaeocystis* so late? This is much later than observations.

We thank the reviewer for this comment. We point out that in section 3.4 of the manuscript, we only describe the carbon cycling for very broad spatial averages (30-90°S and 60-90°S). Admittedly, this makes it difficult to compare the simulated timing of maximum POC production of *Phaeocystis* to available observations taken at a more regional scale. In fact, the timing of peak *Phaeocystis* POC production and its peak contribution to total POC production is earlier in the Ross Sea (~November/December, see Fig. 12 below) than between 60-90°S, thus reconciling our model results with the observations. As a response to a comment by reviewer #3, the carbon cycling figures for the Ross Sea (Fig. 12 below) were added to the supplementary material of the revised version of the manuscript.

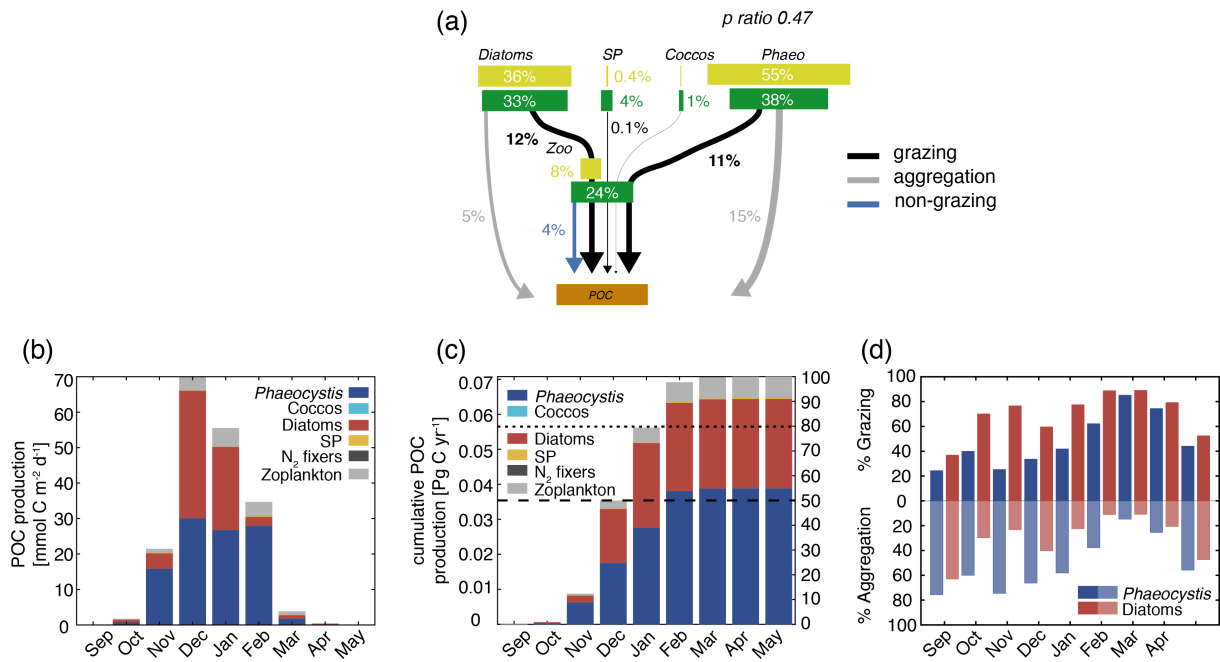


Fig. 12: Carbon cycling in the Ross Sea: The upper panel corresponds to Fig. 6 in the main text, the lower panels shows the quantities from Fig. 7 for the Ross Sea.

SC65: Line 525: I find this result hard to believe when the model is not taking into account changing cellular iron quotas as iron limitation shifts.

The Fe:C uptake ratio of the different phytoplankton PFTs in ROMS-BEC varies as a function of the Fe concentrations (and thereby also the cellular iron quotas). Please see our answer to GC1 for more details.

SC66: Line 539: More than K_{Fe} needs to be constrained with environmental data. Alpha, Fe:C, P_{max} are all also sensitive to light/iron limitation conditions.

Agreed. We have rephrased the sentence as follows:

“Thus, in order to include light-iron interactions in future modeling efforts with *Phaeocystis* and to assess their impact on the competition of *Phaeocystis* with diatoms throughout the SO, additional measurements are needed for how k_{Fe}, but also e.g. αPI and the Fe:C uptake ratio of phytoplankton vary as a function of the surrounding light level.”

SC67: Line 546: There is agreement in some conditions, but elsewhere there seems to be large discrepancies. Additionally, surface chlorophyll variability is not represented well by the model.

While the simulated distribution of chlorophyll concentrations in ROMS-BEC is admittedly far from in perfect agreement with observation, we point the reviewer to our answers of e.g. SC 46 & SC 47, demonstrating that important features of the variability in *Phaeocystis* chlorophyll concentrations are simulated by the model. Accordingly, we have rephrased the sentence as follows:

„Furthermore, the simulated spatio-temporal variability of the high-latitude phytoplankton community structure is in agreement with that suggested by available pigment data (Fig. 2).“

SC68: Line 555: It would be useful to conduct more sensitivity experiments while varying the aggregation parameter alongside other model parameters, in light of this finding.

Please see our comment to GC1 above.

SC69: Line 565: This paragraph seems somewhat redundant with the above paragraph. Please restructure.

We have combined the two paragraphs into a single, slightly modified paragraph in the revised manuscript. It reads:

Loss processes, such as aggregation and grazing, clearly matter for the competitive advantage of one PFT over another, but these loss processes are generally not well quantified and often not studied with sufficient detail. For example, while the modeling study by Le Quéré et al. (2016) demonstrates the importance of such top-down control for total SO phytoplankton biomass concentrations, an analysis of the impact on phytoplankton community structure is yet to be done. In fact, in the literature, only few studies discuss the role of top-down factors for the relative importance of *Phaeocystis* and diatoms in the high-latitude SO (Granéli et al., 1993; van Hilst and Smith, 2002). Consequently, very little quantitative information exists to constrain model parameters (see section 2.1) or to validate the simulated non-grazing mortality, grazing, or aggregation loss rates of *Phaeocystis* and diatoms over time. In agreement with our results, aggregation has been suggested to be an important process facilitating high POC export when *Phaeocystis* biomass is high (Asper and Smith, 1999; Ducklow et al., 2015; Asper and Smith, 2019), but to what extent this process significantly contributes to the observed relative importance of *Phaeocystis* and diatoms throughout the year in the high-latitude SO remains largely unknown. Certainly, the simulated aggregation rates in the model and their impact on spatio-temporal distributions of PFT biomass concentrations and rates of NPP are associated with substantial uncertainty due to the immediate conversion of biomass to sinking detritus in the model, the equal treatment of POC originating from all PFTs, the neglect of disaggregation, and due to the calculation of aggregation rates based on the biomass concentrations of individual PFTs rather than all PFTs or even particles combined (see e.g. Turner, 2015). Given that the simulated biomass distributions in ROMS-BEC are most sensitive to differences in parameters describing non-grazing mortality (e.g. viral lysis) and aggregation (Fig. A2 & S11), any changes in these loss processes will significantly impact the relative abundance of *Phaeocystis* and diatoms in the SO. Additionally, as discussed in Nissen et al. (2018), the lack of multiple zooplankton groups in the SO model (Le Quéré et al., 2016) and the parametrization of the single zooplankton grazer using fixed prey preferences and separate grazing on each prey using a Holling Type II function (Holling, 1959), which thus precludes a saturation of feeding at high total phytoplankton biomass, are major limitations of ROMS-BEC. To what extent accounting implicitly for grazing by higher trophic levels in the non-grazing mortality term makes up for not including more zooplankton PFTs remains unclear. Nevertheless, by changing the overall coupling between phytoplankton and zooplankton and through the distinct grazing preferences of the different zooplankton types, the addition of larger zooplankton grazers would likely change the simulated temporal evolution of *Phaeocystis* and diatom biomass in the model (Le Quéré et al., 2016). Therefore, the above mentioned uncertainties should be addressed by future in situ or laboratory measurements in order to better constrain the simulated biomass loss processes, as our findings suggest these to be necessary to explain the seasonal evolution of the relative importance of *Phaeocystis* and diatoms in the high-latitude SO.

SC70: Line 579: Please provide uncertainty on this percentage.

In agreement with our answer to GC1, we have added the spatial variability of the contribution of *Phaeocystis* to SO NPP in the revised manuscript. For the estimation of the contribution of SO *Phaeocystis* to global NPP we have used the simulated integrated NPP of *Phaeocystis* in ROMS-BEC, whose uncertainty is not straightforward to quantify and is beyond the scope of this study (see GC1). The respective part of the manuscript now reads:

“Based on our model results, *Phaeocystis* is a substantial contributor to global NPP and POC export. Comparing the integrated NPP and POC export between 30-90° S in ROMS-BEC with data-based estimates of global NPP and POC export suggests that SO *Phaeocystis* alone contribute about 5% to globally integrated NPP (58 ± 7 Pg C yr⁻¹, Buitenhuis et al., 2013), and about the same percentage to global POC export (9.1 ± 0.2 Pg C yr⁻¹, DeVries and Weber, 2017). Thereby, our simulated contribution of *Phaeocystis* to global NPP is higher than that found in the previous modeling study by Wang and Moore (2011), particularly at higher latitudes, where Wang and Moore (2011) diagnosed a contribution of 23% to NPP south of 60°S ($46 \pm 21\%$ in ROMS-BEC).”

SC71: Line 587: Please propagate this uncertainty into your NPP, POC, and export estimates. Please see our answer to GC1 above.

SC72: Line 590: Considering the discrepancies between the observations and the model, please include confidence intervals on your estimates. Please see our answer to GC1 above.

SC73: Line 608: Why can't you assess these effects? Assessing horizontal fluxes of model tracers should be relatively straightforward.

We completely agree with the reviewer in that the assessment of the simulated physical fluxes of the biogeochemical tracers would allow for a quantification of the spatial/temporal decoupling of POC production and export. However, particle sinking of e.g. POC is currently treated implicitly in ROMS-BEC, meaning that particles are instantaneously distributed in the vertical and remineralized following an exponential curve (Lima et al., 2014). Therefore, sinking particles are not laterally advected with physical fluxes in the version of ROMS-BEC used here, making it impossible to assess the decoupling between POC production and export. In the revised version of the manuscript, we have rephrased this part of the manuscript to better explain the implications of the implicit particle treatment. It now reads:

“In this regard, the simulated strong temporal coupling between POC fluxes and biomass distributions in ROMS-BEC is a direct result of the model formulations describing particle sinking (particles sink implicitly, i.e., they are not laterally advected, Lima et al., 2014).”

The implementation of an explicit treatment of sinking particles, which are then subject to lateral fluxes with ocean circulation, is on-going work in the research group at ETH Zürich, but goes beyond our study.

SC74: Line 616: How are you accounting for variability in mixed layer depth in the DMSP calculation?

In the calculation presented in the manuscript, we are not accounting for any variability in mixed layer depth at the moment, but instead use the approximated DMS production integrated over the top 10 m (calculated using a range of conversion efficiencies to get from the DMSP produced by *Phaeocystis* to DMS). Assuming that all of the DMS produced in this uppermost layer will quickly exchange with the atmosphere, we acknowledge that this is a very rough *upper* estimate. When integrating over greater depths, e.g. the mixed layer, our assumption will be less justified, as DMS produced at greater depths will at least partly be degraded before escaping to the atmosphere (see e.g. Stefels et al., 2007). However, as we are currently not explicitly modeling the cycling of DMS in ROMS-BEC, we have decided to only present the calculation for the uppermost ocean layer, where the assumption of quick exchange is most justified.

SC75: Line 640: These topics should be discussed in your methods. The rationale for excluding solitary *Phaeocystis* needs to be justified.

Please see our answers to comments SC15 & SC18 above.

SC76: Line 669: These non-Redfieldian dynamics should be straightforward to implement in the model, and would be an interesting sensitivity study.

We completely agree with the reviewer in that the assessment of non-Redfieldian stoichiometry of diatoms and *Phaeocystis* for the simulated Southern Ocean-wide nutrient distributions and export fluxes should be a key focus of the modeling community. However, unfortunately, we do not agree with the reviewer in the amount of work its implementation would involve. While the implementation of non-Redfieldian stoichiometry in phytoplankton nutrient uptake might seem rather easy (and is currently already done e.g. for the Fe:C uptake ratio, see GC1 above), it requires the implementation of several additional biogeochemical tracers to track the non-Redfieldian nutrient uptake stoichiometry not only through phytoplankton biomass, but also through all particle classes and zooplankton. As a result, this exercise certainly goes beyond a simple sensitivity experiment and unfortunately beyond the scope of this work.

SC77: Line 689: It may be worth testing a range of parameters to get a general sense of the sensitivity of export. I'd imagine this would be useful for many people to see

We agree with the reviewer that a thorough assessment of the sensitivity of the simulated carbon routing to the chosen model parameters would be interesting, but note that this analysis would be computationally expensive and is beyond the scope of this study. For this study, parameters were chosen to best fit the observed pattern and magnitude of export fluxes.

Cited literature

- Alvain, S., Moulin, C., Dandonneau, Y., & Loisel, H. (2008). Seasonal distribution and succession of dominant phytoplankton groups in the global ocean: A satellite view. *Global Biogeochemical Cycles*, 22(3), GB3001. <https://doi.org/10.1029/2007GB003154>
- Arrigo, K. R., van Dijken, G. L., Alderkamp, A., Erickson, Z. K., Lewis, K. M., Lowry, K. E., Joy-Warren, H. L., Middag, R., Nash-Arrigo, J. E., Selz, V., & van de Poll, W. (2017). Early Spring Phytoplankton Dynamics in the Western Antarctic Peninsula. *Journal of Geophysical Research: Oceans*, 122(12), 9350–9369. <https://doi.org/10.1002/2017JC013281>
- Balch, W. M., Drapeau, D. T., Bowler, B. C., Lyczkowski, E., Booth, E. S., & Alley, D. (2011). The contribution of coccolithophores to the optical and inorganic carbon budgets during the Southern Ocean Gas Exchange Experiment: New evidence in support of the “Great Calcite Belt” hypothesis. *Journal of Geophysical Research*, 116, C00F06. <https://doi.org/10.1029/2011JC006941>
- Buesseler, K. O., Boyd, P. W., Black, E. E., & Siegel, D. A. (2020). Metrics that matter for assessing the ocean biological carbon pump. *Proceedings of the National Academy of Sciences*, 117(18), 9679–9687. <https://doi.org/10.1073/pnas.1918114117>
- Bopp, L., Resplandy, L., Orr, J. C., Doney, S. C., Dunne, J. P., Gehlen, M., Halloran, P., Heinze, C., Ilyina, T., Séférian, R., Tjiputra, J., & Vichi, M. (2013). Multiple stressors of ocean ecosystems in the 21st century: projections with CMIP5 models. *Biogeosciences*, 10(10), 6225–6245. <https://doi.org/10.5194/bg-10-6225-2013>
- Boyd, P. W. (2019). Physiology and iron modulate diverse responses of diatoms to a warming Southern Ocean (supplement). *Nature Climate Change*, 9(2), 148–152. <https://doi.org/10.1038/s41558-018-0389-1>
- Buma, A. G. J., Bano, N., Veldhuis, M. J. W., & Kraay, G. W. (1991). Comparison of the pigmentation of two strains of the prymnesiophyte *Phaeocystis* sp. *Netherlands Journal of Sea Research*, 27(2), 173–182. [https://doi.org/10.1016/0077-7579\(91\)90010-X](https://doi.org/10.1016/0077-7579(91)90010-X)
- Carvalho, F., Kohut, J., Oliver, M. J., Sherrell, R. M., & Schofield, O. (2016). Mixing and phytoplankton dynamics in a submarine canyon in the West Antarctic Peninsula. *Journal of Geophysical Research: Oceans*, 121(7), 5069–5083. <https://doi.org/10.1002/2016JC011650>
- Dale, A. W., Nickelsen, L., Scholz, F., Hensen, C., Oschlies, A., & Wallmann, K. (2015). A revised global estimate of dissolved iron fluxes from marine sediments. *Global Biogeochemical Cycles*, 29(5), 691–707. <https://doi.org/10.1002/2014GB005017>
- DiTullio, G. R., Grebmeier, J. M., Arrigo, K. R., Lizotte, M. P., Robinson, D. H., Leventer, A., ... Dunbar, R. B. (2000). Rapid and early export of *Phaeocystis antarctica* blooms in the Ross Sea, Antarctica. *Nature*, 404(6778), 595–598. <https://doi.org/10.1038/35007061>
- Eppley, R. W. (1972). Temperature and phytoplankton growth in the sea. *Fishery Bulletin*, 70(4).
- Geider, R. J., MacIntyre, H. L., & Kana, T. M. (1998). A dynamic regulatory model of phytoplankton acclimation to light, nutrients, and temperature. *Limnology and Oceanography*, 43(4), 679–694. <https://doi.org/10.4319/lo.1998.43.4.0679>
- Green, S. E., & Sambrotto, R. N. (2006). Plankton community structure and export of C, N, P and Si in the Antarctic Circumpolar Current. *Deep Sea Research Part II: Topical Studies in Oceanography*, 53(5–7), 620–643. <https://doi.org/10.1016/j.jsr.2006.01.022>

- Johnson, R., Strutton, P. G., Wright, S. W., McMinin, A., & Meiners, K. M. (2013). Three improved satellite chlorophyll algorithms for the Southern Ocean. *Journal of Geophysical Research: Oceans*, *118*(7), 3694–3703. <https://doi.org/10.1002/jgrc.20270>
- Laufkötter, C., Vogt, M., Gruber, N., Aumont, O., Bopp, L., Doney, S. C., ... Völker, C. (2016). Projected decreases in future marine export production: the role of the carbon flux through the upper ocean ecosystem. *Biogeosciences*, *13*(13), 4023–4047. <https://doi.org/10.5194/bg-13-4023-2016>
- Lee, S., Hwang, J., Ducklow, H. W., Hahm, D., Lee, S. H., Kim, D., ... Shin, H. C. (2017). Evidence of minimal carbon sequestration in the productive Amundsen Sea polynya. *Geophysical Research Letters*, *44*(15), 7892–7899. <https://doi.org/10.1002/2017GL074646>
- Le Quéré, C., Harrison, S. P., Colin Prentice, I., Buitenhuis, E. T., Aumont, O., Bopp, L., ... Wolf-Gladrow, D. (2005). Ecosystem dynamics based on plankton functional types for global ocean biogeochemistry models. *Global Change Biology*, *11*, 2016–2040. <https://doi.org/10.1111/j.1365-2486.2005.1004.x>
- Lima, I. D., Lam, P. J., & Doney, S. C. (2014). Dynamics of particulate organic carbon flux in a global ocean model. *Biogeosciences*, *11*(4), 1177–1198. <https://doi.org/10.5194/bg-11-1177-2014>
- Locarnini, R. A., Mishonov, A. V., Antonov, J. I., Boyer, T. P., Garcia, H. E., Baranova, O. K., ... Seidov, D. (2013). *World Ocean Atlas 2013, Volume 1: Temperature* (Vol. 1). Retrieved from <http://www.nodc.noaa.gov/OC5/indprod.html>
- Losa, S. N., Dutkiewicz, S., Losch, M., Oelker, J., Soppa, M. A., Trimborn, S., Xi, H., and Bracher, A.: On modeling the Southern Ocean Phytoplankton Functional Types, *Biogeosciences Discussions*, <https://doi.org/10.5194/bg-2019-289>, 2019
- Mahowald, N. M., Engelstaedter, S., Luo, C., Sealy, A., Artaxo, P., Benitez-Nelson, C., Bonnet, S., Chen, Y., Chuang, P. Y., Cohen, D. D., Dulac, F., Herut, B., Johansen, A. M., Kubilay, N., Losno, R., Maenhaut, W., Paytan, A., Prospero, J. M., Shank, L. M., & Siefert, R. L. (2009). Atmospheric Iron Deposition: Global Distribution, Variability, and Human Perturbations. *Annual Review of Marine Science*, *1*(1), 245–278. <https://doi.org/10.1146/annurev.marine.010908.163727>
- McGillicuddy, D. J., Sedwick, P. N., Dinniman, M. S., Arrigo, K. R., Bibby, T. S., Greenan, B. J. W., ... Dijken, G. L. (2015). Iron supply and demand in an Antarctic shelf ecosystem. *Geophysical Research Letters*, *42*(19), 8088–8097. <https://doi.org/10.1002/2015GL065727>
- Moore, J. K., & Braucher, O. (2008). Sedimentary and mineral dust sources of dissolved iron to the world ocean. *Biogeosciences*, *5*(3), 631–656. <https://doi.org/10.5194/bg-5-631-2008>
- Nissen, C., Vogt, M., Münnich, M., Gruber, N., & Haumann, F. A. (2018). Factors controlling coccolithophore biogeography in the Southern Ocean. *Biogeosciences*, *15*(22), 6997–7024. <https://doi.org/10.5194/bg-15-6997-2018>
- Reigstad, M., & Wassmann, P. (2007). Does *Phaeocystis* spp. contribute significantly to vertical export of organic carbon? In *Phaeocystis, major link in the biogeochemical cycling of climate-relevant elements* (pp. 217–234). Springer Netherlands. https://doi.org/10.1007/978-1-4020-6214-8_16
- Sarthou, G., Timmermans, K. R., Blain, S., & Tréguer, P. (2005). Growth physiology and fate of diatoms in the ocean: a review. *Journal of Sea Research*, *53*(1–2), 25–42. <https://doi.org/10.1016/j.seares.2004.01.007>

- Sauzède, R., Lavigne, H., Claustre, H., Uitz, J., Schmechtig, C., D'Ortenzio, F., Guinet, C., & Pesant, S. (2015). Vertical distribution of chlorophyll *a* concentration and phytoplankton community composition from in situ fluorescence profiles: a first database for the global ocean. *Earth System Science Data*, 7(2), 261–273. <https://doi.org/10.5194/essd-7-261-2015>
- Schoemann, V., Becquevort, S., Stefels, J., Rousseau, V., & Lancelot, C. (2005). Phaeocystis blooms in the global ocean and their controlling mechanisms: a review. *Journal of Sea Research*, 53(1–2), 43–66. <https://doi.org/10.1016/j.seares.2004.01.008>
- Smith, W. O., Dennett, M. R., Mathot, S., & Caron, D. A. (2003). The temporal dynamics of the flagellated and colonial stages of *Phaeocystis antarctica* in the Ross Sea. *Deep Sea Research Part II: Topical Studies in Oceanography*, 50(3–4), 605–617. [https://doi.org/10.1016/S0967-0645\(02\)00586-6](https://doi.org/10.1016/S0967-0645(02)00586-6)
- Stefels, J., Steinke, M., Turner, S., Malin, G., & Belviso, S. (2007). Environmental constraints on the production and removal of the climatically active gas dimethylsulphide (DMS) and implications for ecosystem modelling. In *Phaeocystis, major link in the biogeochemical cycling of climate-relevant elements* (pp. 245–275). Dordrecht: Springer Netherlands. https://doi.org/10.1007/978-1-4020-6214-8_18
- Strzepek, R. F., Boyd, P. W., & Sunda, W. G. (2019). Photosynthetic adaptation to low iron, light, and temperature in Southern Ocean phytoplankton. *Proceedings of the National Academy of Sciences*, 116(10), 4388–4393. <https://doi.org/10.1073/pnas.1810886116>
- Strzepek, R. F., Maldonado, M. T., Hunter, K. A., Frew, R. D., & Boyd, P. W. (2011). Adaptive strategies by Southern Ocean phytoplankton to lessen iron limitation: Uptake of organically complexed iron and reduced cellular iron requirements. *Limnology and Oceanography*, 56(6), 1983–2002. <https://doi.org/10.4319/lo.2011.56.6.1983>
- Swan, C. M., Vogt, M., Gruber, N., & Laufkoetter, C. (2016). A global seasonal surface ocean climatology of phytoplankton types based on CHEMTAX analysis of HPLC pigments. *Deep Sea Research Part I: Oceanographic Research Papers*, 109, 137–156. <https://doi.org/10.1016/j.dsr.2015.12.002>
- Thomalla, S. J., Fauchereau, N., Swart, S., & Monteiro, P. M. S. (2011). Regional scale characteristics of the seasonal cycle of chlorophyll in the Southern Ocean. *Biogeosciences*, 8(10), 2849–2866. <https://doi.org/10.5194/bg-8-2849-2011>
- Vogt, M., O'Brien, C., Peloquin, J., Schoemann, V., Breton, E., Estrada, M., ... Peperzak, L. (2012). Global marine plankton functional type biomass distributions: *Phaeocystis* spp. *Earth System Science Data*, 4(1), 107–120. <https://doi.org/10.5194/essd-4-107-2012>
- Wang, S., & Moore, J. K. (2011). Incorporating *Phaeocystis* into a Southern Ocean ecosystem model. *Journal of Geophysical Research*, 116(C1), C01019. <https://doi.org/10.1029/2009JC005817>
- Yager, P., Sherrell, R., Stammerjohn, S., Ducklow, H., Schofield, O., Ingall, E., ... van Dijken, G. (2016). A carbon budget for the Amundsen Sea Polynya, Antarctica: Estimating net community production and export in a highly productive polar ecosystem. *Elementa: Science of the Anthropocene*, 4, 000140. <https://doi.org/10.12952/journal.elementa.000140>
- Yang, E. J., Jiang, Y., & Lee, S. (2016). Microzooplankton herbivory and community structure in the Amundsen Sea, Antarctica. *Deep Sea Research Part II: Topical Studies in Oceanography*, 123, 58–68. <https://doi.org/10.1016/j.dsr2.2015.06.001>

Factors controlling the competition between *Phaeocystis* and diatoms in the Southern Ocean and implications for carbon export fluxes

Cara Nissen¹ and Meike Vogt¹

¹Institute for Biogeochemistry and Pollutant Dynamics, ETH Zürich, Universitätstrasse 16, 8092 Zürich, Switzerland

Correspondence: C. Nissen (cara.nissen@usys.ethz.ch)

Abstract. The high-latitude Southern Ocean phytoplankton community is shaped by the competition between *Phaeocystis* and silicifying diatoms, with the relative abundance of these two groups controlling primary and export production, the production of dimethylsulfide, the ratio of silicic acid and nitrate available in the water column, and the structure of the food web. Here, we investigate this competition using a regional physical-biogeochemical-ecological model (ROMS-BEC) configured at eddy-permitting resolution for the Southern Ocean south of 35° S. We ~~extended-improved~~ ROMS-BEC by adding an explicit parameterization of *Phaeocystis* colonies, so that the model, together with the previous addition of an explicit coccolithophore type, now includes all biogeochemically relevant Southern Ocean phytoplankton types. We find that *Phaeocystis* contribute 46% ± 21% (1σ in space) and 40 ± 20% to annual NPP and POC export south of 60° S, respectively, making them an important contributor to high-latitude carbon cycling. In our simulation, the relative importance of *Phaeocystis* and diatoms is mainly controlled by ~~the temporal~~ spatio-temporal variability in temperature and iron availability. ~~The~~ In addition, in more coastal areas, such as the Ross Sea, the higher light sensitivity of *Phaeocystis* at low irradiances promotes the succession from *Phaeocystis* to diatoms ~~in more coastal areas, such as the Ross Sea. Still, differences~~. Differences in the biomass loss rates, such as aggregation or grazing by zooplankton, need to be considered to explain the simulated seasonal biomass evolution and carbon export fluxes.

15 1 Introduction

Phytoplankton production in the Southern Ocean (SO) regulates not only the uptake of anthropogenic carbon in marine food-webs, but also controls global primary production via the lateral export of nutrients to lower latitudes (e.g. Sarmiento et al., 2004; Palter et al., 2010). The amount and stoichiometry of these laterally exported nutrients is determined by the combined action of multiple types of phytoplankton with differing ecological niches and nutrient requirements. Yet, despite their important role, the drivers of phytoplankton biogeography and competition and the relative contribution of different phytoplankton groups to SO carbon cycling are still poorly quantified. Today, the SO phytoplankton community is largely dominated by silicifying diatoms that efficiently fix and transport carbon from the surface ocean to depth (e.g. Swan et al., 2016) and have been suggested to be the major contributor to SO carbon export (Buesseler, 1998; Smetacek et al., 2012). However, calcifying coccolithophores and dimethylsulfide (DMS) producing *Phaeocystis* have been found to contribute in a significant way to total phytoplankton

25 biomass [in summer/fall](#) at subantarctic (Balch et al., 2016; Nissen et al., 2018) and [in spring/summer](#) at high latitudes, respectively (Smith and Gordon, 1997; Arrigo et al., 1999; DiTullio et al., 2000; Poulton et al., 2007) (Smith and Gordon, 1997; Arrigo et al., 1999), thus suggesting that the succession and competition of different plankton groups governs biogeochemical cycles at the (sub)regional scale. As climate change is expected to differentially impact the competitive fitness of different phytoplankton groups and ultimately their contribution to total net primary production (NPP; IPCC, 2014; Constable et al., 2014; Deppeler and Davidson, 2017), with a likely increase in the relative importance of coccolithophores and *Phaeocystis* in a warming world at the expense of diatoms (Bopp et al., 2005; Winter et al., 2013; Rivero-Calle et al., 2015), the resulting change in SO phytoplankton community structure is likely to affect global nutrient and carbon distributions, ocean carbon uptake, and marine food web structure (Smetacek et al., 2004). While a number of recent studies have elucidated the importance of coccolithophores for subantarctic carbon cycling (e.g. Rosengard et al., 2015; Balch et al., 2016; Nissen et al., 2018; Rigual Hernández et al., 2020), few estimates quantify the role of present and future high-latitude SO phytoplankton community structure for ecosystem services such as NPP and carbon export (e.g. Wang and Moore, 2011; Yager et al., 2016).

Phaeocystis blooms in the SO have been regularly observed in early spring at high SO latitudes (especially in the Ross Sea, see e.g. Smith et al., 2011), thus preceding those of diatoms (Green and Sambrotto, 2006; Peloquin and Smith, 2007; Alvain et al., 2008; Arrigo et al., 2017; Ryan-Keogh et al., 2017), and *Phaeocystis* can dominate over diatoms in terms of carbon biomass at regional and sub-annual scales (e.g. Smith and Gordon, 1997; Alvain et al., 2008; Leblanc et al., 2012; Vogt et al., 2012; Ben Mustapha et al., 2014). Nevertheless, *Phaeocystis* is not routinely included as a phytoplankton functional type (PFT) in global biogeochemical models, possibly a result of the limited number of biomass validation data (Vogt et al., 2012) and its complex life cycle (Schoemann et al., 2005). In particular, *Phaeocystis* is difficult to model because traits linked to biogeochemistry-related ecosystem services, such as size and carbon content, vary due to its complex multi-stage life cycle. Its alternation between solitary cells of a few μm in diameter and gelatinous colonies of several mm to cm in diameter (e.g. Rousseau et al., 1994; Peperzak, 2000; Chen et al., 2002; Bender et al., 2018) directly impacts community biomass partitioning and the relative importance of aggregation, viral lysis, and grazing for *Phaeocystis* biomass losses, its susceptibility to zooplankton grazing relative to that of diatoms (Granéli et al., 1993; Smith et al., 2003), and ultimately the export of particulate organic carbon (POC; Schoemann et al., 2005). With *Phaeocystis* colonies typically dominating over solitary cells during the SO growing season (Smith et al., 2003) [and with larger cells being more likely to form aggregates and less likely to be grazed by microzooplankton](#) (Granéli et al., 1993; Caron et al., 2000; Schoemann et al., 2005; Nejtgaard et al., 2007), *Phaeocystis* biomass loss via aggregation possibly increases in relative importance at the expense of grazing as more colonies are formed and colony size increases (Tang et al., 2008). Altogether, this implies a complex seasonal variability in the magnitude and pathways of carbon transfer to depth as the phytoplankton community changes throughout the year, which is **difficult** [expensive](#) to comprehensively assess through in situ studies and therefore calls for marine ecosystem models.

Across those marine ecosystem models including a *Phaeocystis* PFT, the representation of its life cycle differs in terms of complexity (Pasquer et al., 2005; Tagliabue and Arrigo, 2005; Wang and Moore, 2011; Le Quéré et al., 2016; Kaufman et al., 2017; Losa et al., 2019). While some models include rather sophisticated parametrizations to describe life cycle transitions (accounting for nutrient concentrations, light levels, and a seed population, see e.g. Pasquer et al., 2005; Kaufman

60 et al., 2017), the majority includes rather simple transition functions (accounting for iron concentrations only, see Losa et al., 2019) or only the colonial life stage of *Phaeocystis* (Tagliabue and Arrigo, 2005; Wang and Moore, 2011; Le Quéré et al., 2016). Despite these differences, all of the models see improvements in the simulated SO phytoplankton biogeography as compared to observations upon the implementation of a *Phaeocystis* PFT. In particular, Wang and Moore (2011) find that *Phaeocystis* contributes substantially to SO integrated annual NPP and POC export (23% and 30% south of 60° S, respectively; Wang and Moore, 2011), implying that models not accounting for *Phaeocystis* possibly overestimate the role of diatoms for high-latitude phytoplankton biomass, NPP, and POC export (Laufkötter et al., 2016). Overall, the link between ecosystem composition, ecosystem function, and global biogeochemical cycling in general (e.g. Siegel et al., 2014; Guidi et al., 2016; Henson et al., 2019) and the contribution of *Phaeocystis* to SO export of POC in particular are still under debate. While some have found blooms of *Phaeocystis* to be important vectors of carbon transfer to depth through the formation of aggregates (Asper and Smith, 1999; DiTullio et al., 2000; Ducklow et al., 2015; Asper and Smith, 2019) (Asper and Smith, 1999; DiTullio et al., 2000), others suggest their biomass losses to be efficiently retained in the upper ocean by local circulation (Lee et al., 2017) and degraded in the upper water column through bacterial and zooplankton activity (Gowing et al., 2001; Accornero et al., 2003; Reigstad and Wassmann, 2007), making *Phaeocystis* a minor contributor to SO POC export (Gowing et al., 2001; Accornero et al., 2003; Reigstad and Wassmann, 2007). This demonstrates the major existing uncertainty in how the high-latitude phytoplankton community structure impacts carbon export fluxes.

In general, the relative importance of different phytoplankton types for total phytoplankton biomass is controlled by a combination of top-down factors, i.e. processes impacting phytoplankton biomass loss such as grazing by zooplankton, aggregation of cells and subsequent sinking, or viral lysis, and bottom-up factors, i.e. physical and biogeochemical variables impacting phytoplankton growth (Le Quéré et al., 2016). The observed spatio-temporal differences in the relative importance of *Phaeocystis* and diatoms in the SO are thought to be largely controlled by differences in light and iron levels, but the relative importance of the different bottom-up factors appears to vary depending on the time and location of the sampling (Arrigo et al., 1998, 1999; Goffart et al., 2000; Sedwick et al., 2000; Garcia et al., 2009; Tang et al., 2009; Mills et al., 2010; Feng et al., 2010; Smith et al., 2011, 2014). Concurrently, while available models agree with the observations on the general importance of light and iron levels, differences in the dominant bottom-up factors controlling the distribution of *Phaeocystis* at high SO latitudes across models are possibly a result of differences in how this phytoplankton type is parametrized (Tagliabue and Arrigo, 2005; Pasquer et al., 2005; Wang and Moore, 2011; Le Quéré et al., 2016; Kaufman et al., 2017; Losa et al., 2019). In this context, whether the model explicitly represents both *Phaeocystis* life stages (Pasquer et al., 2005; Kaufman et al., 2017; Losa et al., 2019) or only the colonial stage (Wang and Moore, 2011; Le Quéré et al., 2016) is key, as single cells are known to have lower iron requirements than *Phaeocystis* colonies (Veldhuis et al., 1991). Besides bottom-up factors, some observational studies suggest that top-down factors are important in controlling the relative importance of *Phaeocystis* and diatoms as well. For instance, van Hilst and Smith (2002) suggest grazing by zooplankton to be an important factor explaining the observed distributions of these two phytoplankton types in the SO, likely resulting from the generally lower grazing pressure on *Phaeocystis* colonies than on diatoms (Granéli et al., 1993; Smith et al., 2003). Yet, further evidence suggests a role for other biomass loss processes such as aggregation and subsequent sinking (Asper and Smith, 1999; Ducklow et al., 2015; Asper and Smith, 2019). Altogether,

95 this calls for a comprehensive quantitative analysis of the relative importance of bottom-up and top-down factors in controlling the competition between *Phaeocystis* and diatoms over the course of the SO growing season and its ramifications for carbon transfer to depth.

In this study, we investigate the competition between *Phaeocystis* and diatoms and its implications for carbon cycling using a regional coupled physical-biogeochemical-ecological model configured at eddy-permitting resolution for the SO (ROMS-BEC, 100 Nissen et al., 2018). To address the missing link between SO phytoplankton biogeography, [ecosystem function](#), and the global carbon cycle, we have added *Phaeocystis* colonies as an additional PFT to the model, so that it includes all ~~major-identified~~ [known](#) biogeochemically relevant phytoplankton types of the SO. ~~We then assess the~~ [\(e.g. Buesseler, 1998; DiTullio et al., 2000\)](#). [Using available observations, such as satellite-derived chlorophyll concentrations, carbon biomass and pigment data, we first validate the simulated phytoplankton distributions and community structure across the SO and then particularly focus](#) 105 [on the temporal variability of diatoms and *Phaeocystis* in the high-latitude SO. After assessing the](#) relative importance of bottom-up and top-down factors in controlling the ~~relative importance~~ [contribution](#) of *Phaeocystis* colonies and diatoms [to total phytoplankton biomass](#) over a complete annual cycle in the high-latitude SO. ~~We show that a correct representation of SO phytoplankton biogeography~~, [we show that the spatially and temporarily varying phytoplankton community composition](#) leaves a distinct, [PFT-specific](#) imprint on upper ocean carbon cycling and POC export across the SO.

110 2 Methods

2.1 ROMS-BEC with explicit *Phaeocystis* colonies

We use a quarter-degree SO setup of the Regional Ocean Modeling System ROMS (latitudinal range from 24° S-78° S, 64 topography-following vertical levels, time step to solve the primitive equations is 1600 s; Shchepetkin and McWilliams, 2005; Haumann, 2016), coupled to the biogeochemical model BEC (Moore et al., 2013), which was recently extended to include 115 an explicit representation of coccolithophores and thoroughly validated in the SO setup (Nissen et al., 2018). BEC resolves the biogeochemical cycling of all macronutrients (C, N, P, Si), as well as the cycling of iron (Fe), the major micronutrient in the SO. The model includes four PFTs – diatoms, coccolithophores, small phytoplankton/SP, and N₂-fixing diazotrophs – and one zooplankton functional type (Moore et al., 2013; Nissen et al., 2018). Here, we extend the version of Nissen et al. (2018) to include an explicit parameterization of colonial *Phaeocystis antarctica*, which is the only [bloom-forming](#) species 120 of *Phaeocystis* occurring in the SO (Schoemann et al., 2005) [and which typically dominates over solitary cells when SO *Phaeocystis* biomass levels are highest \(Smith et al., 2003\)](#). For the remainder of this manuscript, we will refer to the new PFT as "*Phaeocystis*". Generally, model parameters for *Phaeocystis* [in the Baseline setup](#) are chosen to represent the colonial form of *Phaeocystis* whenever information is available in the literature (see e.g. review by Schoemann et al., 2005), [and model parameters were tuned to maximize the model-data agreement in the spatio-temporal variability of the phytoplankton](#) 125 [community structure between ROMS-BEC and all available observations \(see also section 2.3.1\)](#). By only simulating the colonial form of *Phaeocystis*, we assume enough solitary cells of *Phaeocystis* to be available for colony formation at any time as part of the SP PFT. As for the other phytoplankton PFTs, growth by *Phaeocystis* is limited by surrounding temperature,

nutrient, and light conditions as outlined in the following (see appendix B for a complete description of the model equations describing phytoplankton growth).

130 As the new PFT in ROMS-BEC represents a single species of *Phaeocystis*, we use an optimum function rather than an Eppley curve (Eppley, 1972) to describe its temperature-limited growth rate $\mu^{\text{PA}}(T)$ (d^{-1} , Schoemann et al., 2005):

$$\mu^{\text{PA}}(T) = \mu_{\text{max}}^{\text{PA}} \cdot e^{-\left(\frac{T-T_{\text{opt}}}{\tau}\right)^2} \quad (1)$$

In the above equation, the maximum growth rate ($\mu_{\text{max}}^{\text{PA}}$) is 1.56 d^{-1} at an optimum temperature (T_{opt}) of 3.6° C and the temperature interval (τ) is 17.51° C and 1.17° C at temperatures below and above 3.6° C , respectively. With these parameters, 135 the simulated growth rate of *Phaeocystis* in ROMS-BEC is zero at temperatures above $\sim 8^\circ \text{ C}$ (in agreement with laboratory experiments with *Phaeocystis antarctica*, see Buma et al., 1991) and higher than that of diatoms for temperatures between $\sim 0\text{-}4^\circ \text{ C}$ (Fig. A1a). We acknowledge that the range of temperatures for which the growth of *Phaeocystis* exceeds that of diatoms is possibly underestimated, as the temperature-limited growth rate by diatoms in ROMS-BEC is overestimated at low 140 temperatures compared to available laboratory data (see Fig. A1a & Eq. B5). Yet, we note that temperature-limited growth by diatoms in the model is tuned to fit the data at the global range of temperatures, in particular for the competition with coccolithophores at subantarctic latitudes (Nissen et al., 2018).

Half-saturation constants for macronutrient limitation are scarce for *P. antarctica* (Schoemann et al., 2005), and macronutrient limitation of *Phaeocystis* is therefore chosen to be identical to that of diatoms in ROMS-BEC (Table 1). As the availability of the micronutrient Fe generally limits phytoplankton growth in the high-latitude SO (Martin et al., 1990a, b) and accordingly 145 in ROMS-BEC (Fig. S1), this choice is not expected to significantly impact the simulated competition between diatoms and *Phaeocystis* in this area. In contrast, differences in the half-saturation constants with respect to dissolved Fe concentrations (k_{Fe}) of *Phaeocystis* and diatoms critically impact the competitive success of *Phaeocystis* relative to diatoms throughout the year (see e.g. Sedwick et al., 2000, 2007). Here, due to their larger size, we assume a higher k_{Fe} for *Phaeocystis* ($0.2 \mu\text{mol m}^{-3}$) than for diatoms ($0.15 \mu\text{mol m}^{-3}$, Table 1). We note however, that the k_{Fe} of *Phaeocystis* has been reported to vary over 150 one order magnitude depending on the ambient light level ($0.045\text{-}0.45 \mu\text{mol m}^{-3}$, see Fig. A1b and Garcia et al., 2009), with lowest values at optimum light levels of around 80 W m^{-2} . Due to the limited number (3) of reported light levels in Garcia et al. (2009) and the associated uncertainty when fitting the data, we refrain from using this k_{Fe} -light-dependency in the *Base-line* simulation, but explore the sensitivity of the simulated seasonality of *Phaeocystis* and diatom biomass to a polynomial fit describing the k_{Fe} of *Phaeocystis* as a function of the light intensity (see Fig. A1b and section 2.2). As a result of the tuning 155 exercise aiming to maximize the fit of *all* simulated PFT biomass fields to available observations, the k_{Fe} of the other PFTs in ROMS-BEC are increased by 25% in this study as compared to in Nissen et al. (2018, see Table 1). For diatoms, this change leads to a better agreement of the k_{Fe} used in ROMS-BEC with values suggested for large SO diatoms by Timmermans et al. (2004), but we acknowledge that the chosen value here is still at the lower end of their suggested range ($0.19\text{-}1.14 \mu\text{mol m}^{-3}$).
[In ROMS-BEC, phytoplankton Fe uptake relative to the uptake of C varies as a function of seawater Fe levels and decreases linearly below a critical concentration which is specific to each PFT's \$k_{\text{Fe}}\$ \(see Eq. B11\). In concert with the seasonal evolution of upper ocean Fe levels, the Fe:C ratios of all PFTs are highest in winter and lowest in summer \(not shown\). As a result of](#) 160

Table 1. BEC parameters controlling phytoplankton growth and loss for the five phytoplankton PFTs diatoms (D), *Phaeocystis* (PA), coccolithophores (C), small phytoplankton (SP), and diazotrophs (NDZ). Z=zooplankton, P=phytoplankton, PI=photosynthesis-irradiance. If not given in section 2.1, the model equations describing phytoplankton growth and loss rates are given in Nissen et al. (2018).

Parameter	Unit	Description	D	PA	C	SP	NDZ [†]
μ_{\max}	d^{-1}	max. growth rate at 30° C	4.6	‡	3.8	3.6	0.9
Q ₁₀		temperature sensitivity	1.55	‡	1.45	1.5	1.5
k _{NO₃}	mmol m^{-3}	half-saturation constant for NO ₃	0.5	0.5	0.3	0.1	1.0
k _{NH₄}	mmol m^{-3}	half-saturation constant for NH ₄	0.05	0.05	0.03	0.01	0.15
k _{PO₄}	mmol m^{-3}	half-saturation constant for PO ₄	0.05	0.05	0.03	0.01	0.02
k _{DOP}	mmol m^{-3}	half-saturation constant for DOP	0.9	0.9	0.3	0.26	0.09
k _{Fe}	$\mu\text{mol m}^{-3}$	half-saturation constant for Fe	0.15	0.2	0.125	0.1	0.5
k _{SiO₃}	mmol m^{-3}	half-saturation constant for SiO ₃	1.0	-	-	-	-
α_{PI}	$\frac{\text{mmol C m}^2}{\text{mg Chl W s}}$	initial slope of PI-curve	0.44	0.63	0.4	0.44	0.38
$\theta_{\text{chl:N,max}}$	$\frac{\text{mg chl}}{\text{mmol N}}$	max. Chl:N ratio	<u>4.0</u>	<u>2.5</u>	<u>2.5</u>	<u>2.5</u>	<u>2.5</u>
$\gamma_{\text{g,max}}$	d^{-1}	max. growth rate of Z grazing on P	3.8	3.6	4.4	4.4	3.0
z _{grz}	mmol m^{-3}	half-saturation constant for ingestion	1.0	1.0	1.05	1.05	1.2
$\gamma_{\text{m},0}$	d^{-1}	linear non-grazing mortality	0.12	0.18	0.12	0.12	0.15
$\gamma_{\text{a},0}$	$\frac{\text{m}^3}{\text{mmol C d}}$	quadratic loss rate in aggregation	0.001	0.005	0.001	0.001	-
r _g	-	fraction of grazing routed to POC	0.3 0.42	<u>0.3</u>	0.2	0.05	0.05

[†] Compared to Nissen et al. (2018), the k_{Fe} of diazotrophs in ROMS-BEC is higher than for all other PFTs, consistent with literature reporting high Fe requirements of *Trichodesmium* (Berman-Frank et al., 2001). Furthermore, the maximum grazing rate on diazotrophs is lowest in the model (Capone, 1997). Still, diazotrophs continue to be a minor player in the SO phytoplankton community, contributing <1% to domain-integrated NPP in ROMS-BEC.

[‡] The temperature-limited growth rate of *Phaeocystis* is calculated based on an optimum function according to Eq. 1 (see also Fig. A1a).

their higher k_{Fe} in the model, *Phaeocystis* generally have lower Fe:C uptake ratios than diatoms. We note that we currently do not include any luxury uptake of Fe by *Phaeocystis* into their gelatinous matrix (Schoemann et al., 2001). Serving as a storage of additional Fe accessible to the *Phaeocystis* colony when Fe in the seawater gets low, this luxury uptake is thought to relieve it from Fe limitation when Fe concentrations become growth limiting (see discussion in Schoemann et al., 2005). We therefore probably overestimate the Fe limitation of *Phaeocystis* growth in ROMS-BEC.

P. antarctica blooms are typically found where and when waters are turbulent and the mixed layer is deep (in comparison to blooms dominated by diatoms, see e.g. Arrigo et al., 1999; Alvain et al., 2008), suggesting that *Phaeocystis* is better in coping with low light levels than diatoms (e.g. Arrigo et al., 1999). In agreement with laboratory experiments (Tang et al., 2009; Mills et al., 2010; Feng et al., 2010), we therefore choose a higher α_{PI} , i.e. a higher sensitivity of growth to increases of photosynthetically active radiation (PAR) at low PAR levels, for *Phaeocystis* than for diatoms in ROMS-BEC (see Table 1).

Our value ($0.63 \text{ mmol C m}^{-2} (\text{mg Chl W s})^{-1}$) corresponds to the average value compiled from available laboratory experiments (Schoemann et al., 2005).

In addition to environmental conditions directly impacting phytoplankton growth rates, loss processes such as grazing, non-grazing mortality, and aggregation impact the simulated biomass levels at any point and time (Moore et al., 2002). Grazing on *Phaeocystis* varies across zooplankton size classes, as a consequence of *Phaeocystis* life forms spanning several orders of magnitude in size (Schoemann et al., 2005). Furthermore, *Phaeocystis* colonies are surrounded by a membrane (Hamm et al., 1999), potentially serving as protection from zooplankton grazing. While small copepods have been shown to graze less on *Phaeocystis* once they form colonies, other larger zooplankton appear to continue grazing on *Phaeocystis* colonies at unchanged rates (Granéli et al., 1993; Schoemann et al., 2005; Nejtgaard et al., 2007) (Granéli et al., 1993; Caron et al., 2000; Schoemann et al., 2005; Nejtgaard et al., 2007). Based on a size-mismatch assumption of the single grazer in ROMS-BEC and *Phaeocystis* colonies, we assume a lower maximum grazing rate on *Phaeocystis* than on diatoms (3.6 d^{-1} and 3.8 d^{-1} , respectively, see $\gamma_{g,\text{max}}$ in Table 1). Upon grazing, we assume the fraction of the grazed phytoplankton biomass that is transformed to sinking POC via zooplankton fecal pellet production to be higher for larger and ballasted cells than for small, unballasted cells. Consequently, the fraction of grazing routed to POC increases from grazing on SP or diazotrophs to coccolithophores, *Phaeocystis*, and diatoms (r_g in Table 1). Consistent with Nissen et al. (2018), we keep a Holling Type II ingestion functional response here (Holling, 1959) and compute grazing on each prey separately (Eq. B14). We refer to Nissen et al. (2018) for a discussion of the relative merits and pitfalls for using Holling Type II versus III.

Non-grazing mortality (such as viral lysis) has been shown to increase under environmental stress for *Phaeocystis* colonies, causing colony disruption and ultimately cell death (van Boekel et al., 1992; Schoemann et al., 2005). To account for processes causing colony disintegration and for grazing by higher trophic levels not explicitly included in ROMS-BEC, *Phaeocystis* in ROMS-BEC experience a higher mortality rate than diatoms (0.18 d^{-1} and 0.12 d^{-1} , respectively, see $\gamma_{m,0}$ in Table 1 & Eq. B16). Thereby, the chosen non-grazing mortality rate of *Phaeocystis* assumed in the model is still lower than the estimated rate of viral lysis for *Phaeocystis* in the North Sea by van Boekel et al. (1992, 0.25 d^{-1}), but we note that data on non-grazing mortality of *P. antarctica* are currently lacking (Schoemann et al., 2005). Furthermore, based on the assumption that for a given biomass concentration, larger cells are more likely than smaller cells to form aggregates and to subsequently stop photosynthesizing and sink as POC, we use a higher quadratic loss rate for *Phaeocystis* (0.005 d^{-1}) than for diatoms (0.001 d^{-1}) in the model (see $\gamma_{a,0}$ in Table 1 & Eq. B18).

In summary, the spatio-temporal variability of the relative importance of *Phaeocystis* and diatoms in ROMS-BEC is controlled by the interplay of the environmental conditions and loss processes, which differentially impact the growth and loss rates of these two PFTs and consequently their competitive fitness in the model. In the following, we will describe the model setup and the simulations that were performed to assess the competition between *Phaeocystis* and diatoms throughout the year in the high-latitude SO. The simulations include a set of sensitivity experiments, with the aim to assess the impact of choices of single parameters or parameterizations on the simulated *Phaeocystis* biogeography.

Table 2. Overview of sensitivity experiments aiming to 1) assess the sensitivity of the simulated *Phaeocystis*-diatom competition to chosen parameter values and parameterizations of *Phaeocystis* (competition experiments, runs 1-8) and 2) assess the sensitivity of the simulated biomass distributions to chosen *Phaeocystis* parameter values (parameter sensitivity experiments, runs 9-22). The results of the parameter sensitivity experiments are discussed in the supplementary material. See Table 1 and section 2.1 for parameter values and parameterizations of *Phaeocystis* in the reference simulation. PA=*Phaeocystis*, D=diatoms.

<u>Competition</u>	Run Name	Description
1	TEMPERATURE	Use μ_{\max}^D , Q_{10}^D , and $\mu_T^{PA} = \mu_{\max}^D \cdot Q_{10}^D \frac{T-T_{\text{ref}}}{10^\circ\text{C}}$ to compute the temperature-limited growth rate of <i>Phaeocystis</i> instead of Eq. 1
2	ALPHA _{PI}	Set α_{PI}^{PA} to α_{PI}^D
3	IRON	Set k_{Fe}^{PA} to k_{Fe}^D
4	GRAZING	Set $\gamma_{g,\max}^{PA}$ to γ_{\max}^D
5	AGGREGATION	Set $\gamma_{a,0}^{PA}$ to $\gamma_{a,0}^D$
6	MORTALITY	Set $\gamma_{m,0}^{PA}$ to $\gamma_{m,0}^D$
7	<u>THETA_N_MAX</u>	<u>Set $\theta_{chl:N,\max}^{PA}$ to $\theta_{chl:N,\max}^D$</u>
8	VARYING_kFE	Use $k_{Fe}^{PA}(I) = 2.776 \cdot 10^{-5} \cdot (I + 20)^2 - 0.00683 \cdot (I + 20) + 0.46$ (with the irradiance I in W m^{-2}) instead of a constant k_{Fe}^{PA}
<u>Parameter sensitivity</u>	<u>Run Name</u>	<u>Description</u>
9	<u>Topt150</u>	<u>Increase T_{opt}^{PA} by 50%</u>
10	<u>Topt50</u>	<u>Decrease T_{opt}^{PA} by 50%</u>
11	<u>kFe150</u>	<u>Increase k_{Fe}^{PA} by 50%</u>
12	<u>kFe50</u>	<u>Decrease k_{Fe}^{PA} by 50%</u>
13	<u>alphaPI150</u>	<u>Increase α_{PI}^{PA} by 50%</u>
14	<u>alphaPI50</u>	<u>Decrease α_{PI}^{PA} by 50%</u>
15	<u>mortality150</u>	<u>Increase $\gamma_{m,0}^{PA}$ by 50%</u>
16	<u>mortality50</u>	<u>Decrease $\gamma_{m,0}^{PA}$ by 50%</u>
17	<u>aggregation150</u>	<u>Increase $\gamma_{a,0}^{PA}$ by 50%</u>
18	<u>aggregation50</u>	<u>Decrease $\gamma_{a,0}^{PA}$ by 50%</u>
19	<u>grazing150</u>	<u>Increase $\gamma_{g,\max}^{PA}$ by 50%</u>
20	<u>grazing50</u>	<u>Decrease $\gamma_{g,\max}^{PA}$ by 50%</u>

205 2.2 Model setup and sensitivity simulations

With few exceptions, we use the same ROMS-BEC model setup as described in detail in Nissen et al. (2018): At the open northern boundary, we use monthly climatological fields for all tracers (Carton and Giese, 2008; Locarnini et al., 2013; Zweng et al., 2013; Garcia et al., 2014b, a; Lauvset et al., 2016; Yang et al., 2017), and the same data sources are used to initialize the model simulations. At the ocean surface, the model is forced with a 2003-normal year forcing for momentum, heat, and freshwater fluxes (Dee et al., 2011). Satellite-derived climatological total chlorophyll concentrations are used to initialize phytoplankton biomass and to constrain it at the open northern boundary in the model (NASA-OBPG, 2014b), and the fields are extrapolated to depth following Morel and Berthon (1989). Due to the addition of *Phaeocystis*, the partitioning of total chlorophyll onto the different phytoplankton PFTs is adjusted compared to Nissen et al. (2018): 90% is attributed to small phytoplankton, 4% to diatoms and coccolithophores, respectively, and 1% to diazotrophs and *Phaeocystis*, respectively. This partitioning is motivated by the phytoplankton community structure at the open northern boundary at 24° S, where small phytoplankton typically dominate and *P. antarctica* are only a minor contributor to phytoplankton biomass (see e.g. Schoemann et al., 2005; Swan et al., 2016). *Phaeocystis* is initialized with a carbon-to-chlorophyll ratio of 60 mg C (mg chl)⁻¹ (same as small phytoplankton and coccolithophores), whereas diatoms are initialized with a ratio of 36 mg C (mg chl)⁻¹ (Sathyendranath et al., 2009).

220 We first run a 30 year long physics-only spin-up, followed by a 10 year long spin-up in the coupled ROMS-BEC setup. Our *Baseline* simulation for this study is then run for an additional 10 years, of which we analyze a daily climatology over the last 5 full seasonal cycles. i.e. from 1 July of year 5 until 30 June of year 10. Apart from having added *Phaeocystis* and adjusted the parameters of the other PFTs as described in section 2.1, the setup of the *Baseline* simulation in this study is thereby identical to the *Baseline* simulation in Nissen et al. (2018). We will evaluate the model's performance with respect to the simulated phytoplankton biogeography in section 3.1 and in the supplementary material.

Furthermore, we perform ~~seven sensitivity experiments~~ two sets of sensitivity experiments (22 simulations in total), in order to 1) assess the sensitivity of the simulated *Phaeocystis* biogeography and the competition of *Phaeocystis* and diatoms to chosen parameters and parameterizations (competition experiments, runs 1-8 in Table 2) ~~-To do so~~ and 2) systematically assess the sensitivity of the simulated biomass distributions to chosen *Phaeocystis* parameter values (parameter experiments, runs 9-22). For the former set, we set the parameters and parameterizations of *Phaeocystis* to those used for diatoms in ROMS-BEC (runs ~~1-6~~ 1-8 in Table 2). Generally, the differences in parameters between *Phaeocystis* and diatoms affect either the simulated ~~growth~~ biomass accumulation rates (runs TEMPERATURE, ALPHA_{PI}, ~~and IRON~~ IRON, and THETA_N_MAX) or loss rates (runs GRAZING, AGGREGATION, and MORTALITY). By successively eradicating the differences between *Phaeocystis* and diatoms, these simulations allow us to directly quantify the impact of parameter differences on the simulated relative importance of *Phaeocystis* for total phytoplankton biomass. To assess the impact of iron-light interactions on the competitive success of *Phaeocystis* at high SO latitudes, we ultimately run a simulation in which the half-saturation constant of iron (k_{Fe}) of *Phaeocystis* is a function of the light intensity, following a polynomial fit of available laboratory data (VARYING_kFE, Fig. A1b; Garcia et al., 2009). For the second set of experiments, we systematically vary *Phaeocystis* growth and loss parameters by

[±50%, and the results of these experiments are discussed in detail in section S2 of the supplementary material.](#) All sensitivity
240 experiments use the same physical and biogeochemical spin-up as the *Baseline* simulation and start from the end of year 10 of
the coupled ROMS-BEC spin-up. Each simulation is then run for an additional 10 years, of which the average over the last 5
full seasonal cycles is analyzed in this study.

2.3 **Analysis framework**[Data and diagnostics used in the model assessment](#)

2.3.1 **Evaluating the simulated phytoplankton community structure**

245 We compare the simulated spatio-temporal variability in phytoplankton biomass and community structure to available obser-
vations of phytoplankton carbon biomass concentrations from the MAREDAT initiative (O'Brien et al., 2013; Leblanc et al.,
2012; Vogt et al., 2012), satellite-derived total chlorophyll concentrations (Fanton d'Andon et al., 2009; Maritorena et al.,
2010), DMS measurements (Curran and Jones, 2000; Lana et al., 2011), the ecological niches suggested for SO phytoplankton
250 taxa (Brun et al., 2015), and the CHEMTAX climatology based on high performance liquid chromatography (HPLC) pigment
data (Swan et al., 2016). The latter provides seasonal estimates of the mixed layer average community composition, which
we compare to the seasonally and top 50 m averaged model output of each phytoplankton's contribution to total chlorophyll
biomass. The CHEMTAX analysis splits the phytoplankton community into diatoms, nitrogen fixers (such as *Trichodesmium*),
pico-phytoplankton (such as *Synechococcus* and *Prochlorococcus*), dinoflagellates, cryptophytes, chlorophytes (all three com-
bined into the single group "Others" here), and haptophytes (such as coccolithophores and *Phaeocystis*). As noted in Swan et al.
255 (2016), the differentiation between coccolithophores and *Phaeocystis* in the CHEMTAX analysis is difficult and prone to error.
Possibly, this is due to the large variability in pigment composition of *Phaeocystis* in response to varying environmental condi-
tions, especially regarding light and iron levels (Smith et al., 2010; Wright et al., 2010). Coccolithophores have been reported
to only grow very slowly at low temperatures (below $\sim 8^\circ\text{C}$, Buitenhuis et al., 2008), and in the SO, their abundance in the high
latitudes south of the polar front is very low (Balch et al., 2016). Therefore, whenever the climatological temperature in the
260 World Ocean Atlas 2013 (Locarnini et al., 2013) is below 2°C at the time and location of the respective HPLC observation, we
re-assign data points identified as "Hapto-6" (hence e.g. *Emiliania huxleyi*) in the CHEMTAX analysis to "Hapto-8" (hence e.g.
Phaeocystis antarctica). Throughout the manuscript, this new category ("Hapto-8 re-assigned") is indicated separately in the
respective figures, and leads to a better correspondence of the functional types included in the CHEMTAX-based climatology
by Swan et al. (2016) and the PFTs in ROMS-BEC.

265 To assess the controlling factors of the simulated PFT distributions in our model, we analyze the simulated summer (December-
March; DJFM) top 50 m average biomass distribution of the different model PFTs south of 40°S in environmental niche space.
To that aim, we bin the simulated carbon biomass concentrations of *Phaeocystis*, diatoms, and coccolithophores in ROMS-BEC
as a function of the temperature [$^\circ\text{C}$], nitrate concentration [mmol m^{-3}], iron concentration [$\mu\text{mol m}^{-3}$], and mixed layer pho-
tosynthetically active radiation (MLPAR; W m^{-2}). Subsequently, we compare the simulated ecological niche to that observed
270 for abundant SO species of each model PFT (such as *Phaeocystis antarctica*, *Fragilariopsis kerguelensis*, *Thalassiosira* sp., or
Emiliania huxleyi, see Brun et al., 2015). In section 3.3 of this manuscript, only the results for *Phaeocystis* and diatoms will

be shown, the corresponding figures for coccolithophores can be found in the supplementary material (Fig. [S8](#) & [S9](#) [S2](#) & [S3](#)). While this analysis informs on possible links between the competitive fitness of a PFT and the environmental conditions it lives in, the assessment is limited to a qualitative inter-comparison due to difficulties in comparing a model PFT to individual
275 phytoplankton species, a sampling bias towards the summer months and the low latitudes, and the neglect of loss processes such as zooplankton grazing to explain biomass distributions. As a consequence, the ecological niche analysis does not allow for the assessment of any temporal variability in PFT biomass concentrations.

In order to assess the simulated seasonality and the seasonal succession of *Phaeocystis* and diatoms, we identify the bloom peak as the day of peak chlorophyll concentrations throughout the year. Besides the timing of the bloom peak, phytoplankton
280 phenology is typically characterized by metrics such as the day of bloom initiation or the day of bloom end (see e.g. Soppa et al., 2016). In this regard, the timing of the bloom start is known to be sensitive to the chosen identification methodology (Thomalla et al., 2015). At high latitudes, the identification of the bloom start based on remotely sensed chlorophyll concentrations is additionally impaired by the large number of missing data in all seasons (even in the summer months, a large part of the SO is sampled by the satellite in less than 5 of the 21 available years, see Fig. [S2](#) [S4](#)), complicating any comparison of the
285 high-latitude satellite-derived bloom start with output from models such as ROMS-BEC. To minimize the uncertainty due to the low data coverage in the region of interest for this study, and as the seasonal succession of *Phaeocystis* and diatoms in the high-latitude SO is mostly inferred from the timing of observed maximum abundances in the literature (e.g. Peloquin and Smith, 2007; Smith et al., 2011), we focus our discussion of the simulated bloom phenology on the timing of the bloom peak (Hashioka et al., 2013). To evaluate the model's performance, we compare the timing of the total chlorophyll bloom peak in
290 the *Baseline* simulation of ROMS-BEC to the bloom timing derived from climatological daily chlorophyll data from Globcolor (climatology from 1998-2018 based on the daily 25 km chlorophyll product, see Fanton d'Andon et al., 2009; Maritorena et al., 2010).

2.3.2 Phytoplankton competition and succession

In ROMS-BEC, phytoplankton biomass P^i (mmol C m^{-3} , $i \in \{PA, D, C, SP, N\}$) is determined by the balance between
295 growth (μ^i) and loss terms (grazing by zooplankton γ_g^i , non-grazing mortality γ_m^i , and aggregation γ_a^i , see appendix B for a full description of the model equations). Here, in order to disentangle the factors controlling the relative importance of *Phaeocystis* and diatoms for total phytoplankton biomass throughout the year, we use the metrics first introduced by Hashioka et al. (2013) and then applied to assess the competition of diatoms and coccolithophores in ROMS-BEC in Nissen et al. (2018). Same as
300 in Nissen et al. (2018), the relative growth ratio μ_{rel}^{ij} of phytoplankton i and j (e.g. diatoms and *Phaeocystis*) is defined as the ratios of their specific growth rates (μ^i , d^{-1}), which in turn depends on environmental dependencies regarding the temperature

T , nutrients N , and irradiance I , following:

$$\begin{aligned}\mu_{\text{rel}}^{\text{DPA}} &= \log \frac{\mu^{\text{D}}}{\mu^{\text{PA}}} \\ &= \log \underbrace{\frac{f^{\text{D}}(T) \cdot \mu_{\text{max}}^{\text{D}}}{\mu_{\text{T}}^{\text{PA}}}}_{\beta_{\text{T}}} + \log \underbrace{\frac{g^{\text{D}}(N)}{g^{\text{PA}}(N)}}_{\beta_{\text{N}} \sim \beta_{\text{Fe}}} + \log \underbrace{\frac{h^{\text{D}}(I)}{h^{\text{PA}}(I)}}_{\beta_{\text{I}}}\end{aligned}\quad (2)$$

In the above equation, the specific growth rate μ^i of each phytoplankton i is calculated as a multiplicative function of a temperature-limited growth rate ($f^{\text{D}}(T) \cdot \mu_{\text{max}}^{\text{D}}$ for diatoms and $\mu_{\text{T}}^{\text{PA}}$ for *Phaeocystis*; see Eq. B5 & Eq. 1), a nutrient limitation term ($g^i(N)$), limitation of each nutrient is calculated using a Michaelis-Menten function, and the most-limiting one is then used here; see Eq. B8), and a light limitation term ($h^i(I)$; see Eq. B9 and Geider et al., 1998). Further, β_{T} , β_{N} , and β_{I} describe the logarithmic ratio of the limitation by temperature, nutrients, and light of growth by diatoms and *Phaeocystis*. Thereby, these terms denote the log-normalized contribution of each environmental factor to the simulated relative growth ratio. At high-latitudes south of 60° S, the ratio of the nutrient limitation of growth β_{N} corresponds to that of the iron limitation β_{Fe} in our model (Fig. S1). Consequently, environmental conditions regarding temperature, iron, and light decide whether the relative growth ratio is positive or negative at a given location and point in time, i.e., which of the two phytoplankton types has a higher specific growth rate and hence a competitive advantage over the other regarding growth.

Similarly, the relative grazing ratio $\gamma_{\text{g,rel}}^{\text{ij}}$ of phytoplankton i and j (e.g. diatoms and *Phaeocystis*) is defined as the ratio of their specific grazing rates (γ_{g}^i , d^{-1}) following:

$$\gamma_{\text{g,rel}}^{\text{DPA}} = \log \frac{\frac{\gamma_{\text{g}}^{\text{PA}}}{P^{\text{PA}}}}{\frac{\gamma_{\text{g}}^{\text{D}}}{P^{\text{D}}}}\quad (3)$$

In ROMS-BEC, grazing on each phytoplankton i is calculated using a Holling Type II ingestion function (Nissen et al., 2018). As described in section 2.1, *Phaeocystis* and diatoms in ROMS-BEC do not only differ in parameters describing the zooplankton grazing pressure they experience, but in parameters describing their non-grazing mortality and aggregation losses as well. Therefore, in accordance with the relative grazing ratio defined above, we define the relative mortality ratio ($\gamma_{\text{m,rel}}^{\text{ij}}$) and the relative aggregation ratio ($\gamma_{\text{a,rel}}^{\text{ij}}$) of phytoplankton i and j (e.g. diatoms and *Phaeocystis*) as the ratio of their specific non-grazing mortality rates (γ_{m}^i , d^{-1}) and aggregation rates (γ_{a}^i , d^{-1}), respectively, following:

$$\gamma_{\text{m,rel}}^{\text{DPA}} = \log \frac{\frac{\gamma_{\text{m}}^{\text{PA}}}{P^{\text{PA}}}}{\frac{\gamma_{\text{m}}^{\text{D}}}{P^{\text{D}}}}\quad (4)$$

$$\gamma_{\text{a,rel}}^{\text{DPA}} = \log \frac{\frac{\gamma_{\text{a}}^{\text{PA}}}{P^{\text{PA}}}}{\frac{\gamma_{\text{a}}^{\text{D}}}{P^{\text{D}}}}\quad (5)$$

Since the total specific loss rate ($\gamma_{\text{total}}^{\text{ij}}$, d^{-1}) of phytoplankton i is the addition of its specific grazing, non-grazing mortality, and aggregation loss rates, the relative total loss ratio $\gamma_{\text{total,rel}}^{\text{ij}}$ of phytoplankton i and j (e.g. diatoms and *Phaeocystis*) is

defined as

$$\gamma_{\text{total,rel}}^{\text{DPA}} = \log \frac{\frac{\gamma_g^{\text{PA}}}{P^{\text{PA}}} + \frac{\gamma_m^{\text{PA}}}{P^{\text{PA}}} + \frac{\gamma_a^{\text{PA}}}{P^{\text{PA}}}}{\frac{\gamma_g^{\text{D}}}{P^{\text{D}}} + \frac{\gamma_m^{\text{D}}}{P^{\text{D}}} + \frac{\gamma_a^{\text{D}}}{P^{\text{D}}}} \quad (6)$$

330 If $\gamma_{\text{total,rel}}^{\text{DPA}}$ is positive, the specific total loss rate of *Phaeocystis* is larger than that of diatoms (and accordingly for the individual loss ratios in Eq. 3-5), and loss processes promote the accumulation of diatom biomass relative to that of *Phaeocystis*. While the maximum grazing rate on *Phaeocystis* is lower than that of diatoms, their non-grazing mortality and aggregation losses are higher (see section 2.1 and Table 1). Ultimately, at any given location and point in time, the interaction between the phytoplankton biomass concentrations (impacting the respective loss rates) and environmental conditions (impacting the
335 respective growth rate) will determine the relative contribution of each phytoplankton type *i* to total phytoplankton biomass. Here, we use these metrics to assess the controls on the simulated seasonal evolution of the relative importance of *Phaeocystis* and diatoms in the high-latitude SO.

3 Results

3.1 Phytoplankton biogeography and community composition in the SO

340 In the 5-PFT *Baseline* simulation of ROMS-BEC, total summer chlorophyll is highest close to the Antarctic continent (>10 mg chl m^{-3}) and decreases northwards to values <1 mg chl m^{-3} close to the open northern boundary (Fig. 1a). While this south-north gradient is in broad agreement with remotely sensed chlorophyll concentrations (Fig. 1b), our model generally overestimates high-latitude chlorophyll levels, which has already been noted for the 4-PFT setup of ROMS-BEC (Nissen et al.,
345 by 18% (40.8 Gg chl in ROMS-BEC between 30-90° S compared to 34.5 Gg chl in the MODIS Aqua chlorophyll product, Table 3, NASA-OBPG, 2014a; Johnson et al., 2013) and satellite derived NPP by 38-42% (17.2 compared to 12.1-12.5 Pg C yr^{-1} , Table 3, Behrenfeld and Falkowski, 1997; O'Malley, last access: 16 May 2016; Buitenhuis et al., 2013). This bias is largest south of 60° S, where NPP and surface chlorophyll are overestimated by a factor 1.8-4.4 and 1.8, respectively (Table 3), and the bias is likely due to a combination of underestimated high-latitude chlorophyll concentrations in satellite-derived
350 products (Johnson et al., 2013) and the missing complexity in the zooplankton compartment in ROMS-BEC, as biases in the simulated physical fields (temperature, light) have been shown to only explain a minor fraction of the simulated high-latitude biomass overestimation (Nissen et al., 2018).

The simulated carbon biomass distributions of colonial *Phaeocystis*, diatoms, coccolithophores, and SP are ~~distinctly different~~
distinct in the model (Fig. 1c-f, showing top 50 m averages). The simulated summer *Phaeocystis* biomass is highest south of
355 50° S, with highest concentrations of 10 mmol C m^{-3} at $\sim 74^\circ$ S. In the model, average *Phaeocystis* biomass concentrations quickly decline to levels <0.1 mmol C m^{-3} north of 50° S (Fig. 1c), a direct result of the restriction of *Phaeocystis* growth to temperatures $< \sim 8^\circ$ C in the model (Fig. A1a). This is in broad agreement with in situ observations, which suggest highest concentrations (>20 mmol C m^{-3}) south of $\sim 75^\circ$ S, and concentrations <5 mmol C m^{-3} north of $\sim 65^\circ$ S (Fig. 1c &

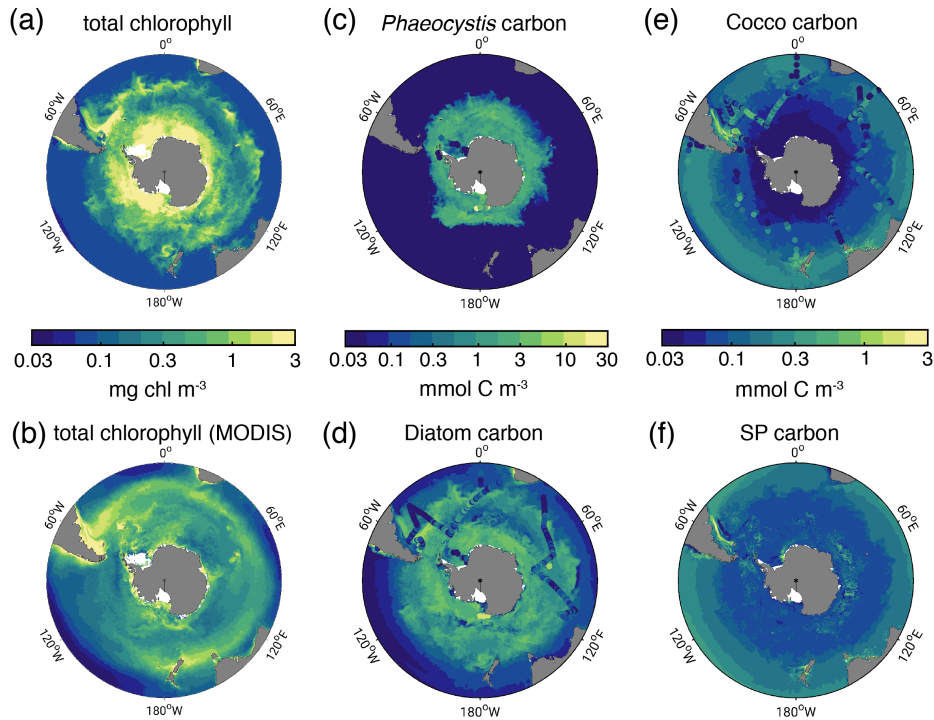


Figure 1. Biomass distributions for December-March (DJFM). Total surface chlorophyll [mg chl m^{-3}] in a) ROMS-BEC and b) MODIS-Aqua climatology (NASA-OBPG, 2014a), using the chlorophyll algorithm by Johnson et al. (2013). c)-f) Mean top 50 m c) *Phaeocystis*, d) diatom, e) coccolithophore, and f) small phytoplankton carbon biomass concentrations [mmol C m^{-3}] in ROMS-BEC. *Phaeocystis*, diatom, and coccolithophore biomass observations from the top 50 m are indicated by colored dots in c), d), and e), respectively (Balch et al., 2016; Saavedra-Pellitero et al., 2014; O'Brien et al., 2013; Vogt et al., 2012; Leblanc et al., 2012; Tyrrell and Charalampopoulou, 2009; Gravalosa et al., 2008; Cubillos et al., 2007). For more details on the biomass evaluation, see Nissen et al. (2018).

Fig. S3a-S5a & b). As a response to the addition of *Phaeocystis* to ROMS-BEC, the simulated high-latitude diatom biomass concentrations decrease compared ~~of~~ to the 4-PFT setup of the model (Nissen et al., 2018). In the 5-PFT setup, the model simulates highest diatom biomass south of 60° S with maximum concentrations of $\sim 7 \text{ mmol C m}^{-3}$ at 72° S (top 50 m mean; $\sim 17 \text{ mmol C m}^{-3}$ in 4-PFT setup) and rapidly declining concentrations north of 60° S (Fig. 1d). Nevertheless, the simulated summer diatom biomass levels are still overestimated compared to carbon biomass estimates (~~Fig. S3c, Leblanc et al., 2012~~) (Fig. S5c, Leblanc et al., 2012) and satellite derived diatom chlorophyll estimates (Soppa et al., 2014, comparison not shown).
 365 In contrast to both *Phaeocystis* and diatoms, the simulated biomass levels of coccolithophores are highest in the subantarctic (highest concentrations of 3 mmol C m^{-3} on the Patagonian Shelf, Fig. 1e & S3d), ~~and~~ Overall, their simulated SO biogeography agrees well with the position of the "Great Calcite Belt" (Balch et al., 2011, 2016) and remains largely unchanged compared to the 4-PFT setup (Nissen et al., 2018).

Table 3. Comparison of ROMS-BEC based phytoplankton biomass, production, and export estimates with available observations (given in parentheses). Data sources are given below the Table. [The reported uncertainty of the contribution of the PFTs to the simulated integrated NPP corresponds to the area-weighted spatial variability of each PFT's contribution to annual NPP \(\$1\sigma\$ in space\).](#)

		ROMS-BEC (Data)	
		30-90° S	60-90° S
Surface chlorophyll biomass	total, annual mean [Gg chl]	40.8 (34.5 ^a)	17.1 (9.5 ^a)
Diatom carbon biomass	0-200m, annual mean [Pg C]	0.059 (global ^b : 0.10-0.94)	0.015
<i>Phaeocystis</i> carbon biomass	0-200m, annual mean [Pg C]	0.019 (global ^b : 0.11-0.71)	0.010
Coccolithophore carbon biomass	0-200m, annual mean [Pg C]	0.012 (global ^b : 0.001-0.03)	0.001
NPP	Pg C yr ⁻¹	17.2 (12.1-12.5 ^c)	3.0 (0.68-1.7 ^c)
	Diatoms [%]	52.0 (±26.2)	49.1 (±19.9)
	<i>Phaeocystis</i> [%]	15.3 (±24.5)	45.8 (±20.7)
	Coccolithophores [%]	14.6 (±15.3)	0.7 (±1.0)
	SP [%]	17.2 (±16.1)	4.5 (±1.9)
POC export at 100m	Pg C yr ⁻¹	3.1 (2.3-2.96 ^d)	0.62 (0.21-0.24 ^d)

^a Monthly climatology from MODIS Aqua (2002-2016, NASA-OBPG, 2014a), SO algorithm (Johnson et al., 2013)

^b The reported estimates from the MAREDAT data base in Buitenhuis et al. (2013) are global estimates of phytoplankton biomass.

^c Monthly climatology from MODIS Aqua VGPM (2002-2016, Behrenfeld and Falkowski, 1997; O'Malley, last access: 16 May 2016), NPP climatology from Buitenhuis et al. (2013, 2002-2016)

^d Monthly output from a biogeochemical inverse model (Schlitzer, 2004) and a data-assimilated model (DeVries and Weber, 2017).

Taken together, the model simulates a phytoplankton community with substantial contributions of coccolithophores and *Phaeocystis* in the subantarctic and high-latitude SO, respectively (Fig. 2a). CHEMTAX data generally support this latitudinal trend (see Fig. 2b-d and section 2.3.1, Swan et al., 2016). Averaged over 30-90° S (60-90° S), the simulated relative contributions of *Phaeocystis*, diatoms, and coccolithophores to total chlorophyll in summer are [20±28%](#) ([33%±34%](#); [subarea mean as shown in Fig. 2b & c ±1σ in space](#)), [68±33%](#) ([64±33%](#)), and [5±17%](#) ([<1±2%](#)), respectively, in good agreement with the CHEMTAX climatology (28% (27%), 46% (48%), and 3% (1%), respectively, [Fig. 2b & e](#)). Acknowledging the uncertainty in the attribution of the group "Other" in the CHEMTAX data to a model PFT ("Other" includes dinoflagellates, cryptophytes, and chlorophytes here, see section 2.3.1), the model also captures the seasonal evolution of the relative importance of *Phaeocystis* and diatoms reasonably well, both averaged over 30-90° S (Fig. 2b) and at high SO latitudes (Fig. 2c-d). The model overestimates the contribution of *Phaeocystis* in fall ([39±14%](#) as compared to 24% in CHEMTAX) and spring ([51±22%](#) as compared to 28%) between 60-90° S and in the Ross Sea, respectively (Fig. 2c-d), but the limited number of data points available in the CHEMTAX climatology in this area and the uncertainty in the attribution of pigments in CHEMTAX to the *Phaeocystis* PFT in ROMS-BEC have to be noted (see section 2.3.1).

In the 4-PFT setup of ROMS-BEC, the simulated summer phytoplankton community south of 60° S was often almost solely composed of diatoms ([Fig. S4 and Nissen et al., 2018](#)) ([Fig. S6 and Nissen et al., 2018](#)), suggesting that the implemen-

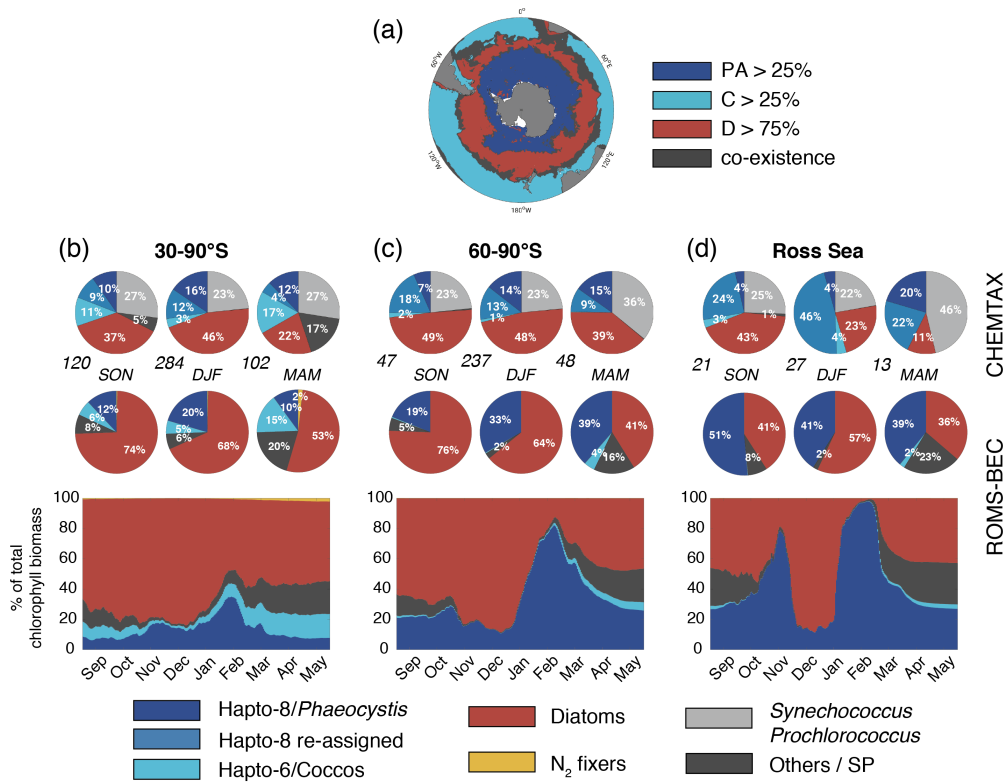


Figure 2. Spatio-temporal distribution of phytoplankton communities in the SO. a) Diatom-dominated phytoplankton community vs. mixed communities with substantial contributions of *Phaeocystis*, coccolithophores and small phytoplankton in ROMS-BEC. Communities in which neither *Phaeocystis* (PA, dark blue) or coccolithophores (C, light blue) contribute >25 % nor diatoms (D, red) contribute >75 % to total annual NPP are classified as co-existence communities (grey). b)-d) Relative contribution of the five phytoplankton PFTs to total chlorophyll biomass [mg chl m^{-3}] for b) 30-90° S, c) 60-90° S, and d) the Ross Sea. The top pie charts denote the climatological mixed layer average community composition suggested by CHEMTAX analysis of HPLC pigments for spring, summer, and fall, respectively (the total number of available observations for a given region and season is given at the lower left side, Swan et al., 2016), and the lower pie charts denote the corresponding community structure in the top 50 m in ROMS-BEC. Note that the categories in the CHEMTAX analysis are not 100% equivalent to the model PFTs. Here, “others” in the CHEMTAX fractions corresponds to dinoflagellates, cryptophytes, and chlorophytes, and “Hapto-8 reassigned” corresponds to the contribution of Hapto-6 where the temperature is $<2^\circ\text{C}$ (see also section 2.3.1). The panels at the bottom denote the daily contribution of each PFT in ROMS-BEC to total surface chlorophyll biomass.

385 (Fig. 2). Concurrently, as the distribution of silicic acid and nitrate is directly impacted by the relative importance of silicifying and non-silicifying phytoplankton, such as *Phaeocystis*, in the community, the addition of *Phaeocystis* to the model led to an improvement in the simulated high-latitude nutrient distributions when comparing to climatological data from the World Ocean Atlas (WOA, Fig. S5d-f, Garcia et al., 2014b) (WOA, Fig. S7d-f, Garcia et al., 2014b). Upon the addition of *Phaeocys-*

390 *tis*, the zonal average location of the silicate front, i.e., the latitude at which nitrate and silicic acid concentrations are equal (Freeman et al., 2018), is shifted northward by $\sim 7^\circ$ C in ROMS-BEC (from 57.1° S in 4-PFT setup to 50° S in 5-PFT setup, see Fig. S6S8). While this is further north than suggested by WOA data (56.5° S, Fig. S6b and Garcia et al., 2014b) (56.5° S, Fig. S8b and Garcia et al., 2014b), this can certainly be expected to affect the competitive fitness of individual phytoplankton types in the subantarctic and possibly at lower latitudes, which we did not assess further in this study. Overall, our model ~~suggests~~ agrees with observational data that *Phaeocystis* is an important member of the high-latitude phytoplankton 395 community. In the remainder of the manuscript, we will therefore explore the temporal variability in the relative importance of diatoms and *Phaeocystis* and its implications for SO carbon cycling in more detail.

3.2 ~~Patterns of phytoplankton~~ Phytoplankton phenology and the seasonal succession of *Phaeocystis* and diatoms

Maximum total chlorophyll concentrations are simulated for the first half of December across latitudes in ROMS-BEC (solid blue line in Fig. 3a). ~~At~~, and at high SO latitudes south of 60° S, ~~this is total chlorophyll blooms start already in late~~ 400 September in the model (not shown). Thereby, the model-derived timing of total chlorophyll bloom start and peak is 2-3 and 1-2 months earlier than suggested by satellite estimates (black line in Fig. 3a), respectively, than satellite-derived estimates (for bloom peak, see black line in Fig. 3a, for bloom start, see e.g. Thomalla et al., 2011). Yet, compared to the 4-PFT setup (dashed blue line in Fig. 3a), the simulated timing of peak chlorophyll levels improved in this study, with peak chlorophyll delayed by on average a week in the model upon the implementation of *Phaeocystis*. The simulated physical biases (i.e., generally too high temperatures and too shallow mixed layer depths, both favoring an earlier onset of the phytoplankton bloom, 405 see Nissen et al., 2018) only partially explain the bias in the simulated timing of maximum chlorophyll levels (see red and green dashed lines in Fig. S7aS9a), suggesting that biological factors must explain the difference between ROMS-BEC and the satellite product. As diatoms dominate the phytoplankton community at peak total chlorophyll concentrations ~~everywhere for~~ all latitudinal averages in the model domain (compare their bloom timing in Fig. 3c to Fig. 3a and to the simulated community 410 composition in Fig. 2b-d, but note that *Phaeocystis* often dominate in coastal areas, not shown), the mismatch in timing is likely related to the representation of this PFT in the model, and is possibly at least partly caused by their comparatively high growth rates at low temperatures (see Fig. A1a).

In contrast to diatoms, maximum zonally averaged chlorophyll concentrations of *Phaeocystis* are simulated for late November or early December across most latitudes in the model (only around 70° S a peak in late January is simulated, Fig. 3b; note 415 that locally, maximum *Phaeocystis* chlorophyll concentrations exceed 10 mg chl m^{-3} , not shown here). Overall, the timing of simulated peak *Phaeocystis* chlorophyll levels corresponds well to the suggested timing of observed maximum seawater DMSP concentrations (peak in November/December in Curran et al., 1998; Curran and Jones, 2000) and the delayed maximum atmospheric DMS concentrations (January/February, e.g. Nguyen et al., 1990; Ayers et al., 1991). This further corroborates the hypothesis that the bias in the timing of maximum total chlorophyll levels in ROMS-BEC is likely caused by how diatoms are 420 parameterized in the model ~~-(see e.g. the rather high temperature-limited growth rate of diatoms at low temperatures compared to available laboratory data, see Fig. A1).~~ Taken together, the model simulates a succession from *Phaeocystis* to diatoms close to the Antarctic continent (south of 72° S, see also Fig. S7bS9b) and in some parts of the open ocean north of 68° S (Fig. 3d

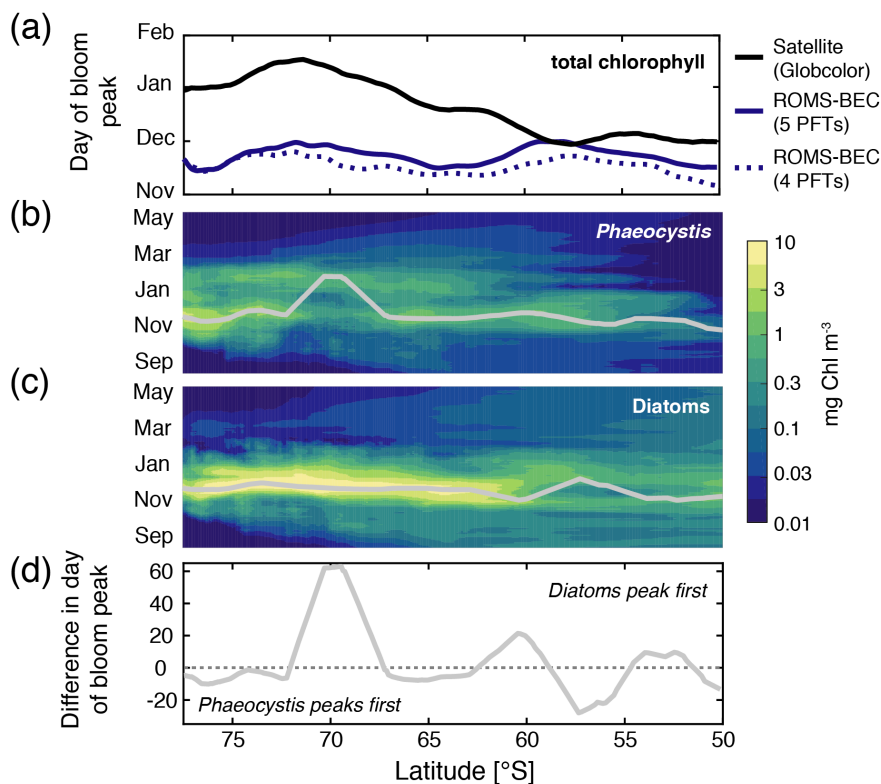


Figure 3. Hovmoller plots south of 50° S of a) the day of maximum total chlorophyll concentrations in a satellite product (black line, Globcolor climatology from 1998-2018 based on the daily 25 km chlorophyll product, see Fanton d'Andon et al., 2009; Maritorena et al., 2010), the *Baseline* simulation of this study (solid blue line), and the *Baseline* simulation of Nissen et al. (2018, dashed blue line; without *Phaeocystis*), and daily surface b) diatom and c) *Phaeocystis* chlorophyll biomass concentrations [mg chl m^{-3}]. Overlain are the average day of the peak concentrations for each latitude (see also section 2.3.1). Panel d) denotes the difference in days in the timing of the bloom peak of diatoms and *Phaeocystis* for each latitude, with negative values denoting a succession from *Phaeocystis* to diatoms throughout the season.

& Fig. S7bS9b). The difference in the timing of the bloom peak between the two PFTs is largely <10 days when averaged zonally, but locally exceeds 30 days when looking at individual grid cells in the model (Fig. S7bS9b), in broad agreement with observations, which suggest up to 2 months between the peak chlorophyll concentrations of *Phaeocystis* and diatoms in the Ross Sea (see e.g. Peloquin and Smith, 2007; Smith et al., 2011). Subsequently, we will assess how environmental conditions and biomass loss processes interact to control the competition between *Phaeocystis* and diatoms at high SO latitudes.

3.3 Drivers of ~~SO phytoplankton~~ the high-latitude biogeography, phenology, and seasonal succession patterns of *Phaeocystis* and diatoms

430 Relating the observed or simulated PFT biomass concentrations to the concurrent environmental conditions allows for an assessment of the ecological niche of the PFT in question. In ROMS-BEC, *Phaeocystis* and diatoms occupy distinct ecological

niches in the *Baseline* simulation, in agreement with their distinct geographic distributions in summer (Fig. 1c-d). Between 40-90° S, the niche center of DJFM average *Phaeocystis* biomass is simulated at a nitrate concentration of 18.8 mmol m⁻³ (inter quartile range (IQR) 16.6-20.5 mmol m⁻³), a temperature of 1.1° C (IQR -0.2-2.6° C), and MLPAR of 27.8 W m⁻² (IQR 24.3-32 W m⁻², Fig. 4a & c). Since the diatom PFT in ROMS-BEC represents multiple species (in contrast to the *Phaeocystis* PFT), diatoms occupy a wider niche in temperature (IQR 0.8-8.5° C, niche center at 5° C) and nitrate (IQR 11-19.5 mmol m⁻³, niche center at 15.5 mmol m⁻³) in the model, which is in agreement with the ecological niches of important SO diatom and *Phaeocystis* species derived by Brun et al. (2015) based on presence/absence observations and species distribution models (Fig. 4a & b). In ROMS-BEC, the niche center is only at marginally higher MLPAR for diatoms than for *Phaeocystis* (28.9 W m⁻² compared to 27.8 W m⁻², respectively, Fig. 4c & d) and is at higher MLPAR for both PFTs than available observations for important SO species suggest (~10 W m⁻² and ~20 W m⁻² for *Phaeocystis* and diatoms, respectively, see Fig. 4c & d). While this bias in the MLPAR niche is consistent with the mixed layer depth bias in ROMS-BEC (~10 m; Nissen et al., 2018), the small difference in the MLPAR niche center between *Phaeocystis* and diatoms implies a minor role for MLPAR in controlling the differences in DJFM average biomass concentrations of these two PFTs (Fig. 1c-d). With regard to iron, the two PFTs do not occupy distinct ecological niches in ROMS-BEC (niche centers at 0.32 μmol m⁻³ for both PFTs, see Fig. S9S3). Yet, as all simulated phytoplankton growth is most limited by iron availability in the high-latitude SO compared to the availability of other nutrients (Fig. S1), this suggests that the spatio-temporal averaging applied for the niche analysis here potentially precludes the assessment of the role of iron in the competition between *Phaeocystis* and diatoms, especially on a sub-seasonal scale. We conclude that the simulated ecological niches of *Phaeocystis* and diatoms are largely in agreement with available observations, but acknowledge the difficulties in comparing the ecological niche of a model PFT to those of individual phytoplankton species or groups, a sampling bias towards temperate and tropical species/strains and the overall low data coverage in the high-latitude SO in Brun et al. (2015), and the limitation of this niche analysis to inform about the role of top-down factors and sub-seasonal environmental variability in controlling the simulated biogeography of phytoplankton types.

The temporal evolution of the relative growth ratio, i.e., the ratio of the specific growth rates of diatoms and *Phaeocystis*, informs about the competitive advantage of one PFT over the other throughout the year due to bottom-up factors and can be broken down into the different environmental contributors for each phytoplankton type at any point in time (Eq. 2). In the 5-PFT *Baseline* simulation of ROMS-BEC, the relative growth ratio is only positive ($\mu^D > \mu^{PA}$) between early December and early February between 60-90° S (μ^D is on average 5% larger than μ^{PA} in summer, but 5-6% smaller in the other seasons, Fig. 5a & c) and only between mid-December and mid-January in the Ross Sea (μ^{PA} is up to 38% larger than μ^D in spring, Fig. 5b & d). Hence, bottom-up factors promote the accumulation of *Phaeocystis* relative to diatom biomass over much of the year, particularly in the Ross Sea. In both areas, as expected from the chosen half-saturation constants ($k_{Fe}^{PA} > k_{Fe}^D$; Table 1), the iron limitation of *Phaeocystis* growth is stronger than that of diatoms in the model, and iron availability is an advantage for diatoms at all times ($\beta_{Fe} > 0$; up to 14% stronger iron limitation of *Phaeocystis* in both areas in summer, blue areas in Fig. 5a-d). Yet, the two subareas differ in the simulated temperature and light limitation of growth of *Phaeocystis* and diatoms. Overall, temperature is limiting diatom growth more than *Phaeocystis* growth in both subareas throughout the year ($\beta_T < 0$), but this difference is

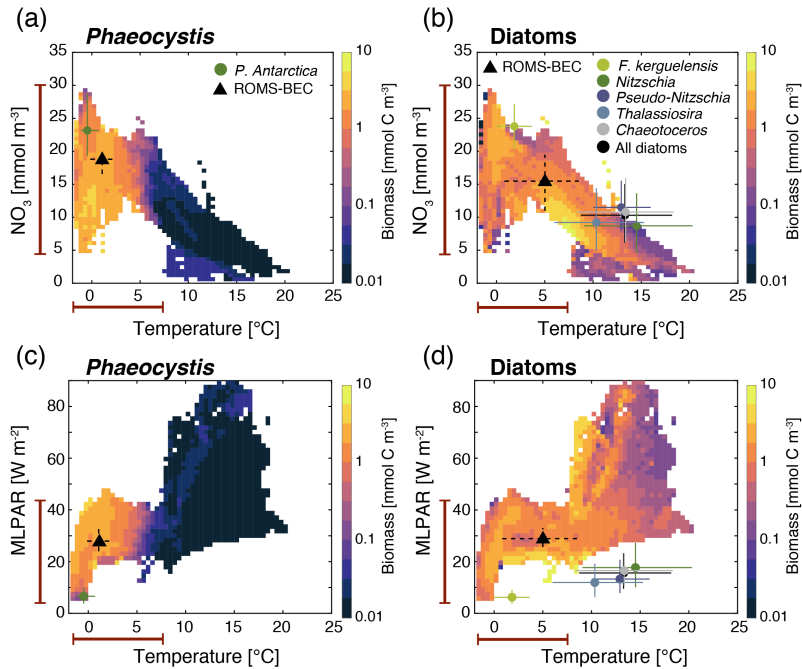


Figure 4. Simulated DJFM average top 50 m average a) & c) *Phaeocystis* and b) & d) diatom carbon biomass concentrations (mmol C m⁻³) south of 40° S as a function of the simulated temperature (° C) and a)-b) nitrate concentrations (mmol N m⁻³) and c)-d) mixed layer PAR levels (W m⁻²). Overlain are the observed ecological niche centers (median) and breadths (inter quartile ranges) for example taxa of the two functional types from Brun et al. (2015, circles and solid lines) and as simulated in ROMS-BEC (triangles and dashed lines; area and biomass weighted). The red bars on the axes indicate the simulated range of the respective environmental condition in ROMS-BEC between 60-90° S and averaged over DJFM and the top 50 m.

rather small in summer between 60-90° S (5%, but up to 19% stronger growth limitation in the Ross Sea, red areas in Fig. 5a-d, see also Fig. A1). Similarly, the difference in light limitation between diatoms and *Phaeocystis* is rather small between 60-90° S (3-4% throughout the year, yellow areas in Fig. 5a & c), implying that their differences in α_{PI} (43% higher for *Phaeocystis*, see Table 1) are balanced by differences in photoacclimation in ROMS-BEC in this area (see Eq. B9 and Geider et al., 1998) (see Eq. B9 and Geider et al., 1998, note that $\theta_{chl:N,max}^D > \theta_{chl:N,max}^{PA}$ see Table 1). In contrast, in the Ross Sea, differences in light limitation between diatoms and *Phaeocystis* are large, especially in spring (the growth of diatoms is 32% more light limited; Fig. 5b & d). Therefore, the difference in light limitation predominantly controls the seasonality of the relative growth ratio (Fig. 5b) and promotes the dominance of *Phaeocystis* over diatoms early in the growing season in this area in our model (Fig. 5j), which is not simulated when averaging over 60-90° S (Fig. 5i). Nevertheless, acknowledging the sensitivity of the simulated *Phaeocystis* and diatom biomass levels to all chosen model parameters describing the growth of the respective PFT (the annual mean biomass changes by >17% and >14% for *Phaeocystis* and diatoms, respectively, in the experiments TEMPERATURE, ALPHA_{PI}, and IRON, Fig. A2 & Fig. S4-S10), the sensitivity simulations support the importance of light

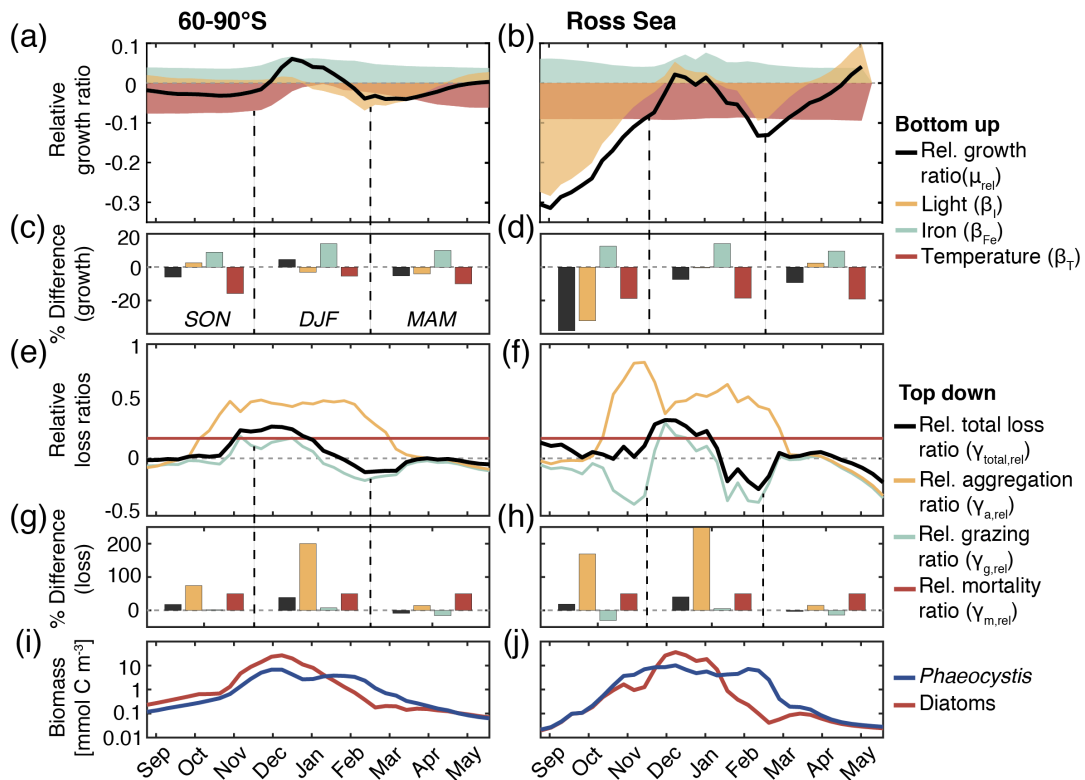


Figure 5. a) & b) Relative growth ratio (black) of diatoms vs. *Phaeocystis*. The colored areas are the contributions of the limitation of growth by light (yellow, β_L), iron (blue, β_{Fe}), and temperature (red, β_T , see Eq. 2). c) & d) Seasonally averaged percent difference between diatoms and *Phaeocystis* in the specific growth rate (black), light limitation (yellow), iron limitation (blue), and temperature limitation (red). Calculated from non-log-transformed ratios, i.e., e.g. black bar corresponds to $10^{\mu_{rel}^{DPA}}$ (see Eq. 2). e) & f) Relative total loss ratio (black) of diatoms vs. *Phaeocystis*, with contributions of the relative grazing ratio (blue), relative non-grazing loss ratio (red), and relative aggregation ratio (yellow, see Eq. 3-6). g) & h) Seasonally averaged percent difference between diatoms and *Phaeocystis* in the total specific loss rate (black), specific aggregation rate (yellow), specific grazing rate (blue), and specific mortality rate (red), calculated from non-log-transformed ratios. i) & j) *Phaeocystis* (blue) and diatom (red) surface carbon biomass concentrations [mmol C m^{-3}]. For all metrics, the left panels are surface averages over 60-90° S and those on the right for the Ross Sea.

in controlling the annual mean high-latitude phytoplankton community structure for both subareas, as the elimination of the
480 differences in α_{PI} between the PFTs results in the largest biomass changes both between 60-90° S (-76% and +52% for
Phaeocystis and diatoms, respectively) and in the Ross Sea (-87% and +86%, Fig. A2). Altogether, in ROMS-BEC, differences
in growth between diatoms and *Phaeocystis* are mostly controlled by seasonal differences in iron/temperature (60-90° S) and
iron/light conditions (Ross Sea), respectively. Still, given the simulated growth advantage of *Phaeocystis* throughout much of
the growing season in both subareas, bottom-up factors alone cannot explain why *Phaeocystis* only dominates over diatoms
485 temporarily (Fig. 5i & j), implying that top-down factors need to be considered to explain their biomass evolution in our model.

In both subareas, the simulated relative total loss ratio is positive throughout spring and summer, implying that the specific total loss rate of *Phaeocystis* is higher than that of diatoms ($\gamma_{\text{total}}^{\text{PA}} > \gamma_{\text{total}}^{\text{D}}$, see Eq. 6), which favors the accumulation of diatom biomass relative to that of *Phaeocystis* (Fig. 5e-h). In fact, the total loss rate of *Phaeocystis* is on average 17%/38% (60-90° S) and 18%/40% (Ross Sea) higher than that of diatoms in spring/summer (Fig. 5g & h), despite the higher prescribed maximum grazing rate on *Phaeocystis* in ROMS-BEC (Table 1). In the model, the relative total loss ratio is only negative in early fall in both subareas ($\gamma_{\text{total}}^{\text{D}} > \gamma_{\text{total}}^{\text{PA}}$, Fig. 5e & f), but the difference between diatoms and *Phaeocystis* in their specific total loss rates is rather small in this season (9% and 3% between 60-90° S and in the Ross Sea, respectively, Fig. 5g & h). In all top-down sensitivity experiments, the simulated change in *Phaeocystis* biomass levels is larger than for the bottom-up experiments (>20% for experiments GRAZING, AGGREGATION, and MORTALITY, see Fig. A2), and the dominance of *Phaeocystis* over diatoms increases in magnitude and duration both between 60-90° S and in the Ross Sea if disadvantages of *Phaeocystis* in the loss processes are eliminated (Fig. S4S10). The simulated seasonality of the total loss ratio is the result of the interplay between losses through grazing, aggregation, and non-grazing mortality of each phytoplankton type in ROMS-BEC (Eq. 6, colors in Fig. 5e-h). Of all three loss pathways, differences in aggregation losses in the *Baseline* simulation are largest between *Phaeocystis* and diatoms both between 60-90° S (up to 200% higher aggregation losses for *Phaeocystis* in summer, yellow in Fig. 5e & g) and in the Ross Sea (up to 250% higher in summer, Fig. 5f & h). In comparison, differences between *Phaeocystis* and diatoms in grazing (up to 16% and 14% between 60-90° S and in the Ross Sea, respectively) and mortality losses (50% everywhere) are considerably smaller (see blue and red areas in Fig. 5e-h, respectively), suggesting that aggregation losses predominantly contribute to the simulated differences in the total loss rates between *Phaeocystis* and diatoms.

In summary, between 60-90° S, the simulated growth advantage of *Phaeocystis* early in the season (facilitated by advantages in the temperature limitation of their growth) are not large enough to outweigh the disadvantages in iron limitation of their growth and in the biomass losses they experience. As a result, in spring and summer, *Phaeocystis* do not accumulate substantial biomass relative to (or even dominate over) diatoms in this subarea in ROMS-BEC. In the Ross Sea, however, the simulated growth advantages of *Phaeocystis* (resulting from advantages in the light and temperature limitation of their growth) are large enough to outweigh the disadvantages in iron limitation and specific biomass loss rates, allowing them to dominate over diatoms early in the growing season in our model and explaining the simulated succession from *Phaeocystis* to diatoms close to the Antarctic continent (see also section 3.2). Ultimately, this simulated spatio-temporal variability in the relative importance of *Phaeocystis* and diatoms has implications for SO carbon cycling, which we will assess in the following.

3.4 Quantifying the importance of *Phaeocystis* for the SO carbon cycle

Phaeocystis is an important member of the SO phytoplankton community in our model, particularly south of 60°S, where it contributes $46 \pm 21\%$ and $40 \pm 20\%$ to total annual NPP and POC formation, respectively (Table 3 & Fig. 6). Even when considering the entire region south of 30°S, the contribution of *Phaeocystis* to NPP ($15 \pm 24\%$) and POC production ($16 \pm 22\%$) is sizeable. The simulated spatial differences in phytoplankton community structure have direct implications for the fate of organic carbon upon biomass loss, and Fig. 6 illustrates the annually integrated importance of different pathways of POC formation related to each PFT in ROMS-BEC. Overall, in our model, the p ratio, i.e., the fraction of NPP that is transformed to

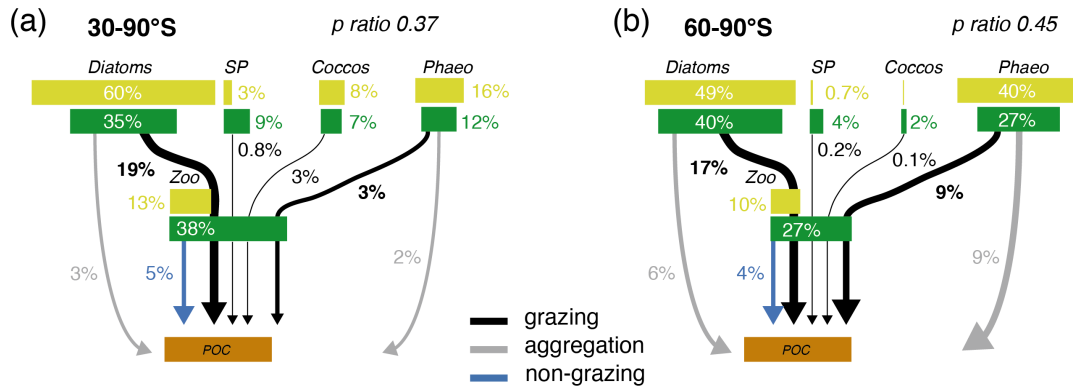


Figure 6. Pathways of particulate organic carbon (POC) formation in the *Baseline* simulation of ROMS-BEC averaged annually over a) 30-90° S and b) 60-90° S. The [results for the Ross Sea are comparable to those between 60-90° S \(see Fig. S11\)](#). The green and yellow boxes show the relative contribution (%) of *Phaeocystis*, diatoms, coccolithophores, small phytoplankton (SP), and zooplankton (Zoo) to the combined phytoplankton and zooplankton biomass (green) and total POC production (yellow) in the top 100 m, respectively. The arrows denote the relative contribution of the different POC production pathways associated with each PFT (black = grazing by zooplankton, grey = aggregation, blue = non-grazing mortality), given as % of total NPP in the top 100 m. Numbers are printed if $\geq 0.1\%$ and rounded to the nearest integer if $> 1\%$. The sum of all arrows gives the POC production efficiency, [i.e., the fraction of NPP which is converted into sinking POC upon biomass loss](#) (p ratio). Note that diazotrophs are not included in this figure due to their minor contribution to NPP in the model domain.

520 sinking POC (Laufkötter et al., 2016), is higher at high latitudes south of 60° S (45%) than the domain average (37%, Fig. 6). This is a direct result of the higher fraction of large phytoplankton types, i.e., *Phaeocystis* and diatoms, in the ecosystem south of 60° S (67% of total carbon biomass) than between 30-90° S (47%; Fig. 6, but see also Fig. 2), facilitating more carbon export relative to NPP in the model. In fact, our model results suggest that these two large phytoplankton types contribute more to POC formation than to total biomass (76% and 89% of total POC formation between 30-90° S and 60-90° S, respectively; 525 compare yellow and green boxes in Fig. 6). Integrated annually, diatoms contribute most of all PFTs to POC formation in our model (60% and 49% between 30-90° S and 60-90° S, respectively, Fig. 6). For both diatoms and *Phaeocystis*, grazing by zooplankton (i.e., the formation of fecal pellets) is the most important pathway of POC production in ROMS-BEC (black arrows in Fig. 6, 9%/52% and 20%/37% of total POC production for *Phaeocystis*/diatoms between 30-90° S and 60-90° S, respectively). Yet, at high latitudes (60-90° S), aggregation of *Phaeocystis* biomass contributes significantly to POC formation 530 (20% of total POC production, 9% of NPP, grey arrows in Fig. 6b). Given that the loss of biomass via a given pathway is a function of the local biomass concentrations of each PFT at any given point in time (see section 2.1 and appendix B), the relative importance of any PFT or biomass loss pathway for total POC formation and hence the total POC produced vary throughout the year.

The seasonal variability in total POC formation is governed by the variability in total chlorophyll concentrations both between 30-90° S and 60-90° S, and peak POC formation rates of $35 \text{ mmol m}^{-2} \text{ d}^{-1}$ (30-90° S) and $65 \text{ mmol m}^{-2} \text{ d}^{-1}$ (60-90° S) 535

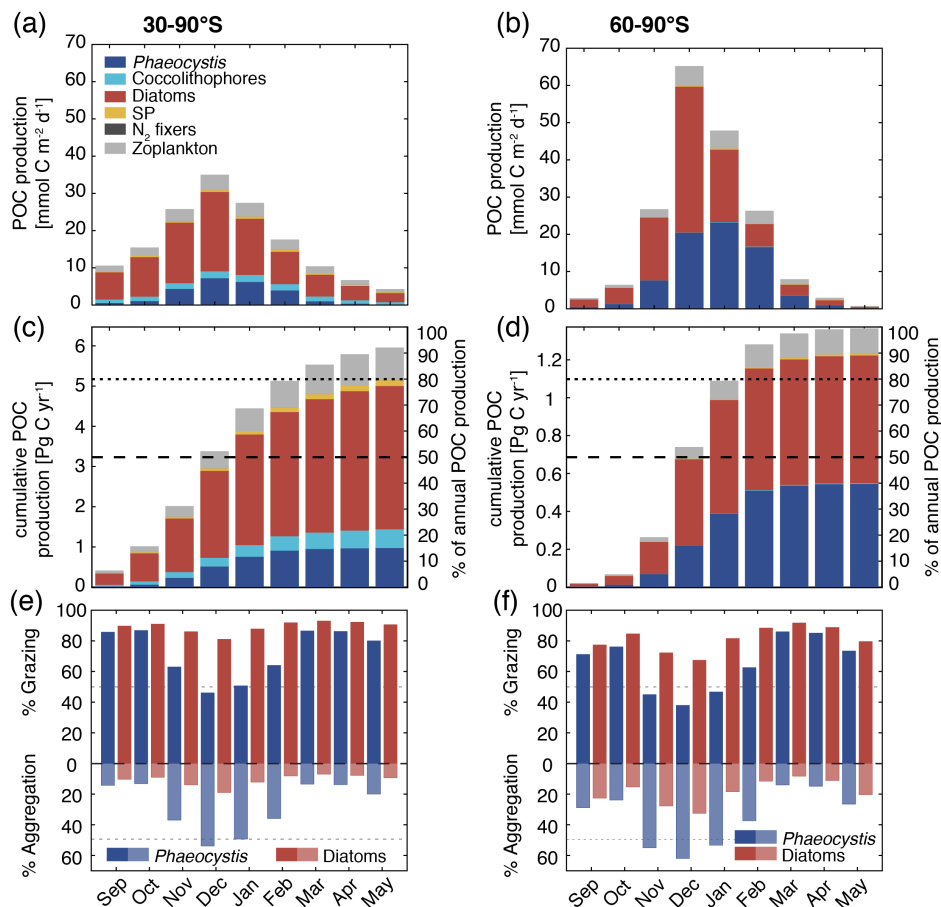


Figure 7. Simulated vertically integrated production of particulate organic carbon (POC) a) & b) as a function of time [$\text{mmol C m}^{-2} \text{d}^{-1}$], c) & d) cumulative over time (absolute production in Pg C yr^{-1} on the left axis and relative to annually integrated production on the right axis), and e) & f) as a function of time via grazing and aggregation, respectively. The colors correspond to the different PFTs in ROMS-BEC, and the panels correspond to averages or integrals over $30\text{-}90^\circ \text{S}$ (left) and $60\text{-}90^\circ \text{S}$ (right), respectively. [The results for the Ross Sea are comparable for those between \$60\text{-}90^\circ \text{S}\$ \(see Fig. S11\).](#)

are simulated for December in ROMS-BEC (Fig. 7a & b; compare to Fig. 3a). Similarly, the contribution of *Phaeocystis* and diatoms to total POC formation closely follows their contribution to total biomass over the year, with the contribution of *Phaeocystis* peaking in January (23%) and February (63%) for $30\text{-}90^\circ \text{S}$ and $60\text{-}90^\circ \text{S}$, respectively (Fig. 7a & b; compare timing to Fig. 2b & c). As a result of the close link between POC formation and chlorophyll concentrations in ROMS-BEC, the majority of the annual POC formation occurs between November and February in our model (64% and 88% south of 30°S and 60°S , respectively, Fig. 7c & d). During these months, the simulated pathways of POC formation differ from the annually integrated perspective in Fig. 6, especially for *Phaeocystis*. While grazing is the most important pathway throughout the year for diatoms in both subareas in our model (red bars in Fig. 7e & f), aggregation of *Phaeocystis* is as important as grazing in December and

January between 30-90° S (blue bars in Fig. 7e) and even dominantly contributes to POC formation between November and
545 January at high SO latitudes (up to 65%, blue bars in Fig. 7f). Altogether, this implies that both spatial and temporal variations
in SO phytoplankton community structure critically impact the fate of carbon beyond the upper ocean.

4 Discussion

4.1 Drivers of phytoplankton biogeography and the competition between *Phaeocystis* and diatoms

In ROMS-BEC, the interplay of iron availability with temperature (60-90° S) and light levels (Ross Sea), respectively, largely
550 controls the competitive fitness of *Phaeocystis* relative to diatoms in the high-latitude SO. Yet, differences in the simulated
biomass loss rates between the two PFTs (in particular via aggregation) need to be considered in order to explain why peak
Phaeocystis biomass levels precede those of diatoms only close to the Antarctic continent in the model. In the literature, the
spatial distribution of *Phaeocystis* and diatoms and the temporal succession from *Phaeocystis* to diatoms is almost exclusively
discussed in terms of light and iron availability (see e.g. Arrigo et al., 1999; Smith et al., 2014). In this context, regions/times of
555 low light and/or high mixed layer depth are typically associated with high *Phaeocystis* abundance (Alvain et al., 2008; Smith
et al., 2014), explaining their bloom in spring, whereas iron availability has been suggested to largely control the magnitude of
the summer diatom bloom (Peloquin and Smith, 2007; Smith et al., 2011). This is in agreement with the simulated dynamics
and parameters chosen in ROMS-BEC, in which the difference in light limitation between growth of *Phaeocystis* and diatoms
facilitates early *Phaeocystis* blooms in the Ross Sea. Yet, it has to be noted that advantages in temperature limitation contribute
560 to the growth advantage of *Phaeocystis* in the high-latitude SO in ROMS-BEC as well and without it, *Phaeocystis* would
contribute substantially less to high-latitude phytoplankton biomass (Fig. A2). Currently, this growth advantage of *Phaeocystis*
at temperatures <4° C is possibly underestimated in the model, as diatom growth at low temperatures is currently overestimated
when comparing to available laboratory measurements (Fig. A1a). Nevertheless, in agreement with Peloquin and Smith (2007)
and Smith et al. (2011), when diatoms reach peak chlorophyll levels in summer in our model, the simulated difference in iron
565 limitation between the two PFTs is largest across the high-latitude SO (Fig. 5a & b), suggesting that any change in summer
iron availability will indeed strongly impact peak diatom and hence total chlorophyll levels in ROMS-BEC.

An important limitation in the assessment of the role of iron in controlling the relative importance of *Phaeocystis* in the
high-latitude phytoplankton community is the assumption of a constant k_{Fe} of *Phaeocystis* in the model ($0.2 \mu\text{mol m}^{-3}$, Table
1). In laboratory experiments, the affinity of *Phaeocystis* for iron has been shown to be sensitive to light (Garcia et al., 2009),
570 which is not accounted for in the *Baseline* simulation of ROMS-BEC. In order to assess the possible effect of a varying
 k_{Fe} on the competition between *Phaeocystis* and diatoms, we fit a polynomial function to describe the k_{Fe} of *Phaeocystis*
as a function of the light level (VARYING_kFE simulation in Table 2, Fig. A1b, Garcia et al., 2009). Acknowledging the
uncertainty in the fit, our model simulates $k_{Fe} < 0.2 \mu\text{mol m}^{-3}$ only at highest light intensities in summer and mostly close
to the surface, and $0.2 \mu\text{mol m}^{-3} < k_{Fe} \leq 0.26 \mu\text{mol m}^{-3}$ elsewhere as a result of low light levels (Fig. S10a-S12a & b).
575 While the contribution of *Phaeocystis* to total NPP is only affected to a lesser extent as a consequence (37% and 13% south of
60° S and 30° S, respectively, instead of 46% and 15% in the *Baseline* simulation), the simulated phytoplankton seasonality

is impacted substantially. The maximum chlorophyll levels of diatoms occur earlier than those of *Phaeocystis* in many more places of the SO compared to the *Baseline* simulation, both in coastal areas and in the open ocean (Fig. S10e-S12c & d). Thus, in order to include light-iron interactions in future modeling efforts with *Phaeocystis* and to assess their impact on the competition of *Phaeocystis* with diatoms throughout the SO, additional measurements are needed for how k_{Fe} varies, but also e.g. α_{PI} and the Fe:C uptake ratio of phytoplankton vary as a function of the surrounding light level. Taken together, given the likely underestimation of the growth advantage of *Phaeocystis* in temperature and at least occasionally in iron in ROMS-BEC, we probably currently underestimate the competitive advantage in growth of *Phaeocystis* relative to diatoms in the model. However, such a potential underestimation in growth advantage does not automatically mean that the contribution of *Phaeocystis* to the phytoplankton community is underestimated as well. This is because of the important role of biomass loss processes to explain why *Phaeocystis* do not outcompete diatoms everywhere in the high latitudes in ROMS-BEC (Fig. 5). Furthermore, the simulated spatio-temporal variability of the high-latitude phytoplankton community structure is in good agreement with available observations agreement with that suggested by available pigment data (Fig. 2).

Loss processes, such as aggregation and grazing, clearly matter for the competitive advantage of one PFT over another, but these loss processes are generally not well quantified and often not studied with sufficient detail. For example, while the modeling study by Le Quéré et al. (2016) demonstrates the importance of such top-down control for total SO phytoplankton biomass concentrations, an analysis of the impact on phytoplankton community structure is yet to be done. In fact, in the literature, only few studies discuss the role of top-down factors for the relative importance of *Phaeocystis* and diatoms in the high-latitude SO (Granéli et al., 1993; van Hilst and Smith, 2002). Consequently, very little quantitative information exists to constrain model parameters (see section 2.1) or to validate the simulated non-grazing mortality, grazing, or aggregation loss rates of *Phaeocystis* and diatoms over time. In agreement with our results, aggregation has been suggested to be an important process facilitating high POC export when *Phaeocystis* biomass is high (Asper and Smith, 1999; Ducklow et al., 2015; Asper and Smith, 2019), but to what extent this process significantly contributes to the observed relative importance of *Phaeocystis* and diatoms throughout the year in the high-latitude SO remains largely unknown.

~~Our findings suggest an important role for biomass loss processes in controlling the relative importance of *Phaeocystis* and diatoms in ROMS-BEC, but very little quantitative information exists to constrain model parameters (see section 2.1) or to validate the simulated non-grazing mortality, grazing, or aggregation loss rates of *Phaeocystis* and diatoms over time.~~ Certainly, the simulated aggregation rates in the model and their impact on spatio-temporal distributions of PFT biomass concentrations and rates of NPP are associated with substantial uncertainty due to the immediate conversion of biomass to sinking detritus in the model, the equal treatment of POC originating from all PFTs, the neglect of disaggregation, and due to the calculation of aggregation rates based on the biomass concentrations of individual PFTs rather than all PFTs or even particles combined (see e.g. Turner, 2015). Given that the simulated biomass distributions in ROMS-BEC are most sensitive to differences in parameters describing non-grazing mortality (e.g. viral lysis) and aggregation (Fig. A2 & S11), any changes in these loss processes will significantly impact the relative abundance of *Phaeocystis* and diatoms in the SO. Additionally, as discussed in Nissen et al. (2018), the lack of multiple zooplankton groups in the SO model (Le Quéré et al., 2016) and the parametrization of the single zooplankton grazer using fixed prey preferences and separate grazing on each prey using a Holling Type II function (Holling,

1959), which thus precludes a saturation of feeding at high total phytoplankton biomass, are major limitations of ROMS-BEC. To what extent accounting implicitly for grazing by higher trophic levels in the non-grazing mortality term makes up for not including more zooplankton PFTs remains unclear. Nevertheless, by changing the overall coupling between phytoplankton and zooplankton and through the distinct grazing preferences of the different zooplankton types, the addition of larger zooplankton grazers would likely change the simulated temporal evolution of *Phaeocystis* and diatom biomass in the model (Le Quéré et al., 2016). Therefore, the above mentioned uncertainties should be addressed by future in situ or laboratory measurements in order to better constrain the simulated biomass loss processes, as our findings suggest these to be necessary to explain the seasonal evolution of the relative importance of *Phaeocystis* and diatoms in the high-latitude SO.

620 4.2 Biogeochemical implications of high-latitude SO **phytoplankton** *Phaeocystis* biogeography

Based on our model results, *Phaeocystis* is a substantial contributor to global NPP and POC export. Comparing the integrated NPP and POC export between 30-90° S in ROMS-BEC with data-based estimates of global NPP and POC export suggests that SO *Phaeocystis* alone contribute about 5% to globally integrated NPP (58 ± 7 Pg C yr⁻¹, Buitenhuis et al., 2013), and about the same percentage to global POC export (9.1 ± 0.2 Pg C yr⁻¹, DeVries and Weber, 2017). Thereby, our simulated contribution of *Phaeocystis* to global NPP is higher than that found in the previous modeling study by Wang and Moore (2011), particularly at higher latitudes, where Wang and Moore (2011) diagnosed a contribution of 23% to NPP south of 60° S ($46 \pm 21\%$ in ROMS-BEC). We interpret the difference to stem primarily from differences in parameter choices of the PFTs between the two models. For example, the lower ratio of the half-saturation constants of iron of *Phaeocystis* and diatoms in our model (25%; Table 1) as compared to the one in Wang and Moore (2011, 125%) leads to a larger growth advantage of *Phaeocystis* over diatoms in our model. In fact, differences in model parameters between *Phaeocystis* and diatoms in ROMS-BEC can alter the simulated contribution of *Phaeocystis* to total NPP from 5-32% and 17-63% between 30-90° S and 60-90° S, respectively (see section 2.2 and also section A1). This illustrates how single model parameters sensitively impact the competitive success of *Phaeocystis* in the SO. Still, the simulated community structure in the *Baseline* simulation with ROMS-BEC is supported by available observations (see section 3.1), giving us confidence in our estimates.

635 The simulated contribution of *Phaeocystis* to POC export in ROMS-BEC (16% and 40% south of 30° S and 60° S) is in broad agreement with the previous estimate from Wang and Moore (2011, 19% and 30% south of 40° S and 60° S, respectively). This is despite the differences in high-latitude phytoplankton community structure between the two models (see above) and demonstrates our on-going limited quantitative understanding of the fate of biomass losses (see also Laufkötter et al., 2016). Across the parameter sensitivity runs in ROMS-BEC (section 2.2), the contribution of *Phaeocystis* to POC production and export varies from 4-23% and 13-59% south of 30° S and 60° S, respectively. In addition to this uncertainty resulting only from the growth and loss parameters of *Phaeocystis* in the model, further uncertainty arises from parameters describing the partitioning of biomass losses amongst dissolved and particulate carbon species, which we did not assess in this study. Acknowledging that the exact numbers are highly sensitive to parameter choices in the model, our analysis reveals how the pathways of POC production, in particular the relative importance of fecal pellets from zooplankton and aggregated phytoplankton cells, are impacted by the simulated spatio-temporal variability in phytoplankton commu-

nity structure throughout the year (Fig. 7). In this regard, the simulated strong temporal coupling between POC fluxes and biomass distributions in ROMS-BEC is a direct result of the model formulations describing particle sinking (Lima et al., 2014) (particles sink implicitly, i.e., they are not laterally advected, Lima et al., 2014). This coupling is supported by observations, e.g., from the Ross Sea, where the POC flux from the upper ocean has been found to be closely linked to biomass levels in the overlying surface layer (with aggregates being an important vector for POC export when *Phaeocystis* dominated the community, Asper and Smith, 1999). Yet, the coupling in our model is potentially too strong in other areas, where reprocessing of POC by zooplankton in the upper ocean or lateral advection of POC could decouple the seasonal evolution of phytoplankton biomass and POC export (e.g. Lam and Bishop, 2007; Stange et al., 2017), the effect of which we can currently not assess. Given the possibly large importance of different POC production pathways for carbon and nutrient cycling through their impact on the remineralization depth of organic matter, these processes should be better constrained in the future, in order to further quantify the imprint of spatio-temporal variations in the relative importance of *Phaeocystis* for the high-latitude cycling of carbon.

Besides its impact on the carbon cycle, *Phaeocystis* is the major contributor to the marine sulphur cycle in the SO through its production of DMSP (Keller et al., 1989; Liss et al., 1994; Stefels et al., 2007). Though not explicitly including the biogeochemical cycling of sulphur, we can nevertheless use model output from ROMS-BEC to obtain an estimate of DMS production by *Phaeocystis* through a simple back-of-the-envelope calculation. Integrating the modeled *Phaeocystis* biomass loss rates via zooplankton grazing and non-grazing mortality over the top 10 m, assuming a molar DMSP:C ratio for *Phaeocystis* of 0.011 (Stefels et al., 2007), and a DMSP-to-DMS conversion efficiency between 0.2-0.7 (the DMS yield depends on the local sulphur demand of bacteria, Stefels et al., 2007; Wang et al., 2015), our estimated annual DMS production by *Phaeocystis* in ROMS-BEC amounts to 3.3-11.5 Tg S and 1.8-6.4 Tg S south of 30° S and 60° S, respectively. Consequently, assuming that all of this DMS production quickly escapes to the atmosphere, our estimates correspond to 11.6-40.1% (30-90° S) and 6.5-22.7% (60-90° S) of the global flux of DMS to the atmosphere previously estimated by Lana et al. (2011, 28.1 Tg S yr⁻¹). Our estimate is an upper bound, however, as not all DMS produced in seawater is readily released to the atmosphere. In fact, a fraction is likely broken down by bacteria, by photolysis, or is mixed down in the water column (see e.g. Simó and Pedrós-Alló, 1999; Stefels et al., 2007). Still, given that other phytoplankton types also produce DMS(P) (Keller et al., 1989; Stefels et al., 2007), the ROMS-BEC-based contribution of SO *Phaeocystis* alone (3.3-11.5 Tg S yr⁻¹) to the global flux of DMS to the atmosphere is in agreement with the flux suggested in Lana et al. (2011, 8.1 Tg S yr⁻¹ south of 30° S, i.e., 29% of their global estimate), and the substantial contribution of SO *Phaeocystis* underpins its major role for the global cycling of sulphur.

4.3 Limitations & Caveats

Our results may be affected by several shortcomings regarding the parameterization of *Phaeocystis*, in particular the representation of its life cycle, the fate of its biomass losses, the temperature and light limitation of its growth, and its nutrient uptake stoichiometry. We considered here only colonial *Phaeocystis*, thereby implicitly assuming that a seed population of solitary cells is always available for colony formation. Not including an explicit parameterization for single cells and hence life cycle transitions might substantially impact both the seasonal *Phaeocystis* biomass evolution and the competition with diatoms, as solitary cells have been proposed to require less iron (Veldhuis et al., 1991) and are possibly subject to higher loss rates due

680 to e.g. zooplankton grazing compared to colonies (Smith et al., 2003; Nejstgaard et al., 2007). The transition from solitary to colonial cells is a function of the seed population and light and nutrient levels (Verity, 2000; Bender et al., 2018), and transition models have been applied in SO marine ecosystem models (e.g. Popova et al., 2007; Kaufman et al., 2017; Losa et al., 2019). For example, in their higher complexity, self-organizing ecosystem model (Follows et al., 2007), Losa et al. (2019) include both life stages of *Phaeocystis* and two types of diatoms to simulate phytoplankton competition at high SO latitudes. While
685 our model results suggest that this is not required to reproduce the observed SO biogeography of *Phaeocystis* and diatoms in ROMS-BEC, it nevertheless highlights the need for further research on the impact of the chosen marine ecosystem complexity on the modeled biogeochemical fluxes (Ward et al., 2013). To date, the implementation of morphotype transitions of *Phaeocystis* into a basin-wide SO model such as ROMS-BEC is severely hindered by data availability. At the moment, 390 *Phaeocystis* biomass observations are included in the MAREDAT data base south of 30° S, and the distinction between solitary and colonial
690 cells is often difficult (Vogt et al., 2012), impeding the basin-wide model evaluation of both *Phaeocystis* life stages. In addition, colonies of *Phaeocystis* are surrounded by a gelatinous matrix, which contains nutrients and carbon (Schoemann et al., 2005), leading to an underestimation of modeled *Phaeocystis* carbon biomass estimates if not accounting for this mucus (Vogt et al., 2012). In ROMS-BEC, this underestimation is likely small, as <20% of the total *Phaeocystis* biomass is reportedly incorporated into the mucus in the SO (Fig. 9 in Vogt et al., 2012). Nevertheless, through its function as a nutrient storage, the mucus
695 promotes the accumulation of *Phaeocystis* biomass relative to other phytoplankton types when the latter become limited by low nutrient availability. While the gelatinous matrix is additionally thought to prevent grazing, the literature on grazing losses of *Phaeocystis* colonies is non-conclusive (Schoemann et al., 2005). This is possibly a result of the large range of sizes of both *Phaeocystis* and the respective grazers, with smaller zooplankton typically grazing less on *Phaeocystis* colonies than larger zooplankton (see reviews by Schoemann et al., 2005; Nejstgaard et al., 2007). As discussed above, the fate of biomass losses
700 of *Phaeocystis* is still poorly constrained (this applies to all model PFTs, see also Laufkötter et al., 2016). Currently, ROMS-BEC treats POC from all formation pathways equal, i.e., once produced, there is no differentiation between POC originating from diatoms or *Phaeocystis* or from grazing or aggregation. In reality, *Phaeocystis* aggregates might be recycled more readily than those from diatoms. This could reconcile our model results, i.e., the substantial simulated contribution of *Phaeocystis* to POC export at 100 m, with observations which suggest that the contribution of *Phaeocystis* to the POC flux across 200 m
705 is small (<5%, Gowing et al., 2001; Accornero et al., 2003; Reigstad and Wassmann, 2007). Furthermore, other functional relationships than those used in ROMS-BEC exist to describe the light and temperature dependent growth of *Phaeocystis* (e.g. Moisan and Mitchell, 2018). In comparison to the equations used in ROMS-BEC (see appendix B), the ones suggested by Moisan and Mitchell (2018) lead to generally lower *Phaeocystis* growth rates, especially at $\text{PAR} < 50 \text{ W m}^{-2}$, suggesting that our biomass estimates at high latitudes and early/late in the season are associated with substantial uncertainty. [As iron-light interactions are key for the simulated Fe:C and Chl:C ratios of SO phytoplankton \(Buitenhuis and Geider, 2010\) and in light of more recent advances regarding our understanding of the adaptation of SO phytoplankton to persisting low levels of light, iron, and temperature \(Strzpek et al., 2019\), a reassessment of model parametrizations describing phytoplankton growth and photoacclimation is advisable in future work.](#) Ultimately, the C:P and N:P nutrient uptake ratios by *Phaeocystis* and diatoms are higher (147 ± 26.7 and 19.2 ± 0.61) and lower (94.3 ± 20.1 and 9.67 ± 0.33), respectively (Arrigo et al., 1999, 2000), than

715 those originally suggested by Redfield and currently used in ROMS-BEC (117:16:1 for C:N:P uptake by *Phaeocystis* and diatoms, Anderson and Sarmiento, 1994). Consequently, this suggests that not accounting for the non-Redfield ratios in nutrient uptake by these PFTs leads to an over(under)estimation of carbon fixation per unit of P and hence POC export where/when *Phaeocystis* (diatoms) dominate the phytoplankton community.

5 Conclusions

720 In this modeling study, we present a thorough assessment of the factors controlling the relative importance of SO *Phaeocystis* and diatoms throughout the year and quantify the implications of the spatio-temporal variability in phytoplankton community structure for POC export. In ROMS-BEC, *Phaeocystis* colonies are an important member of the SO phytoplankton community, contributing 15% (16%) to total annual NPP (POC export) south of 30° S. Moreover, their contribution is threefold higher south of 60° S in our model. Given that our results imply a contribution of approximately 5% of SO *Phaeocystis* colonies to
725 total global NPP and POC export, respectively, we recommend the inclusion of an explicit representation of *Phaeocystis* in ecosystem models of the SO. This will allow for a more realistic representation of the SO phytoplankton community structure, in particular the relative importance of silicifying diatoms and non-silicifying phytoplankton, which we here find to significantly impact the simulated high-latitude carbon fluxes and nutrient distributions. Follow-up studies with both regional SO and global marine ecosystem models should more closely assess what the impact of this simulated change in the relative
730 concentrations of silicic acid and nitrate in the high-latitude SO is on subantarctic and low latitude phytoplankton dynamics.

On a basin-scale, we find that the competition of *Phaeocystis* and diatoms is controlled by seasonal differences in temperature and iron availability, but that variations in light levels are critical on a local scale. Yet, our model suggests that the relative importance of *Phaeocystis* and diatoms over a complete annual cycle is ultimately determined by differences in their biomass loss rates (such as zooplankton grazing and aggregation, Le Quére et al., 2016), which in turn impacts the formation of sinking
735 particles and hence carbon transfer to depth. Despite knowing of the importance of top-down factors for global phytoplankton biomass distributions (Behrenfeld, 2014) and for the formation of sinking particles (e.g. Steinberg and Landry, 2017), model parameters describing the fate of carbon after its fixation during photosynthesis are still surprisingly uncertain (Laufkötter et al., 2016), complicating the assessment of the role of biomass loss processes in regulating global biogeochemical cycles.

Environmental conditions in the SO have changed considerably in the last million years (see e.g. Martínez-García et al.,
740 2014), as well as during the past decades (Constable et al., 2014), and are projected to change further during this century (IPCC, 2014). These changes will impact the competitive fitness of *Phaeocystis* and diatoms (see e.g. Hancock et al., 2018; Boyd, 2019) and hence affect the entire phytoplankton community with likely repercussions for the entire food web (Smetacek et al., 2004). Consequently, based on our results, future laboratory and modeling studies should assess how uncertainties in marine ecosystem models surrounding e.g. the parameterization of the life cycle of *Phaeocystis* and the fate of biomass losses
745 impact the simulated relative importance of this phytoplankton type and carbon transfer to depth at high SO latitudes. Thereby, such studies will allow us to better constrain how potential future changes in the high-latitude phytoplankton community structure impact global biogeochemical cycles.

750 Appendix A: Evaluating the simulated phytoplankton dynamics in ROMS-BEC

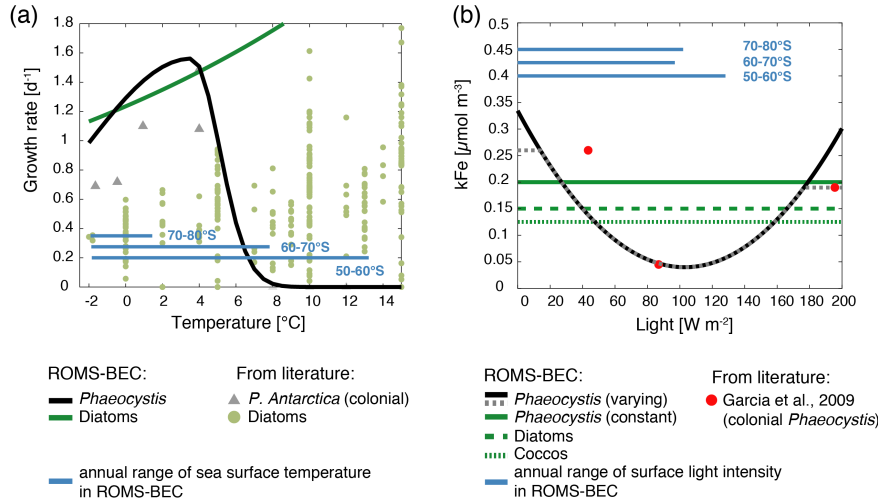


Figure A1. a) Growth rates of *Phaeocystis antarctica* colonies as a function of temperature (conditions of nutrients and light are non-limiting) in laboratory data (grey triangles, see compilation by Schoemann et al., 2005) and as used in ROMS-BEC (black line, see Eq. 1). Green circles and the green line show the temperature-limited growth rate of diatoms in laboratory data (see compilation by Le Quéré et al., 2016) and as used in ROMS-BEC, respectively (see also Table 1). b) Half-saturation constant of Fe (k_{Fe}) of *Phaeocystis* as a function of light intensity I ($W m^{-2}$) in laboratory data (red circles) and the polynomial fit ($k_{Fe}^{PA}(I) = 2.776 \cdot 10^{-5} \cdot (I + 20)^2 - 0.00683 \cdot (I + 20) + 0.46$) without (black) and with (dashed grey, as used in ROMS-BEC in simulation VARYING_kFe, see Table 2) the correction at low and high light intensities to restrict k_{Fe} to the range measured in the laboratory experiments by Garcia et al. (2009). The green lines correspond to the half-saturation constants used for *Phaeocystis* (solid), diatoms (dashed), and coccolithophores (dotted) in the *Baseline* simulation in this study (see Table 1). In both panels, the blue lines correspond to the simulated annual range in a) sea surface temperature [$^{\circ}C$] and b) light intensity [$W m^{-2}$] between 50-60° S, 60-70° S, and 70-80° S, respectively.

A1 Sensitivity of *Phaeocystis* biogeography to chosen parameter values differences between *Phaeocystis* and diatoms

We assess the sensitivity of the simulated annual mean *Phaeocystis* biogeography to parameter choices by performing a set of sensitivity experiments (runs 1-6 competition experiments, runs 1-8 in Table 2). Overall, the simulated surface *Phaeocystis* biomass concentrations change by $\gtrsim \pm 50\%$ for each of the experiments in the high-latitude SO (Fig. A2). Between 60-90° S and in the Ross Sea, the largest increase-increases in *Phaeocystis* biomass concentrations is simulated for are simulated for THETA_N_MAX (+332% and +217%, respectively, Fig. A2b & c) and AGGREGATION (+112% and +96%, respectively, Fig. A2b & c), whereas the strongest decline is simulated for ALPHA_{PI} (-76% and -87%, respectively, Fig. A2b & c). As

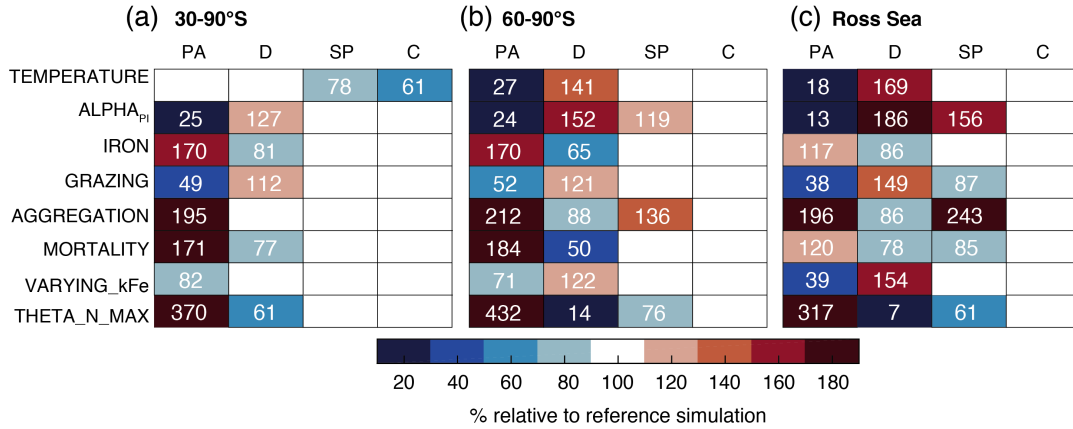


Figure A2. Annual mean surface chlorophyll concentrations of *Phaeocystis* (PA), diatoms (D), small phytoplankton (SP), and coccolithophores (C) in the [parameter-competition](#) sensitivity simulations (see section 2.2 and [runs 1-8 in Table 2](#)) relative to the *Baseline* simulation. The model output is averaged over a) 30-90° S, b) 60-90° S, and c) the Ross Sea. Numbers are only printed if the relative change exceeds $\pm 10\%$

a response to changes in *Phaeocystis* parameters, diatom biomass changes overall more than that of SP on a basin scale, suggesting *Phaeocystis* is indeed mostly competing with diatoms for resources in the high-latitude SO. Between 60-90° S, the magnitude of change is similar for the experiments TEMPERATURE (-73%), ALPHA_{PI} (-76%), and IRON (+70%), while in the Ross Sea, the response in IRON is substantially smaller (+17%) than that for the other two experiments (-82% and -87% for TEMPERATURE and ALPHA_{PI}, respectively; Fig. A2b & c). This supports our findings from section 3.3, namely that the difference in light sensitivity between *Phaeocystis* and diatoms is more important in coastal areas than on a basin scale in controlling the relative importance of *Phaeocystis* for total phytoplankton biomass.

765 Appendix B: BEC equations: Phytoplankton growth & loss

Any change in phytoplankton biomass P [mmol C m⁻³] of phytoplankton i ($i \in \{PA, D, C, SP, N\}$) over time is determined by the balance of growth and loss terms:

$$\frac{dP^i}{dt} = \text{Growth} - \text{Loss} \quad (\text{B1})$$

$$= \mu^i \cdot P^i - \gamma^i(P^i) \cdot P^i \quad (\text{B2})$$

$$= \mu^i \cdot P^i - \gamma_g^i(P^i) \cdot P^i - \gamma_m^i \cdot P^i - \gamma_a^i(P^i) \cdot P^i \quad (\text{B3})$$

In the above equation, γ_g denotes the loss by zooplankton grazing, γ_m the loss by non-grazing mortality, and γ_a the loss by aggregation.

770 B1 Phytoplankton growth

The specific growth rate μ^i [day⁻¹] of phytoplankton i ($i \in \{D, C, SP, N\}$, i.e., all but *Phaeocystis*) is determined by the maximum growth rate μ_{\max}^i (Table 1) and modifications due to temperature (T), nutrients (N) and irradiance (I), following:

$$\mu^i = \mu_{\max}^i \cdot f^i(T) \cdot g^i(N) \cdot h^i(I) \quad (\text{B4})$$

The temperature function $f(T)$ is an exponential function, which is modified by the constant Q_{10} specific to every phytoplankton i (Table 1):

$$f^i(T) = Q_{10}^i \cdot \exp\left(\frac{T - T_{\text{ref}}}{10^\circ\text{C}}\right) \quad (\text{B5})$$

775 Note that for *Phaeocystis* in ROMS-BEC, an optimum temperature function is used (Eq. 1), as this PFT is parametrized to only represent *Phaeocystis antarctica* in the SO application of this study (see section 2.1).

First, the limitation of growth of phytoplankton i ($i \in \{PA, D, C, SP, N\}$) by the surrounding nutrient $L^i(N)$ is calculated individually for each nutrient (nitrogen, phosphorus, iron for all phytoplankton, silicate for diatoms only) following a Michaelis-Menten function (see Table 1 for half-saturation constants k_N^i). Accordingly, the limitation factor is calculated as

780 follows for iron (Fe) and silicate (SiO₃):

$$L^i(N) = \frac{N}{N + k_N^i} \quad (\text{B6})$$

For nitrogen and phosphorus, the combined limitation by nutrient N and M (nitrate (NO₃) and ammonium (NH₄) for nitrogen, phosphate (PO₄) and dissolved organic phosphorus (DOP) for phosphorus) is accounted for following:

$$L^i(N, M) = \frac{N}{k_N^i + N + M \cdot (k_N^i/k_M^i)} + \frac{M}{k_M^i + M + N \cdot (k_M^i/k_N^i)} \quad (\text{B7})$$

In the model, the phytoplankton growth rate is then only limited by the most limiting nutrient:

$$g^i(N) = \min(L^i(\text{NO}_3, \text{NH}_4), L^i(\text{PO}_4, \text{DOP}), L^i(\text{Fe}), L^i(\text{SiO}_3)) \quad (\text{B8})$$

785 The light limitation function $h^i(I)$ includes the effects of photoacclimation by including the chlorophyll-to-carbon ratio θ^i $\frac{\theta^i}{\text{chl:C}}$ and the growth of the respective phytoplankton i ($i \in \{PA, D, C, SP, N\}$) limited by nutrients and temperature:

$$h^i(I) = 1 - \exp\left(-1 \cdot \frac{\alpha_{PI}^i \cdot \theta^i \cdot I}{\mu_{\max}^i \cdot g^i(N) \cdot f^i(T)} \cdot \frac{\alpha_{PI}^i \cdot \theta^i_{\text{chl:C}} \cdot I}{\mu_{\max}^i \cdot g^i(N) \cdot f^i(T)}\right) \quad (\text{B9})$$

Here, same as in Nissen et al. (2018), growth by coccolithophores is set to zero at PAR levels $< 1 \text{ W m}^{-2}$ (Zondervan, 2007) and is linearly reduced at temperatures $< 6^\circ\text{C}$ following:

$$\mu^C = \mu^C \cdot \frac{\max(T + 2^\circ\text{C}, 0)}{8^\circ\text{C}} \quad (\text{B10})$$

Coccolithophore calcification amounts to 20% of their photosynthetic growth at any location and point in time in ROMS-BEC.

Diazotroph growth is zero at temperatures $<14^{\circ}\text{C}$.

790 In BEC, the Fe:C ratio $\theta_{\text{Fe:C}}^i$ [$\mu\text{mol mol}^{-3}$] of growth by phytoplankton i varies between the maximum Fe:C ratio $\theta_{\text{Fe:C,max}}^i$ at high seawater Fe concentrations and the minimum Fe:C ratio $\theta_{\text{Fe:C,min}}^i$ at very low Fe concentrations. Below a critical surrounding Fe concentration, which depends on each PFT's half-saturation constant of iron k_{Fe}^i (see Table 1), the ratio is reduced from the maximum Fe:C ratio following:

$$\theta_{\text{Fe:C}}^i = \theta_{\text{Fe:C,max}}^i \quad (\text{B11})$$

$$\theta_{\text{Fe:C}}^i = \max\left(\theta_{\text{Fe:C}}^i \cdot \frac{[\text{Fe}]}{9 \cdot k_{\text{Fe}}^i}, \theta_{\text{Fe:C,min}}^i\right) \quad \text{where } [\text{Fe}] < 9 \cdot k_{\text{Fe}}^i \quad (\text{B12})$$

795 For this study, $\theta_{\text{Fe:C,max}}^i$ is 60 for diazotrophs and 20 for all other PFTs, and $\theta_{\text{Fe:C,min}}^i$ is 12 for diazotrophs and 3 for all other PFTs.

B2 Phytoplankton loss

In ROMS-BEC, the corrected phytoplankton biomass P^i is used to compute loss rates of phytoplankton biomass, to prevent phytoplankton biomass loss at very low biomass levels:

$$P^i = \max(P^i - c_{\text{loss}}^i, 0) \quad (\text{B13})$$

800 In this equation, c_{loss}^i is the threshold of phytoplankton biomass P^i below which no losses occur ($c_{\text{loss}}^{\text{N}}=0.022 \text{ mmol C m}^{-3}$ and $c_{\text{loss}}^{\text{PA,D,C,SP}}=0.04 \text{ mmol C m}^{-3}$).

The single zooplankton grazer Z [mmol C m^{-3}] feeds on the respective phytoplankton P^i [mmol C m^{-3}] at a grazing rate γ_{g}^i [$\text{mmol C m}^{-3} \text{ day}^{-1}$] that is given by:

$$\gamma_{\text{g}}^i = \gamma_{\text{max}}^i \cdot f^Z(T) \cdot Z \cdot \frac{P^i}{Z_{\text{grz}}^i + P^i} \quad (\text{B14})$$

with

$$f^Z(T) = 1.5 \cdot \exp\left(\frac{T - T_{\text{ref}}}{-10^{\circ}\text{C}}\right) \quad (\text{B15})$$

805 The non-grazing mortality rate γ_{m}^i [$\text{mmol C m}^{-3} \text{ day}^{-1}$] of phytoplankton i [mmol C m^{-3}] is the product of a maximum mortality rate m_0^i [day^{-1}] scaled by the temperature function $f^i(T)$ with the modified phytoplankton biomass P^i :

$$\gamma_{\text{m}}^i = m_0^i \cdot f^i(T) \cdot P^i \quad (\text{B16})$$

with m_0^i being 0.15 day^{-1} for diazotrophs and 0.12 day^{-1} for all other phytoplankton.

Phytoplankton P^i [mmol C m^{-3}] aggregate at an aggregation rate γ_{a}^i [$\text{mmol C m}^{-3} \text{ day}^{-1}$] which is computed with the quadratic mortality rate constants $\gamma_{\text{a},0}^i$ ($[\text{m}^3 (\text{mmol C})^{-1} \text{ d}^{-1}]$, Table 1) and :

$$\gamma_{\text{a}}^i = \min(\gamma_{\text{a,max}}^i \cdot P^i, \gamma_{\text{a},0}^i \cdot P^i \cdot P^i) \quad (\text{B17})$$

$$\gamma_{\text{a}}^i = \max(\gamma_{\text{a,min}}^i \cdot P^i, \gamma_{\text{a}}^i) \quad (\text{B18})$$

In ROMS-BEC, $\gamma_{a,\min}^i$ is 0.01 day^{-1} for small phytoplankton and coccolithophores and 0.02 day^{-1} for *Phaeocystis* and
810 diatoms, and with $\gamma_{a,\max}^i$ being 0.9 day^{-1} for *Phaeocystis*, diatoms, coccolithophores, and small phytoplankton. Note that
phytoplankton immediately stop photosynthesizing upon aggregation and that aggregation losses do not occur for diazotrophs
in ROMS-BEC.

Author contributions. MV and CN conceived the study. CN set up the model simulations, performed the analysis, and wrote the paper. MV
contributed to the interpretation of the results and the writing of the paper.

815 *Competing interests.* The authors declare that they have no conflict of interest.

Acknowledgements. We acknowledge all the scientists who contributed phytoplankton and zooplankton cell count data to the MAREDAT
initiative and William Balch, Helen Smith, Mariem Saavedra-Pellitero, Gustaaf Hallegraeff, José-Abel Flores, and Alex Poulton for providing
additional cell count data. Furthermore, GlobColour data (<http://globcolour.info>) used in this study has been developed, validated, and
distributed by ACRI-ST, France. We would like to thank Nicolas Gruber, Matthias Münnich, and Domitille Louchard for valuable discussions
820 and Damian Loher for technical support. Additionally, we would like to thank Gianna Ferrari for the analysis of early ROMS-BEC simulations
with *Phaeocystis*. Ultimately, we thank ~~two~~four reviewers for their valuable reviews and comments, which have improved the quality of
the manuscript. This research was financially supported by the Swiss Federal Institute of Technology Zürich (ETH Zürich) and the Swiss
National Science Foundation (project SOGate, grant no. 200021_153452). The simulations were performed at the HPC cluster of ETH
Zürich, Euler, which is located in the Swiss Supercomputing Center (CSCS) in Lugano and operated by ETH ITS Scientific IT Services in
825 Zürich. Model output is available upon request to the corresponding author, Cara Nissen (cara.nissen@usys.ethz.ch).

References

- Accornero, A., Manno, C., Esposito, F., and Gambi, M. C.: The vertical flux of particulate matter in the polynya of Terra Nova Bay. Part II. Biological components, *Antarctic Science*, 15, S0954102003001 214, <https://doi.org/10.1017/S0954102003001214>, 2003.
- Alvain, S., Moulin, C., Dandonneau, Y., and Loisel, H.: Seasonal distribution and succession of dominant phytoplankton groups in the global
830 ocean: A satellite view, *Global Biogeochemical Cycles*, 22, GB3001, <https://doi.org/10.1029/2007GB003154>, 2008.
- Anderson, L. A. and Sarmiento, J. L.: Redfield ratios of remineralization determined by nutrient data analysis, *Global Biogeochemical Cycles*, 8, 65–80, <https://doi.org/10.1029/93GB03318>, 1994.
- Arrigo, K. R., Weiss, A. M., and Smith, W. O.: Physical forcing of phytoplankton dynamics in the southwestern Ross Sea, *Journal of Geophysical Research: Oceans*, 103, 1007–1021, <https://doi.org/10.1029/97JC02326>, 1998.
- 835 Arrigo, K. R., Robinson, D. H., Worthen, D. L., Dunbar, R. B., DiTullio, G. R., VanWoert, M. L., and Lizotte, M. P.: Phytoplankton community structure and the drawdown of nutrients and CO₂ in the Southern Ocean, *Science*, 283, 365–367, <https://doi.org/10.1126/science.283.5400.365>, 1999.
- Arrigo, K. R., DiTullio, G. R., Dunbar, R. B., Robinson, D. H., VanWoert, M., Worthen, D. L., and Lizotte, M. P.: Phytoplankton taxonomic variability in nutrient utilization and primary production in the Ross Sea, *Journal of Geophysical Research: Oceans*, 105, 8827–8846,
840 <https://doi.org/10.1029/1998JC000289>, 2000.
- Arrigo, K. R., van Dijken, G. L., Alderkamp, A.-C., Erickson, Z. K., Lewis, K. M., Lowry, K. E., Joy-Warren, H. L., Middag, R., Nash-Arrigo, J. E., Selz, V., and van de Poll, W.: Early Spring Phytoplankton Dynamics in the Western Antarctic Peninsula, *Journal of Geophysical Research: Oceans*, 122, 9350–9369, <https://doi.org/10.1002/2017JC013281>, 2017.
- Asper, V. L. and Smith, W. O.: Particle fluxes during austral spring and summer in the southern Ross Sea, Antarctica, *Journal of Geophysical Research: Oceans*, 104, 5345–5359, <https://doi.org/10.1029/1998JC900067>, 1999.
- 845 Asper, V. L. and Smith, W. O.: Variations in the abundance and distribution of aggregates in the Ross Sea, Antarctica, *Elem Sci Anth*, 7, 23, <https://doi.org/10.1525/elementa.355>, <https://www.elementascience.org/article/10.1525/elementa.355/>, 2019.
- Ayers, G. P., Ivey, J. P., and Gillett, R. W.: Coherence between seasonal cycles of dimethyl sulphide, methanesulphonate and sulphate in marine air, *Nature*, 349, 404–406, <https://doi.org/10.1038/349404a0>, 1991.
- 850 Balch, W. M., Drapeau, D. T., Bowler, B. C., Lyczkowski, E., Booth, E. S., and Alley, D.: The contribution of coccolithophores to the optical and inorganic carbon budgets during the Southern Ocean Gas Exchange Experiment: New evidence in support of the "Great Calcite Belt" hypothesis, *Journal of Geophysical Research*, 116, C00F06, <https://doi.org/10.1029/2011JC006941>, 2011.
- Balch, W. M., Bates, N. R., Lam, P. J., Twining, B. S., Rosengard, S. Z., Bowler, B. C., Drapeau, D. T., Garley, R., Lubelczyk, L. C., Mitchell, C., and Rauschenberg, S.: Factors regulating the Great Calcite Belt in the Southern Ocean and its biogeochemical significance, *Global Biogeochemical Cycles*, 30, 1199–1214, <https://doi.org/10.1002/2016GB005414>, 2016.
- 855 Behrenfeld, M. J.: Climate-mediated dance of the plankton, *Nature Climate Change*, 4, 880–887, <https://doi.org/10.1038/nclimate2349>, 2014.
- Behrenfeld, M. J. and Falkowski, P. G.: Photosynthetic rates derived from satellite-based chlorophyll concentration, *Limnology and Oceanography*, 42, 1–20, <https://doi.org/10.4319/lo.1997.42.1.0001>, 1997.
- Ben Mustapha, Z. B., Alvain, S., Jamet, C., Loisel, H., and Dessailly, D.: Automatic classification of water-leaving radiance anomalies from
860 global SeaWiFS imagery: Application to the detection of phytoplankton groups in open ocean waters, *Remote Sensing of Environment*, 146, 97–112, <https://doi.org/10.1016/j.rse.2013.08.046>, 2014.

- Bender, S. J., Moran, D. M., McIlvin, M. R., Zheng, H., McCrow, J. P., Badger, J., DiTullio, G. R., Allen, A. E., and Saito, M. A.: Colony formation in *Phaeocystis antarctica*: connecting molecular mechanisms with iron biogeochemistry, *Biogeosciences*, 15, 4923–4942, <https://doi.org/10.5194/bg-15-4923-2018>, 2018.
- 865 Berman-Frank, I., Cullen, J. T., Shaked, Y., Sherrell, R. M., and Falkowski, P. G.: Iron availability, cellular iron quotas, and nitrogen fixation in *Trichodesmium*, *Limnology and Oceanography*, 46, 1249–1260, <https://doi.org/10.4319/lo.2001.46.6.1249>, 2001.
- Bopp, L., Aumont, O., Cadule, P., Alvain, S., and Gehlen, M.: Response of diatoms distribution to global warming and potential implications: A global model study, *Geophysical Research Letters*, 32, 1–4, <https://doi.org/10.1029/2005GL023653>, 2005.
- Boyd, P. W.: Physiology and iron modulate diverse responses of diatoms to a warming Southern Ocean, *Nature Climate Change*, 9, 148–152, <https://doi.org/10.1038/s41558-018-0389-1>, 2019.
- 870 Brun, P., Vogt, M., Payne, M. R., Gruber, N., O'Brien, C. J., Buitenhuis, E. T., Le Quéré, C., Leblanc, K., and Luo, Y.-W.: Ecological niches of open ocean phytoplankton taxa, *Limnology and Oceanography*, 60, 1020–1038, <https://doi.org/10.1002/lno.10074>, 2015.
- Buesseler, K. O.: The decoupling of production and particulate export in the surface ocean, *Global Biogeochemical Cycles*, 12, 297–310, <https://doi.org/10.1029/97GB03366>, 1998.
- 875 Buitenhuis, E. T. and Geider, R. J.: A model of phytoplankton acclimation to iron-light colimitation, *Limnology and Oceanography*, 55, 714–724, <https://doi.org/10.4319/lo.2009.55.2.0714>, 2010.
- Buitenhuis, E. T., Pangerc, T., Franklin, D. J., Le Quéré, C., and Malin, G.: Growth rates of six coccolithophorid strains as a function of temperature, *Limnology and Oceanography*, 53, 1181–1185, <https://doi.org/10.4319/lo.2008.53.3.1181>, 2008.
- Buitenhuis, E. T., Hashioka, T., and Le Quéré, C.: Combined constraints on global ocean primary production using observations and models, *Global Biogeochemical Cycles*, 27, 847–858, <https://doi.org/10.1002/gbc.20074>, 2013.
- 880 Buma, A. G. J., Bano, N., Veldhuis, M. J. W., and Kraay, G. W.: Comparison of the pigmentation of two strains of the prymnesiophyte *Phaeocystis* sp., *Netherlands Journal of Sea Research*, 27, 173–182, [https://doi.org/10.1016/0077-7579\(91\)90010-X](https://doi.org/10.1016/0077-7579(91)90010-X), 1991.
- Capone, D. G.: *Trichodesmium*, a Globally Significant Marine Cyanobacterium, *Science*, 276, 1221–1229, <https://doi.org/10.1126/science.276.5316.1221>, 1997.
- 885 Caron, D. A., Dennett, M. R., Lonsdale, D. J., Moran, D. M., and Shalapyonok, L.: Microzooplankton herbivory in the Ross Sea, Antarctica, *Deep Sea Research Part II: Topical Studies in Oceanography*, 47, 3249–3272, [https://doi.org/10.1016/S0967-0645\(00\)00067-9](https://doi.org/10.1016/S0967-0645(00)00067-9), 2000.
- Carton, J. A. and Giese, B. S.: A reanalysis of ocean climate using Simple Ocean Data Assimilation (SODA), *Monthly Weather Review*, 136, 2999–3017, <https://doi.org/10.1175/2007MWR1978.1>, 2008.
- Chen, Y.-Q., Wang, N., Zhang, P., Zhou, H., and Qu, L.-H.: Molecular evidence identifies bloom-forming *Phaeocystis* (Prymnesiophyta) from coastal waters of southeast China as *Phaeocystis globosa*, *Biochemical Systematics and Ecology*, 30, 15–22, [https://doi.org/10.1016/S0305-1978\(01\)00054-0](https://doi.org/10.1016/S0305-1978(01)00054-0), 2002.
- 890 Constable, A. J., Melbourne-Thomas, J., Corney, S. P., Arrigo, K. R., Barbraud, C., Barnes, D. K. A., Bindoff, N. L., Boyd, P. W., Brandt, A., Costa, D. P., Davidson, A. T., Ducklow, H. W., Emmerson, L., Fukuchi, M., Gutt, J., Hindell, M. A., Hofmann, E. E., Hosie, G. W., Iida, T., Jacob, S., Johnston, N. M., Kawaguchi, S., Kokubun, N., Koubbi, P., Lea, M.-A., Makhado, A., Massom, R. A., Meiners, K., Meredith, M. P., Murphy, E. J., Nicol, S., Reid, K., Richerson, K., Riddle, M. J., Rintoul, S. R., Smith, W. O., Southwell, C., Stark, J. S., Sumner, M., Swadling, K. M., Takahashi, K. T., Trathan, P. N., Welsford, D. C., Weimerskirch, H., Westwood, K. J., Wienecke, B. C., Wolf-Gladrow, D., Wright, S. W., Xavier, J. C., and Ziegler, P.: Climate change and Southern Ocean ecosystems I: how changes in physical habitats directly affect marine biota, *Global Change Biology*, 20, 3004–3025, <https://doi.org/10.1111/gcb.12623>, 2014.

- Cubillos, J. C., Wright, S. W., Nash, G., de Salas, M. F., Griffiths, B., Tilbrook, B., Poisson, A., and Hallegraeff, G. M.: Calcification morphotypes of the coccolithophorid *Emiliania huxleyi* in the Southern Ocean: changes in 2001 to 2006 compared to historical data, *Marine Ecology Progress Series*, 348, 47–54, <https://doi.org/10.3354/meps07058>, 2007.
- Curran, M. A. J. and Jones, G. B.: Dimethyl sulfide in the Southern Ocean: Seasonality and flux, *Journal of Geophysical Research: Atmospheres*, 105, 20 451–20 459, <https://doi.org/10.1029/2000JD900176>, 2000.
- Curran, M. A. J., Jones, G. B., and Burton, H.: Spatial distribution of dimethylsulfide and dimethylsulfoniopropionate in the Australasian sector of the Southern Ocean, *Journal of Geophysical Research: Atmospheres*, 103, 16 677–16 689, <https://doi.org/10.1029/97JD03453>, 1998.
- Dee, D. P., Uppala, S. M., Simmons, A. J., Berrisford, P., Poli, P., Kobayashi, S., Andrae, U., Balmaseda, M. A., Balsamo, G., Bauer, P., Bechtold, P., Beljaars, A. C. M., van de Berg, L., Bidlot, J., Bormann, N., Delsol, C., Dragani, R., Fuentes, M., Geer, A. J., Haimberger, L., Healy, S. B., Hersbach, H., Hólm, E. V., Isaksen, L., Kållberg, P., Köhler, M., Matricardi, M., McNally, A. P., Monge-Sanz, B. M., Morcrette, J.-J., Park, B.-K., Peubey, C., de Rosnay, P., Tavolato, C., Thépaut, J.-N., and Vitart, F.: The ERA-Interim reanalysis: configuration and performance of the data assimilation system, *Quarterly Journal of the Royal Meteorological Society*, 137, 553–597, <https://doi.org/10.1002/qj.828>, 2011.
- Deppeler, S. L. and Davidson, A. T.: Southern Ocean phytoplankton in a changing climate, *Frontiers in Marine Science*, 4, 40, <https://doi.org/10.3389/fmars.2017.00040>, 2017.
- DeVries, T. and Weber, T.: The export and fate of organic matter in the ocean: New constraints from combining satellite and oceanographic tracer observations, *Global Biogeochemical Cycles*, 31, 535–555, <https://doi.org/10.1002/2016GB005551>, 2017.
- DiTullio, G. R., Grebmeier, J. M., Arrigo, K. R., Lizotte, M. P., Robinson, D. H., Leventer, A., Barry, J. P., VanWoert, M. L., and Dunbar, R. B.: Rapid and early export of *Phaeocystis antarctica* blooms in the Ross Sea, Antarctica, *Nature*, 404, 595–598, <https://doi.org/10.1038/35007061>, 2000.
- Ducklow, H. W., Wilson, S. E., Post, A. F., Stammerjohn, S. E., Erickson, M., Lee, S., Lowry, K. E., Sherrell, R. M., and Yager, P. L.: Particle flux on the continental shelf in the Amundsen Sea Polynya and Western Antarctic Peninsula, *Elementa: Science of the Anthropocene*, 3, 000 046, <https://doi.org/10.12952/journal.elementa.000046>, 2015.
- Eppley, R. W.: Temperature and phytoplankton growth in the sea, *Fishery Bulletin*, 70, 1972.
- Fanton d’Andon, O., Mangin, A., Lavender, S., Antoine, D., Maritorena, S., Morel, A., Barrot, G., Demaria, J., and Pinnock, S.: GlobColour - the European Service for Ocean Colour, in: Proceedings of the 2009 IEEE International Geoscience & Remote Sensing Symposium, IEEE International Geoscience & Remote Sensing Symposium (IGARSS), ISBN: 9781424433957, 2009.
- Feng, Y., Hare, C. E., Rose, J. M., Handy, S. M., DiTullio, G. R., Lee, P. A., Smith, W. O., Peloquin, J., Tozzi, S., Sun, J., Zhang, Y., Dunbar, R. B., Long, M. C., Sohst, B., Lohan, M., and Hutchins, D. A.: Interactive effects of iron, irradiance and CO₂ on Ross Sea phytoplankton, *Deep Sea Research Part I: Oceanographic Research Papers*, 57, 368–383, <https://doi.org/10.1016/j.dsr.2009.10.013>, 2010.
- Follows, M. J., Dutkiewicz, S., Grant, S., and Chisholm, S. W.: Emergent biogeography of microbial communities in a model ocean, *Science*, 315, 1843–6, <https://doi.org/10.1126/science.1138544>, 2007.
- Freeman, N. M., Lovenduski, N. S., Munro, D. R., Krumhardt, K. M., Lindsay, K., Long, M. C., and MacLennan, M.: The variable and changing Southern Ocean silicate front: Insights from the CESM large ensemble, *Global Biogeochemical Cycles*, 32, 752–768, <https://doi.org/10.1029/2017GB005816>, 2018.
- Garcia, H. E., Locarnini, R. A., Boyer, T. P., Antonov, J. I., Baranova, O., Zweng, M., Reagan, J., and Johnson, D.: World Ocean Atlas 2013, Volume 3: Dissolved oxygen, apparent oxygen utilization, and oxygen saturation, NOAA Atlas NESDIS 75, 3, 27 pp, 2014a.

- Garcia, H. E., Locarnini, R. A., Boyer, T. P., Antonov, J. I., Baranova, O. K., Zweng, M. M., Reagan, J. R., and Johnson, D. R.: World Ocean Atlas 2013, Volume 4 : Dissolved inorganic nutrients (phosphate, nitrate, silicate), NOAA Atlas NESDIS 76, 4, 25 pp, 2014b.
- 940 Garcia, N. S., Sedwick, P. N., and DiTullio, G. R.: Influence of irradiance and iron on the growth of colonial *Phaeocystis antarctica*: implications for seasonal bloom dynamics in the Ross Sea, Antarctica, Aquatic Microbial Ecology, 57, 203–220, <https://doi.org/10.3354/ame01334>, 2009.
- Geider, R. J., MacIntyre, H. L., and Kana, T. M.: A dynamic regulatory model of phytoplankton acclimation to light, nutrients, and temperature, Limnology and Oceanography, 43, 679–694, <https://doi.org/10.4319/lo.1998.43.4.0679>, 1998.
- Goffart, A., Catalano, G., and Hecq, J.: Factors controlling the distribution of diatoms and *Phaeocystis* in the Ross Sea, Journal of Marine Systems, 27, 161–175, [https://doi.org/10.1016/S0924-7963\(00\)00065-8](https://doi.org/10.1016/S0924-7963(00)00065-8), 2000.
- 945 Gowing, M. M., Garrison, D. L., Kunze, H. B., and Winchell, C. J.: Biological components of Ross Sea short-term particle fluxes in the austral summer of 1995–1996, Deep Sea Research Part I: Oceanographic Research Papers, 48, 2645–2671, [https://doi.org/10.1016/S0967-0637\(01\)00034-6](https://doi.org/10.1016/S0967-0637(01)00034-6), 2001.
- Granéli, E., Granéli, W., Rabbani, M. M., Daugbjerg, N., Fransz, G., Roudy, J. C., and Alder, V. A.: The influence of copepod and krill grazing on the species composition of phytoplankton communities from the Scotia Weddell sea, Polar Biology, 13, 201–213, <https://doi.org/10.1007/BF00238930>, 1993.
- 950 Gravalosa, J. M., Flores, J.-A., Sierro, F. J., and Gersonde, R.: Sea surface distribution of coccolithophores in the eastern Pacific sector of the Southern Ocean (Bellingshausen and Amundsen Seas) during the late austral summer of 2001, Marine Micropaleontology, 69, 16–25, <https://doi.org/10.1016/j.marmicro.2007.11.006>, 2008.
- 955 Green, S. E. and Sambrotto, R. N.: Plankton community structure and export of C, N, P and Si in the Antarctic Circumpolar Current, Deep Sea Research Part II: Topical Studies in Oceanography, 53, 620–643, <https://doi.org/10.1016/j.dsr2.2006.01.022>, 2006.
- Guidi, L., Chaffron, S., Bittner, L., Eveillard, D., Larhlimi, A., Roux, S., Darzi, Y., Audic, S., Berline, L., Brum, J. R., Coelho, L. P., Espinoza, J. C. I., Malviya, S., Sunagawa, S., Dimier, C., Kandels-Lewis, S., Picheral, M., Poulain, J., Searson, S., Stemmann, L., Not, F., Hingamp, P., Speich, S., Follows, M., Karp-Boss, L., Boss, E., Ogata, H., Pesant, S., Weissenbach, J., Wincker, P., Acinas, S. G., Bork, P., de Vargas, C., Iudicone, D., Sullivan, M. B., Raes, J., Karsenti, E., Bowler, C., and Gorsky, G.: Plankton networks driving carbon export in the oligotrophic ocean, Nature, 532, 465–470, <https://doi.org/10.1038/nature16942>, 2016.
- 960 Hamm, C. E., Simson, D. A., Merkel, R., and Smetacek, V.: Colonies of *Phaeocystis globosa* are protected by a thin but tough skin, Marine Ecology Progress Series, 187, 101–111, <https://doi.org/10.3354/meps187101>, 1999.
- Hancock, A. M., Davidson, A. T., McKinlay, J., McMinn, A., Schulz, K. G., and van den Eenden, R. L.: Ocean acidification changes the structure of an Antarctic coastal protistan community, Biogeosciences, 15, 2393–2410, <https://doi.org/10.5194/bg-15-2393-2018>, 2018.
- 965 Hashioka, T., Vogt, M., Yamanaka, Y., Le Quéré, C., Buitenhuis, E. T., Aita, M. N., Alvain, S., Bopp, L., Hirata, T., Lima, I., Salliey, S., and Doney, S. C.: Phytoplankton competition during the spring bloom in four plankton functional type models, Biogeosciences, 10, 6833–6850, <https://doi.org/10.5194/bg-10-6833-2013>, 2013.
- Haumann, F. A.: Southern Ocean response to recent changes in surface freshwater fluxes, PhD Thesis, ETH Zürich, <https://doi.org/10.3929/ethz-b-000166276>, 2016.
- 970 Henson, S. A., Le Moigne, F., and Giering, S.: Drivers of Carbon Export Efficiency in the Global Ocean, Global Biogeochemical Cycles, p. 2018GB006158, <https://doi.org/10.1029/2018GB006158>, 2019.
- Holling, C. S.: The components of predation as revealed by a study of small-mammal predation of the European pine sawfly, The Canadian Entomologist, 91, 293–320, <https://doi.org/10.4039/Ent91293-5>, 1959.

- 975 IPCC: Climate change 2013 - The physical science basis: Working group I contribution to the fifth assessment report of the Intergovernmental Panel on Climate Change, Cambridge University Press, <https://doi.org/10.1017/CBO9781107415324>, 2014.
- Johnson, R., Strutton, P. G., Wright, S. W., McMinn, A., and Meiners, K. M.: Three improved satellite chlorophyll algorithms for the Southern Ocean, *Journal of Geophysical Research-Oceans*, 118, 3694–3703, <https://doi.org/10.1002/jgrc.20270>, 2013.
- Kaufman, D. E., Friedrichs, M. A. M., Smith, W. O., Hofmann, E. E., Dinniman, M. S., and Hemmings, J. C. P.: Climate change impacts
980 on southern Ross Sea phytoplankton composition, productivity, and export, *Journal of Geophysical Research: Oceans*, 122, 2339–2359, <https://doi.org/10.1002/2016JC012514>, 2017.
- Keller, M. D., Bellows, W. K., and Guillard, R. R. L.: Dimethyl sulfide production in marine phytoplankton, in: *Biogenic Sulfur in the Environment*, edited by Saltzman, E. S. and Cooper, W. J., vol. 393 of *ACS Symposium Series*, pp. 167–182, American Chemical Society, <https://doi.org/10.1021/bk-1989-0393>, ISBN: 0-8412-1612-6, 1989.
- 985 Lam, P. J. and Bishop, J. K. B.: High biomass, low export regimes in the Southern Ocean, *Deep Sea Research Part II: Topical Studies in Oceanography*, 54, 601–638, <https://doi.org/10.1016/j.dsr2.2007.01.013>, 2007.
- Lana, A., Bell, T. G., Simó, R., Vallina, S. M., Ballabrera-Poy, J., Kettle, A. J., Dachs, J., Bopp, L., Saltzman, E. S., Stefels, J., Johnson, J. E., and Liss, P. S.: An updated climatology of surface dimethylsulfide concentrations and emission fluxes in the global ocean, *Global Biogeochemical Cycles*, 25, 1–17, <https://doi.org/10.1029/2010GB003850>, 2011.
- 990 Laufkötter, C., Vogt, M., Gruber, N., Aumont, O., Bopp, L., Doney, S. C., Dunne, J. P., Hauck, J., John, J. G., Lima, I. D., Seferian, R., and Völker, C.: Projected decreases in future marine export production: the role of the carbon flux through the upper ocean ecosystem, *Biogeosciences*, 13, 4023–4047, <https://doi.org/10.5194/bg-13-4023-2016>, 2016.
- Lauvset, S. K., Key, R. M., Olsen, A., Van Heuven, S., Velo, A., Lin, X., Schirnick, C., Kozyr, A., Tanhua, T., Hoppema, M., Jutterström, S., Steinfeldt, R., Jeansson, E., Ishii, M., Perez, F. F., Suzuki, T., and Watelet, S.: A new global interior ocean mapped climatology: The
995 $1^{\circ} \times 1^{\circ}$ GLODAP version 2, *Earth System Science Data*, 8, 325–340, <https://doi.org/10.5194/essd-8-325-2016>, 2016.
- Le Quéré, C., Buitenhuis, E. T., Moriarty, R., Alvain, S., Aumont, O., Bopp, L., Chollet, S., Enright, C., Franklin, D. J., Geider, R. J., Harrison, S. P., Hirst, A. G., Larsen, S., Legendre, L., Platt, T., Prentice, I. C., Rivkin, R. B., Sailley, S., Sathyendranath, S., Stephens, N., Vogt, M., and Vallina, S. M.: Role of zooplankton dynamics for Southern Ocean phytoplankton biomass and global biogeochemical cycles, *Biogeosciences*, 13, 4111–4133, <https://doi.org/10.5194/bg-13-4111-2016>, 2016.
- 1000 Leblanc, K., Arístegui, J., Armand, L., Assmy, P., Beker, B., Bode, A., Breton, E., Cornet, V., Gibson, J., Gosselin, M.-P., Kopczynska, E., Marshall, H., Peloquin, J., Piontkovski, S., Poulton, A. J., Quéguiner, B., Schiebel, R., Shipe, R., Stefels, J., van Leeuwe, M. A., Varela, M., Widdicombe, C., and Yallop, M.: A global diatom database - abundance, biovolume and biomass in the world ocean, *Earth System Science Data*, 4, 149–165, <https://doi.org/10.5194/essd-4-149-2012>, 2012.
- Lee, S. H., Hwang, J., Ducklow, H. W., Hahm, D., Lee, S. H., Kim, D., Hyun, J.-H., Park, J., Ha, H. K., Kim, T.-W., Yang, E. J., and Shin,
1005 H. C.: Evidence of minimal carbon sequestration in the productive Amundsen Sea polynya, *Geophysical Research Letters*, 44, 7892–7899, <https://doi.org/10.1002/2017GL074646>, 2017.
- Lima, I. D., Lam, P. J., and Doney, S. C.: Dynamics of particulate organic carbon flux in a global ocean model, *Biogeosciences*, 11, 1177–1198, <https://doi.org/10.5194/bg-11-1177-2014>, 2014.
- Liss, P. S., Malin, G., Turner, S. M., and Holligan, P. M.: Dimethyl sulphide and *Phaeocystis*: A review, *Journal of Marine Systems*, 5, 41–53,
1010 [https://doi.org/10.1016/0924-7963\(94\)90015-9](https://doi.org/10.1016/0924-7963(94)90015-9), 1994.

- Locarnini, R. A., Mishonov, A. V., Antonov, J. I., Boyer, T. P., Garcia, H. E., Baranova, O. K., Zweng, M. M., Paver, C. R., Reagan, J. R., Johnson, D. R., Hamilton, M., and Seidov, D.: World Ocean Atlas 2013, Volume 1: Temperature, NOAA Atlas NESDIS 73, 1, 40 pp, 2013.
- 1015 Losa, S. N., Dutkiewicz, S., Losch, M., J., O., Soppa, M. A., Trimborn, S., Xi, H., , and Bracher, A.: On modeling the Southern Ocean Phytoplankton Functional Types, Biogeosciences Discussion, <https://doi.org/10.5194/bg-2019-289>, 2019.
- Maritorea, S., Fanton D'Andon, O., Mangin, A., and Siegel, D. A.: Merged satellite ocean color data products using a bio-optical model: Characteristics, benefits and issues, Remote Sensing of Environment, 114, 1791–1804, <https://doi.org/10.1016/j.rse.2010.04.002>, 2010.
- Martin, J. H., Fitzwater, S. E., and Gordon, R. M.: Iron deficiency limits phytoplankton growth in Antarctic waters, Global Biogeochemical Cycles, 4, 5–12, <https://doi.org/10.1029/GB004i001p00005>, 1990a.
- 1020 Martin, J. H., Gordon, R. M., and Fitzwater, S. E.: Iron in Antarctic waters, Nature, 345, 156–158, <https://doi.org/10.1038/345156a0>, 1990b.
- Martínez-García, A., Sigman, D. M., Ren, H., Anderson, R. F., Straub, M., Hodell, D. a., Jaccard, S. L., Eglinton, T. I., and Haug, G. H.: Iron fertilization of the Subantarctic ocean during the last ice age., Science, 343, 1347–50, <https://doi.org/10.1126/science.1246848>, 2014.
- Mills, M. M., Kropuenske, L. R., van Dijken, G. L., Alderkamp, A.-C., Berg, G. M., Robinson, D. H., Welschmeyer, N. A., and Arrigo, K. R.: Photophysiology in two Southern Ocean phytoplankton taxa: photosynthesis of *Phaeocystis Antarctica* (Prymnesiophyceae) and *Fragilariopsis cylindrus* (Bacillariophyceae) under simulated mixed-layer irradiance, Journal of Phycology, 46, 1114–1127, <https://doi.org/10.1111/j.1529-8817.2010.00923.x>, 2010.
- 1025 Moisan, T. A. and Mitchell, B. G.: Modeling Net Growth of *Phaeocystis antarctica* Based on Physiological and Optical Responses to Light and Temperature Co-limitation, Frontiers in Marine Science, 4, 1–15, <https://doi.org/10.3389/fmars.2017.00437>, 2018.
- Moore, J. K., Doney, S. C., Kleypas, J. A., Glover, D. M., and Fung, I. Y.: An intermediate complexity marine ecosystem model for the global domain, Deep-Sea Research Part II, 49, 403–462, [https://doi.org/10.1016/S0967-0645\(01\)00108-4](https://doi.org/10.1016/S0967-0645(01)00108-4), 2002.
- 1030 Moore, J. K., Lindsay, K., Doney, S. C., Long, M. C., and Misumi, K.: Marine ecosystem dynamics and biogeochemical cycling in the Community Earth System Model [CESM1(BGC)]: Comparison of the 1990s with the 2090s under the RCP4.5 and RCP8.5 scenarios, Journal of Climate, 26, 9291–9312, <https://doi.org/10.1175/JCLI-D-12-00566.1>, 2013.
- Morel, A. and Berthon, J.-F.: Surface pigments, algal biomass profiles, and potential production of the euphotic layer: Relationships reinvestigated in view of remote-sensing applications, Limnology and Oceanography, 34, 1545–1562, <https://doi.org/10.4319/lo.1989.34.8.1545>, 1989.
- 1035 NASA-OBPG: NASA Goddard Space Flight Center, Ocean Ecology Laboratory, Ocean Biology Processing Group, Moderate-resolution Imaging Spectroradiometer (MODIS) Aqua Chlorophyll Data, <https://doi.org/10.5067/AQUA/MODIS/L3M/CHL/2014>, 2014a.
- NASA-OBPG: NASA Goddard Space Flight Center, Ocean Ecology Laboratory, Ocean Biology Processing Group, Sea-viewing Wide Field-of-view Sensor (SeaWiFS) Chlorophyll Data, <https://doi.org/10.5067/ORBVIEW-2/SEAWIFS/L3M/CHL/2014>, 2014b.
- 1040 Nejtgaard, J. C., Tang, K. W., Steinke, M., Dutz, J., Koski, M., Antajan, E., and Long, J. D.: Zooplankton grazing on *Phaeocystis*: a quantitative review and future challenges, in: *Phaeocystis*, major link in the biogeochemical cycling of climate-relevant elements, vol. 83, pp. 147–172, Springer Netherlands, <https://doi.org/10.1007/s10533-007-9098-y>, 2007.
- Nguyen, B. C., Mihalopoulos, N., and Belviso, S.: Seasonal variation of atmospheric dimethylsulfide at Amsterdam Island in the southern Indian Ocean, Journal of Atmospheric Chemistry, 11, 123–141, <https://doi.org/10.1007/BF00053671>, 1990.
- 1045 Nissen, C. and Vogt, M.: ROMS-BEC model data: Factors controlling the competition between *Phaeocystis* and diatoms in the Southern Ocean and implications for carbon export fluxes, <https://doi.org/10.3929/ethz-b-000409193>, 2020.

- Nissen, C., Vogt, M., Münnich, M., Gruber, N., and Haumann, F. A.: Factors controlling coccolithophore biogeography in the Southern Ocean, *Biogeosciences*, 15, 6997–7024, <https://doi.org/10.5194/bg-15-6997-2018>, 2018.
- 1050 O'Brien, C. J., Peloquin, J. A., Vogt, M., Heinle, M., Gruber, N., Ajani, P., Andruleit, H., Arístegui, J., Beaufort, L., Estrada, M., Karentz, D., Kopczyńska, E., Lee, R., Poulton, A. J., Pritchard, T., and Widdicombe, C.: Global marine plankton functional type biomass distributions: coccolithophores, *Earth System Science Data*, 5, 259–276, <https://doi.org/10.5194/essd-5-259-2013>, 2013.
- O'Malley, R.: Ocean Productivity website, data downloaded from <http://www.science.oregonstate.edu/ocean.productivity/index.php>, last access: 16 May 2016.
- 1055 Palter, J. B., Sarmiento, J. L., Gnanadesikan, A., Simeon, J., and Slater, R. D.: Fueling export production: nutrient return pathways from the deep ocean and their dependence on the Meridional Overturning Circulation, *Biogeosciences*, 7, 3549–3568, <https://doi.org/10.5194/bg-7-3549-2010>, 2010.
- Pasquer, B., Laruelle, G., Becquevort, S., Schoemann, V., Goosse, H., and Lancelot, C.: Linking ocean biogeochemical cycles and ecosystem structure and function: results of the complex SWAMCO-4 model, *Journal of Sea Research*, 53, 93–108, <https://doi.org/10.1016/j.seares.2004.07.001>, 2005.
- 1060 Peloquin, J. A. and Smith, W. O.: Phytoplankton blooms in the Ross Sea, Antarctica: Interannual variability in magnitude, temporal patterns, and composition, *Journal of Geophysical Research*, 112, C08 013, <https://doi.org/10.1029/2006JC003816>, 2007.
- Peperzak, L.: Observations of flagellates in colonies of *Phaeocystis globosa* (Prymnesiophyceae); a hypothesis for their position in the life cycle, *Journal of Plankton Research*, 22, 2181–2203, <https://doi.org/10.1093/plankt/22.12.2181>, 2000.
- 1065 Popova, E. E., Pollard, R. T., Lucas, M. I., Venables, H. J., and Anderson, T. R.: Real-time forecasting of ecosystem dynamics during the CROZEX experiment and the roles of light, iron, silicate, and circulation, *Deep Sea Research Part II: Topical Studies in Oceanography*, 54, 1966–1988, <https://doi.org/10.1016/j.dsr2.2007.06.018>, 2007.
- Poulton, A. J., Moore, M. C., Seeyave, S., Lucas, M. I., Fielding, S., and Ward, P.: Phytoplankton community composition around the Crozet Plateau, with emphasis on diatoms and *Phaeocystis*, *Deep Sea Research Part II: Topical Studies in Oceanography*, 54, 2085–2105, <https://doi.org/10.1016/j.dsr2.2007.06.005>, 2007.
- 1070 Reigstad, M. and Wassmann, P.: Does *Phaeocystis* spp. contribute significantly to vertical export of organic carbon?, in: *Phaeocystis*, major link in the biogeochemical cycling of climate-relevant elements, vol. 83, pp. 217–234, Springer Netherlands, https://doi.org/10.1007/978-1-4020-6214-8_16, http://link.springer.com/10.1007/978-1-4020-6214-8_16, 2007.
- Rigual Hernández, A. S., Trull, T. W., Nodder, S. D., Flores, J. A., Bostock, H., Abrantes, F., Eriksen, R. S., Sierro, F. J., Davies, D. M., Ballegeer, A.-M., Fuertes, M. A., and Northcote, L. C.: Coccolithophore biodiversity controls carbonate export in the Southern Ocean, *Biogeosciences*, 17, 245–263, <https://doi.org/10.5194/bg-17-245-2020>, 2020.
- Rivero-Calle, S., Gnanadesikan, A., Del Castillo, C. E., Balch, W. M., and Guikema, S. D.: Multidecadal increase in North Atlantic coccolithophores and the potential role of rising CO₂, *Science*, 350, 1533–1537, <https://doi.org/10.1126/science.aaa8026>, 2015.
- Rosengard, S. Z., Lam, P. J., Balch, W. M., Auro, M. E., Pike, S., Drapeau, D., and Bowler, B.: Carbon export and transfer to depth across the Southern Ocean Great Calcite Belt, *Biogeosciences*, 12, 3953–3971, <https://doi.org/10.5194/bg-12-3953-2015>, 2015.
- 1080 Rousseau, V., Vaultot, D., Casotti, R., Cariou, V., Lenz, J., Gunkel, J., and Baumann, M.: The life cycle of *Phaeocystis* (Prymnesiophyceae): evidence and hypotheses, *Journal of Marine Systems*, 5, 23–39, [https://doi.org/10.1016/0924-7963\(94\)90014-0](https://doi.org/10.1016/0924-7963(94)90014-0), 1994.
- Ryan-Keogh, T. J., DeLizo, L. M., Smith, W. O., Sedwick, P. N., McGillicuddy, D. J., Moore, C. M., and Bibby, T. S.: Temporal progression of photosynthetic-strategy in phytoplankton in the Ross Sea, Antarctica, *Journal of Marine Systems*,

- 1085 166, 87–96, <https://doi.org/10.1016/j.jmarsys.2016.08.014>, <http://dx.doi.org/10.1016/j.jmarsys.2016.08.014><https://linkinghub.elsevier.com/retrieve/pii/S0924796316302688>, 2017.
- Saavedra-Pellitero, M., Baumann, K.-H., Flores, J.-A., and Gersonde, R.: Biogeographic distribution of living coccolithophores in the Pacific sector of the Southern Ocean, *Marine Micropaleontology*, 109, 1–20, <https://doi.org/10.1016/j.marmicro.2014.03.003>, 2014.
- Sarmiento, J. L., Gruber, N., Brzezinski, M. A., and Dunne, J. P.: High-latitude controls of thermocline nutrients and low latitude biological productivity., *Nature*, 427, 56–60, <https://doi.org/10.1038/nature02127>, 2004.
- 1090 Sathyendranath, S., Stuart, V., Nair, A., Oka, K., Nakane, T., Bouman, H., Forget, M. H., Maass, H., and Platt, T.: Carbon-to-chlorophyll ratio and growth rate of phytoplankton in the sea, *Marine Ecology Progress Series*, 383, 73–84, <https://doi.org/10.3354/meps07998>, 2009.
- Schlitzer, R.: Export production in the Equatorial and North Pacific derived from dissolved oxygen, nutrient and carbon data, *J. Oceanogr.*, 60, 53–62, <https://doi.org/10.1023/B:JOCE.0000038318.38916.e6>, 2004.
- 1095 Schoemann, V., Wollast, R., Chou, L., and Lancelot, C.: Effects of photosynthesis on the accumulation of Mn and Fe by *Phaeocystis* colonies, *Limnology and Oceanography*, 46, 1065–1076, <https://doi.org/10.4319/lo.2001.46.5.1065>, 2001.
- Schoemann, V., Becquevort, S., Stefels, J., Rousseau, V., and Lancelot, C.: *Phaeocystis* blooms in the global ocean and their controlling mechanisms: a review, *Journal of Sea Research*, 53, 43–66, <https://doi.org/10.1016/j.seares.2004.01.008>, 2005.
- Sedwick, P. N., DiTullio, G. R., and Mackey, D. J.: Iron and manganese in the Ross Sea, Antarctica: Seasonal iron limitation in Antarctic shelf waters, *Journal of Geophysical Research*, 105, 11 321, <https://doi.org/10.1029/2000JC000256>, 2000.
- 1100 Sedwick, P. N., Garcia, N. S., Riseman, S. F., Marsay, C. M., and DiTullio, G. R.: Evidence for high iron requirements of colonial *Phaeocystis antarctica* at low irradiance, in: *Phaeocystis*, major link in the biogeochemical cycling of climate-relevant elements, vol. 83, pp. 83–97, Springer Netherlands, https://doi.org/10.1007/978-1-4020-6214-8_8, 2007.
- Shchepetkin, A. F. and McWilliams, J. C.: The regional oceanic modeling system (ROMS): a split-explicit, free-surface, topography-following-coordinate oceanic model, *Ocean Modeling*, 9, 347–404, <https://doi.org/10.1016/j.ocemod.2004.08.002>, 2005.
- 1105 Siegel, D. A., Buesseler, K. O., Doney, S. C., Salliey, S. F., Behrenfeld, M. J., and Boyd, P. W.: Global assessment of ocean carbon export by combining satellite observations and food-web models, *Global Biogeochemical Cycles*, 28, 181–196, <https://doi.org/10.1002/2013GB004743>, 2014.
- Simó, R. and Pedrós-Alló, C.: Role of vertical mixing in controlling the oceanic production of dimethyl sulphide, *Nature*, 402, 396–399, <https://doi.org/10.1038/46516>, 1999.
- 1110 Smetacek, V., Assmy, P., and Henjes, J.: The role of grazing in structuring Southern Ocean pelagic ecosystems and biogeochemical cycles, *Antarct. Sci.*, 16, 541–558, <https://doi.org/10.1017/S0954102004002317>, 2004.
- Smetacek, V., Klaas, C., Strass, V. H., Assmy, P., Montresor, M., Cisewski, B., Savoye, N., Webb, A., D’Ovidio, F., Arrieta, J. M., Bathmann, U., Bellerby, R., Berg, G. M., Croot, P., Gonzalez, S., Henjes, J., Herndl, G. J., Hoffmann, L. J., Leach, H., Losch, M., Mills, M. M., Neill, C., Peeken, I., Röttgers, R., Sachs, O., Sauter, E., Schmidt, M. M., Schwarz, J., Terbrüggen, A., and Wolf-Gladrow, D.: Deep carbon export from a Southern Ocean iron-fertilized diatom bloom, *Nature*, 487, 313–319, <https://doi.org/10.1038/nature11229>, 2012.
- 1115 Smith, W. O. and Gordon, L. I.: Hyperproductivity of the Ross Sea (Antarctica) polynya during austral spring, *Geophysical Research Letters*, 24, 233–236, <https://doi.org/10.1029/96GL03926>, 1997.
- Smith, W. O., Dennett, M. R., Mathot, S., and Caron, D. A.: The temporal dynamics of the flagellated and colonial stages of *Phaeocystis antarctica* in the Ross Sea, *Deep Sea Research Part II: Topical Studies in Oceanography*, 50, 605–617, [https://doi.org/10.1016/S0967-0645\(02\)00586-6](https://doi.org/10.1016/S0967-0645(02)00586-6), 2003.
- 1120

- Smith, W. O., Dinniman, M. S., Tozzi, S., DiTullio, G. R., Mangoni, O., Modigh, M., and Saggiomo, V.: Phytoplankton photosynthetic pigments in the Ross Sea: Patterns and relationships among functional groups, *Journal of Marine Systems*, 82, 177–185, <https://doi.org/10.1016/j.jmarsys.2010.04.014>, 2010.
- 1125 Smith, W. O., Shields, A. R., Dreyer, J. C., Peloquin, J. A., and A., V.: Interannual variability in vertical export in the Ross Sea: Magnitude, composition, and environmental correlates, *Deep Sea Research Part I: Oceanographic Research Papers*, 58, 147–159, <https://doi.org/10.1016/j.dsr.2010.11.007>, 2011.
- Smith, W. O., Ainley, D. G., Arrigo, K. R., and Dinniman, M. S.: The Oceanography and Ecology of the Ross Sea, *Annual Review of Marine Science*, 6, 469–487, <https://doi.org/10.1146/annurev-marine-010213-135114>, 2014.
- 1130 Soppa, M., Hirata, T., Silva, B., Dinter, T., Peeken, I., Wiegmann, S., and Bracher, A.: Global retrieval of diatom abundance based on phytoplankton pigments and satellite data, *Remote Sensing*, 6, 10089–10 106, <https://doi.org/10.3390/rs61010089>, 2014.
- Soppa, M., Völker, C., and Bracher, A.: Diatom phenology in the Southern Ocean: mean patterns, trends and the role of climate Oscillations, *Remote Sensing*, 8, 420, <https://doi.org/10.3390/rs8050420>, 2016.
- Stange, P., Bach, L. T., Le Moigne, F. A. C., Taucher, J., Boxhammer, T., and Riebesell, U.: Quantifying the time lag between organic matter production and export in the surface ocean: Implications for estimates of export efficiency, *Geophysical Research Letters*, 44, 268–276, <https://doi.org/10.1002/2016GL070875>, 2017.
- 1135 Stefels, J., Steinke, M., Turner, S., Malin, G., and Belviso, S.: Environmental constraints on the production and removal of the climatically active gas dimethylsulphide (DMS) and implications for ecosystem modelling, in: *Phaeocystis*, major link in the biogeochemical cycling of climate-relevant elements, pp. 245–275, Springer Netherlands, https://doi.org/10.1007/978-1-4020-6214-8_18, 2007.
- 1140 Steinberg, D. K. and Landry, M. R.: Zooplankton and the ocean carbon cycle, *Annual Review of Marine Science*, 9, 413–444, <https://doi.org/10.1146/annurev-marine-010814-015924>, 2017.
- Strzepek, R. F., Boyd, P. W., and Sunda, W. G.: Photosynthetic adaptation to low iron, light, and temperature in Southern Ocean phytoplankton, *Proceedings of the National Academy of Sciences*, 116, 4388–4393, <https://doi.org/10.1073/pnas.1810886116>, <http://www.pnas.org/lookup/doi/10.1073/pnas.1810886116>, 2019.
- 1145 Swan, C. M., Vogt, M., Gruber, N., and Laufkötter, C.: A global seasonal surface ocean climatology of phytoplankton types based on CHEMTAX analysis of HPLC pigments, *Deep-Sea Research Part I*, 109, 137–156, <https://doi.org/10.1016/j.dsr.2015.12.002>, 2016.
- Tagliabue, A. and Arrigo, K. R.: Iron in the Ross Sea: 1. Impact on CO₂ fluxes via variation in phytoplankton functional group and non-Redfield stoichiometry, *Journal of Geophysical Research: Oceans*, 110, 1–15, <https://doi.org/10.1029/2004JC002531>, 2005.
- Tang, K. W., Smith, W. O., Elliott, D. T., and Shields, A. R.: Colony size of *Phaeocystis Antarctica* (Prymnesiophyceae) as influenced by zooplankton grazers, *Journal of Phycology*, 44, 1372–1378, <https://doi.org/10.1111/j.1529-8817.2008.00595.x>, 2008.
- 1150 Tang, K. W., Smith, W. O., Shields, A. R., and Elliott, D. T.: Survival and recovery of *Phaeocystis antarctica* (Prymnesiophyceae) from prolonged darkness and freezing, *Proceedings of the Royal Society B: Biological Sciences*, 276, 81–90, <https://doi.org/10.1098/rspb.2008.0598>, 2009.
- Thomalla, S. J., Fauchereau, N., Swart, S., and Monteiro, P. M. S.: Regional scale characteristics of the seasonal cycle of chlorophyll in the Southern Ocean, *Biogeosciences*, 8, 2849–2866, <https://doi.org/10.5194/bg-8-2849-2011>, 2011.
- 1155 Thomalla, S. J., Racault, M.-F., Swart, S., and Monteiro, P. M. S.: High-resolution view of the spring bloom initiation and net community production in the Subantarctic Southern Ocean using glider data, *ICES Journal of Marine Science: Journal du Conseil*, 72, 1999–2020, <https://doi.org/10.1093/icesjms/fsv105>, 2015.

- 1160 Timmermans, K. R., van der Wagt, B., and de Baar, H. J. W.: Growth rates, half saturation constants, and silicate, nitrate, and phosphate depletion in relation to iron availability of four large open-ocean diatoms from the Southern Ocean, *Limnology and Oceanography*, 49, 2141–2151, <https://doi.org/10.4319/lo.2004.49.6.2141>, 2004.
- Turner, J. T.: Zooplankton fecal pellets, marine snow, phytodetritus and the ocean's biological pump, *Progress in Oceanography*, 130, 205–248, <https://doi.org/10.1016/j.pocean.2014.08.005>, 2015.
- 1165 Tyrrell, T. and Charalampopoulou, A.: Coccolithophore size, abundance and calcification across Drake Passage (Southern Ocean), 2009, <https://doi.org/10.1594/PANGAEA.771715>, 2009.
- van Boekel, W. H. M., Hansen, F. C., Riegman, R., and Bak, R. P. M.: Lysis-induced decline of a *Phaeocystis* spring bloom and coupling with the microbial foodweb, *Marine Ecology Progress Series*, 81, 269–276, <https://doi.org/10.3354/meps081269>, 1992.
- van Hilst, C. M. and Smith, W. O.: Photosynthesis/irradiance relationships in the Ross Sea, Antarctica, and their control by phytoplankton assemblage composition and environmental factors, *Marine Ecology Progress Series*, 226, 1–12, <https://doi.org/10.3354/meps226001>, 1170 2002.
- Veldhuis, M. J. W., Colijn, F., and Admiraal, W.: Phosphate Utilization in *Phaeocystis pouchetii* (*Haptophyceae*), *Marine Ecology*, 12, 53–62, <https://doi.org/10.1111/j.1439-0485.1991.tb00083.x>, 1991.
- Verity, P. G.: Grazing experiments and model simulations of the role of zooplankton in *Phaeocystis* food webs, *Journal of Sea Research*, 43, 317–343, [https://doi.org/10.1016/S1385-1101\(00\)00025-3](https://doi.org/10.1016/S1385-1101(00)00025-3), 2000.
- 1175 Vogt, M., O'Brien, C., Peloquin, J., Schoemann, V., Breton, E., Estrada, M., Gibson, J., Karentz, D., Van Leeuwe, M. A., Stefels, J., Widdicombe, C., and Peperzak, L.: Global marine plankton functional type biomass distributions: *Phaeocystis* spp., *Earth System Science Data*, 4, 107–120, <https://doi.org/10.5194/essd-4-107-2012>, 2012.
- Wang, S. and Moore, J. K.: Incorporating *Phaeocystis* into a Southern Ocean ecosystem model, *Journal of Geophysical Research*, 116, C01 019, <https://doi.org/10.1029/2009JC005817>, 2011.
- 1180 Wang, S., Elliott, S., Maltrud, M., and Cameron-Smith, P.: Influence of explicit *Phaeocystis* parameterizations on the global distribution of marine dimethyl sulfide, *Journal of Geophysical Research: Biogeosciences*, 120, 2158–2177, <https://doi.org/10.1002/2015JG003017>, 2015.
- Ward, B. A., Schartau, M., Oschlies, A., Martin, A. P., Follows, M. J., and Anderson, T. R.: When is a biogeochemical model too complex? Objective model reduction and selection for North Atlantic time-series sites, *Progress in Oceanography*, 116, 49–65, 1185 <https://doi.org/10.1016/j.pocean.2013.06.002>, 2013.
- Winter, A., Henderiks, J., Beaufort, L., Rickaby, R. E. M., and Brown, C. W.: Poleward expansion of the coccolithophore *Emiliania huxleyi*, *Journal of Plankton Research*, 36, 316–325, <https://doi.org/10.1093/plankt/fbt110>, 2013.
- Wright, S. W., van den Enden, R. L., Pearce, I., Davidson, A. T., Scott, F. J., and Westwood, K. J.: Phytoplankton community structure and stocks in the Southern Ocean (30–80°E) determined by CHEMTAX analysis of HPLC pigment signatures, *Deep-Sea Research Part II*, 57, 1190 758–778, <https://doi.org/10.1016/j.dsr2.2009.06.015>, 2010.
- Yager, P. L., Sherrell, R. M., Stammerjohn, S. E., Ducklow, H. W., Schofield, O. M. E., Ingall, E. D., Wilson, S. E., Lowry, K. E., Williams, C. M., Riemann, L., Bertilsson, S., Alderkamp, A.-C., Dinasquet, J., Logares, R., Richert, I., Sipler, R. E., Melara, A. J., Mu, L., Newstead, R. G., Post, A. F., Swalethorp, R., and van Dijken, G. L.: A carbon budget for the Amundsen Sea Polynya, Antarctica: Estimating net community production and export in a highly productive polar ecosystem, *Elementa: Science of the Anthropocene*, 4, 000 140, 1195 <https://doi.org/10.12952/journal.elementa.000140>, 2016.

- Yang, E. J., Jiang, Y., and Lee, S. H.: Microzooplankton herbivory and community structure in the Amundsen Sea, Antarctica, *Deep Sea Research Part II: Topical Studies in Oceanography*, 123, 58–68, <https://doi.org/10.1016/j.dsr2.2015.06.001>, 2016.
- Yang, S., Gruber, N., Long, M. C., and Vogt, M.: ENSO-driven variability of denitrification and suboxia in the Eastern Tropical Pacific Ocean, *Global Biogeochemical Cycles*, 31, 1470–1487, <https://doi.org/10.1002/2016GB005596>, 2017.
- 1200 Zondervan, I.: The effects of light, macronutrients, trace metals and CO₂ on the production of calcium carbonate and organic carbon in coccolithophores—A review, *Deep-Sea Research Part II*, 54, 521–537, <https://doi.org/10.1016/j.dsr2.2006.12.004>, 2007.
- Zweng, M. M., Reagan, J. R., Antonov, J. I., Mishonov, A. V., Boyer, T. P., Garcia, H. E., Baranova, O. K., Johnson, D. R., Seidov, D., and Bidlle, M. M.: *World Ocean Atlas 2013, Volume 2: Salinity*, NOAA Atlas NESDIS 74, 2, 39 pp, 2013.

Supplementary material

The supporting information provides additional figures [in section S1](#) with respect to the nutrient limitation of phytoplankton growth in ROMS-BEC (S1), the [ecological niche analysis \(S2-S3\)](#), the data coverage in a SO satellite derived chlorophyll product ([S2S4](#)), the model evaluation ([S3-S6S5-S8](#)), the bloom timing ([S7S9](#)), the [ecological niche analysis \(S8-S9\)](#), and the [sensitivity simulations \(S10-S11\)](#) [competition sensitivity simulations \(S10\)](#), [carbon cycling in the Ross Sea \(S11\)](#), and the results when using a varying half-saturation constant of iron for *Phaeocystis* growth (S12). In section S2, results of the parameter sensitivity simulations are described (Table S1-S3, Fig. S13).

S1: Additional figures

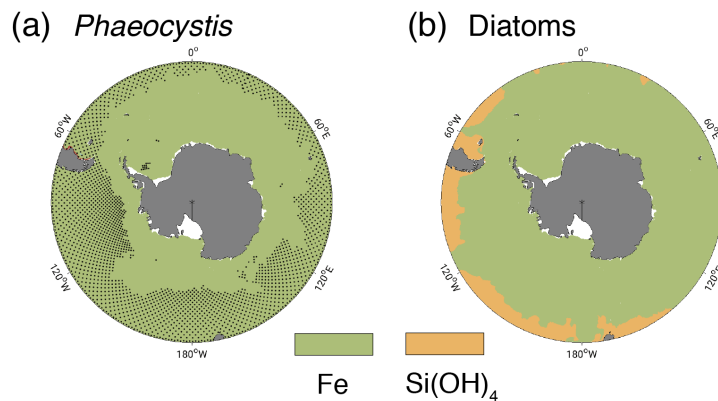


Figure S1: Annual mean most limiting nutrient at the surface south of 45° S for growth rates of a) *Phaeocystis* and b) diatoms in the *Baseline* simulation of ROMS-BEC. High-latitude phytoplankton growth in the model is most limited by either iron (green) or silicic acid (yellow, diatoms only). The stippling in panel a) denotes areas where peak monthly mean chlorophyll concentrations of *Phaeocystis* do not exceed 0.1 mg chl m⁻³.

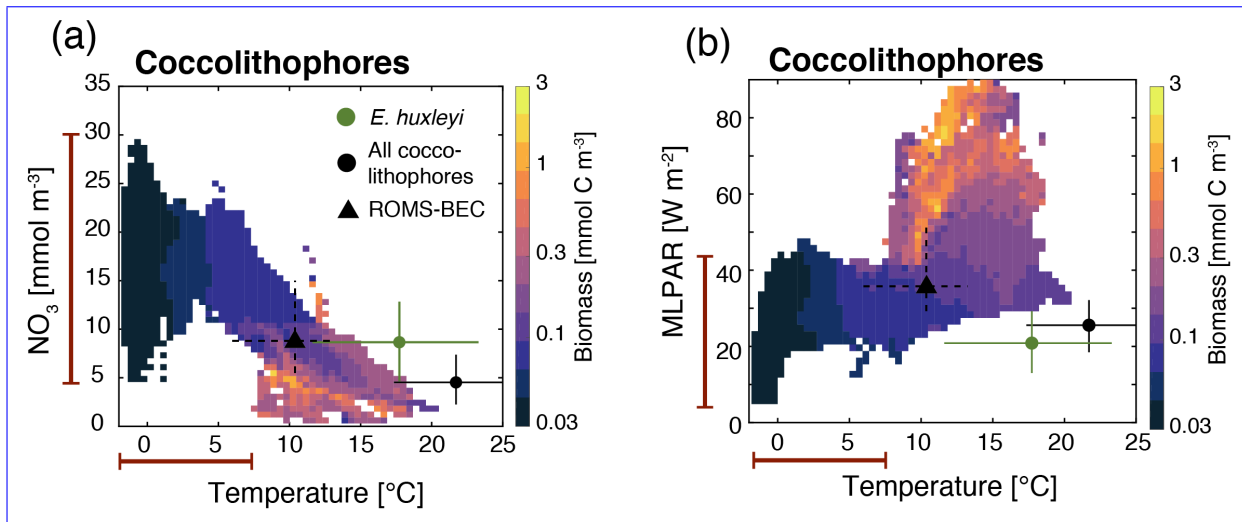


Figure S2: Simulated DJFM average top 50 m average coccolithophore carbon biomass concentrations (mmol C m⁻³) south of 40° S as a function of the simulated temperature (° C) and a) nitrate concentrations (mmol N m⁻³) and b) mixed layer PAR levels (W m⁻²). Overlain are the observed ecological niche centers (median) and breadths (inter quartile ranges) for example taxa from Brun et al. (2015, circles) and as simulated in ROMS-BEC (triangles and dashed lines; area and biomass weighted). The red bars on the axes indicate the simulated range of the respective environmental condition in ROMS-BEC between 60-90° S and averaged over DJFM and the top 50 m.

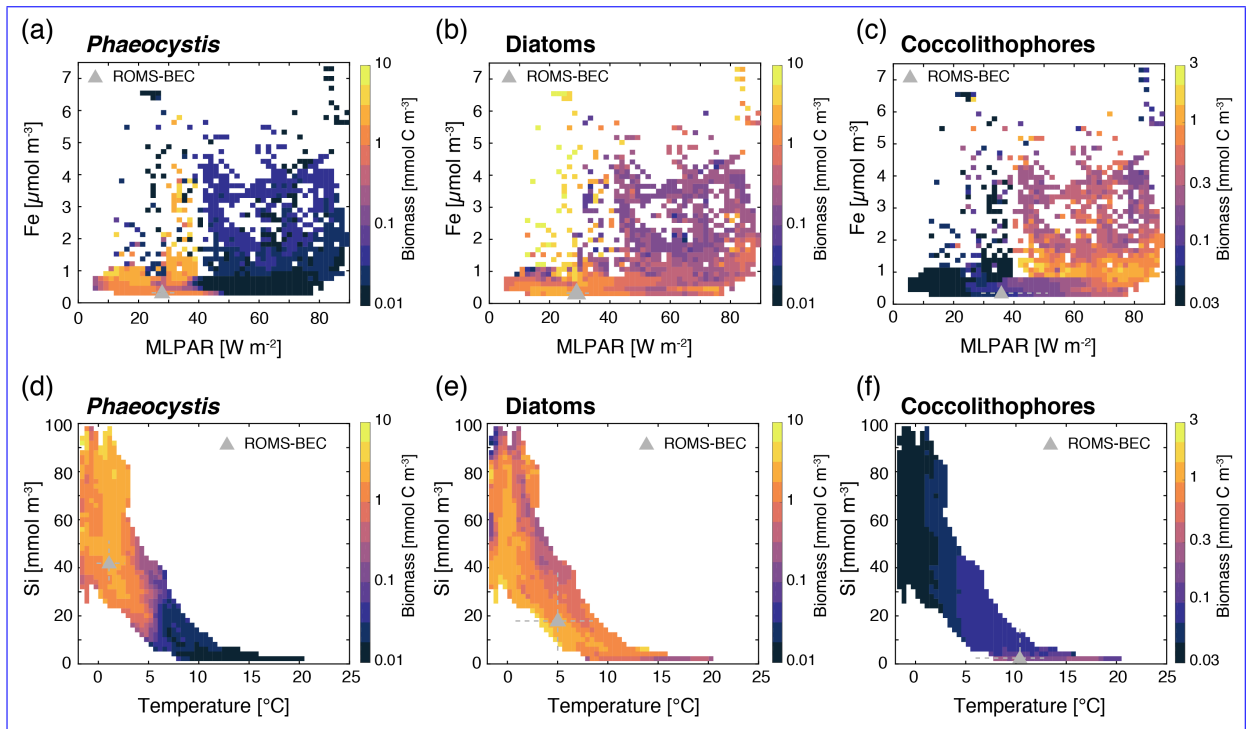


Figure S3: Simulated DJFM average top 50 m average a) *Phaeocystis*, b) diatom, and c) coccolithophore carbon biomass concentrations (mmol C m^{-3}) south of 40°S as a function of the simulated a)-c) dissolved iron concentrations ($\mu\text{mol Fe m}^{-3}$) and mixed layer PAR levels (W m^{-2}) and d)-f) temperature ($^\circ \text{C}$) and dissolved silicic acid concentrations [mmol Si m^{-3}] in the 5-PFT *Baseline* simulation of ROMS-BEC. Overlain are the simulated area and biomass weighted ecological niche centers (median, triangle) and breadths (inter quartile ranges, dashed lines) for the three functional types.

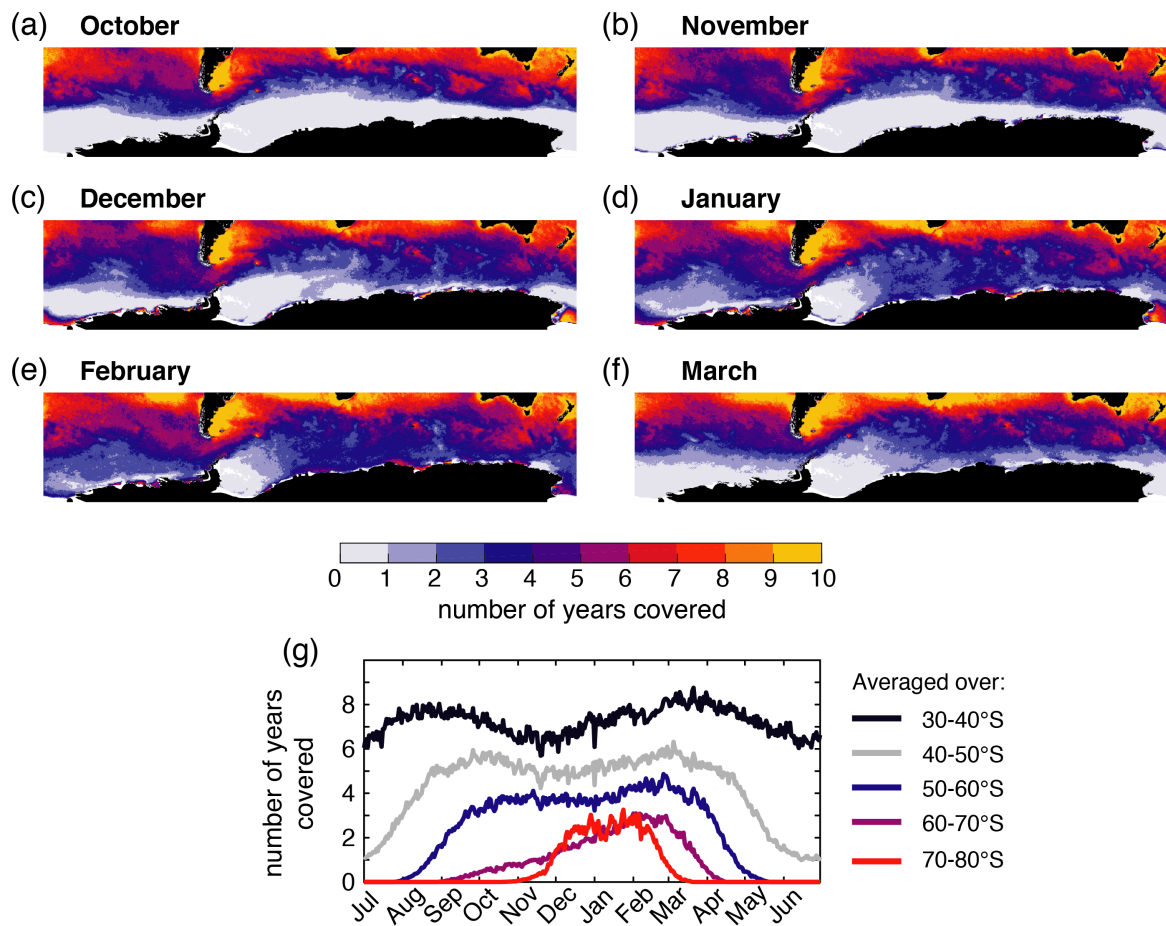


Figure S2S4: Assessment of the SO data coverage in the climatological (1998-2018, i.e. 21 years) daily Globcolor chlorophyll product (Fantón d'Andon et al., 2009; Maritorena et al., 2010): a)-f) Average number of years available for the calculation of the climatological chlorophyll concentration at each grid cell for each of the shown months (October-March), respectively. No minimum number of "days with data coverage" is required for a given month to be counted as "data available" (i.e. one day of data coverage in a month is enough for that month to be counted as "covered" in the respective year). g) Average number of years available for the calculation of the climatological chlorophyll concentration on each day for 10° latitudinal bands across the SO.

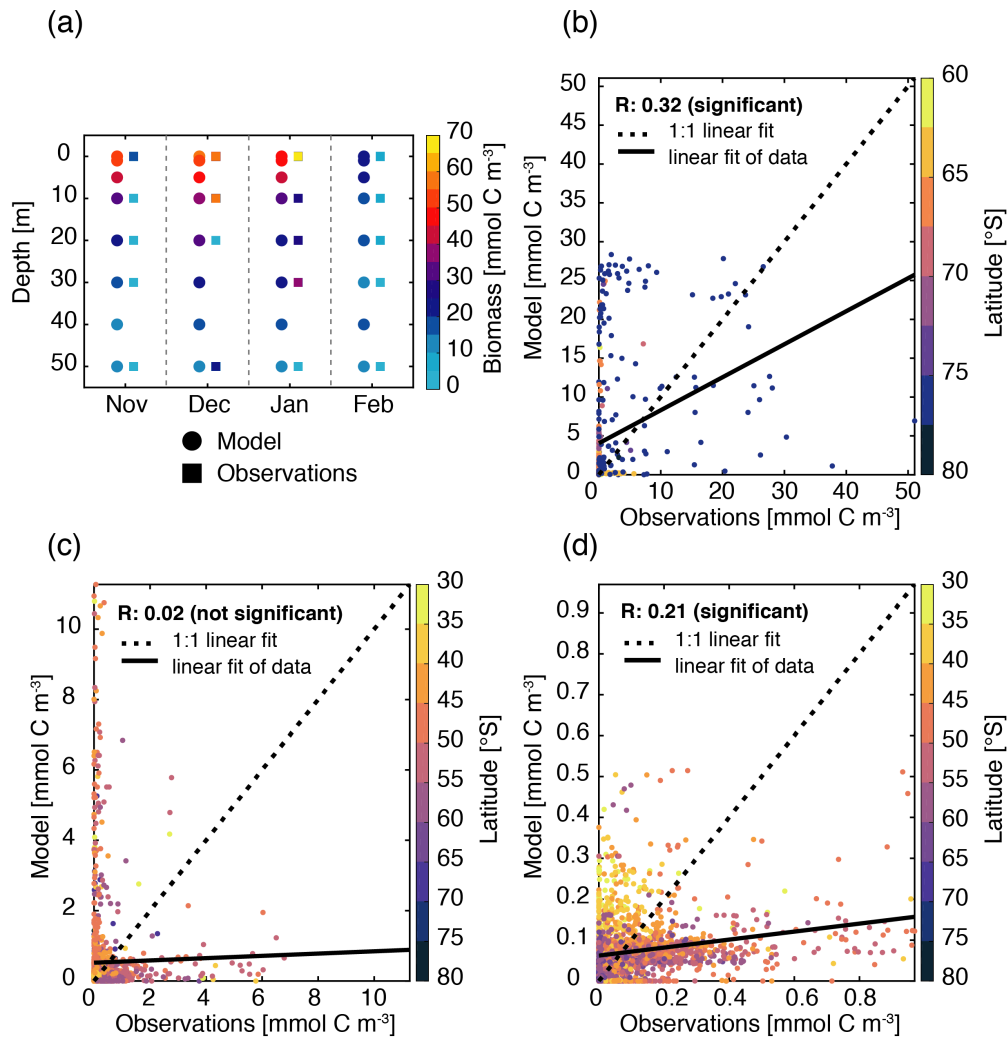


Figure S3S5: Validation of a) & b) *Phaeocystis*, c) diatom, and d) coccolithophore carbon biomass [mmol C m⁻³]. Panel a) shows the maximum *Phaeocystis* carbon biomass concentrations [mmol C m⁻³] in ROMS-BEC (circles) and in observations (squares, Vogt et al., 2012) for each month between November-February and in the the upper 50 meters of the water column. For panels b)-d), the model output is colocated with observations in space and time, and observational data from all months and from above 1000 m are considered here (Balch et al., 2016; Saavedra-Pellitero et al., 2014; O'Brien et al., 2013; Vogt et al., 2012; Leblanc et al., 2012; Tyrrell and Charalampopoulou, 2009; Gravalosa et al., 2008; Cubillos et al., 2007). For more details on the biomass evaluation, see Nissen et al. (2018). The dotted line shows the perfect linear 1:1 fit, whereas the solid line is the actual fit of the data (linear regression). Pearson correlation coefficients of these regressions are given in the top right, those for *Phaeocystis* and coccolithophores are statistically significant ($p < 0.05$). Points are color-coded according to the sampling latitude.

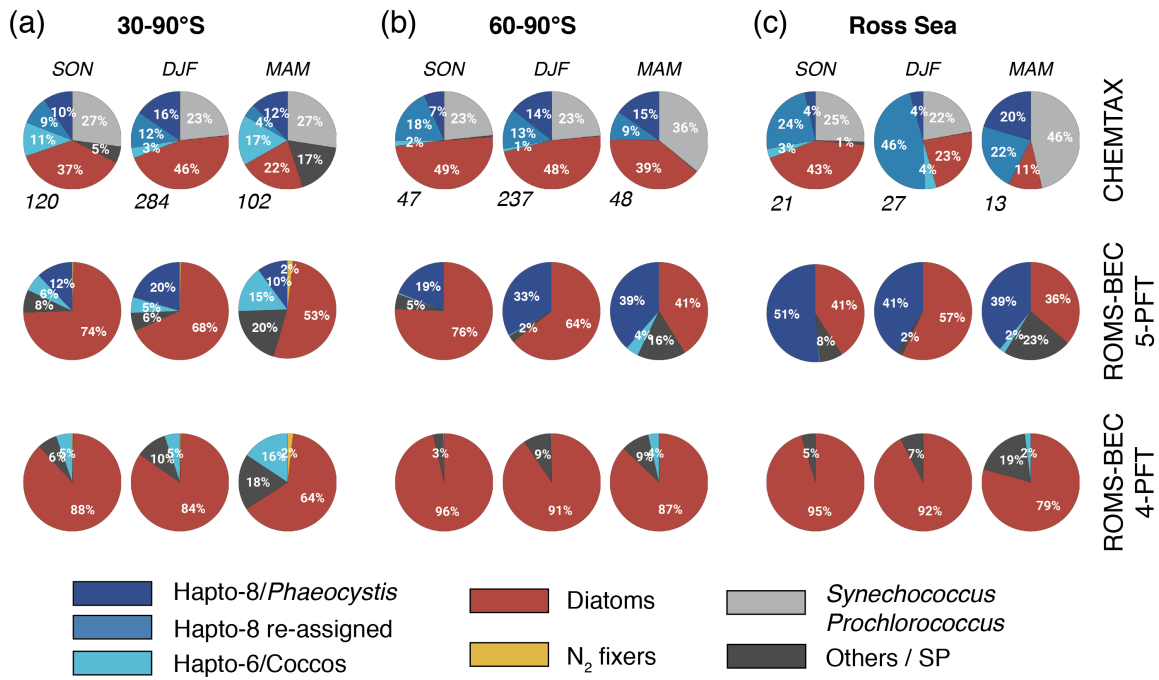


Figure S4S6: a)-c) Relative contribution of the five phytoplankton PFTs to total chlorophyll biomass [mg chl m^{-3}] for a) 30-90° S, b) 60-90° S, and c) the Ross Sea. The top pie charts denote the climatological mixed layer average community composition suggested by CHEMTAX analysis of HPLC pigments for spring, summer, and fall, respectively (the total number of available observations for a given region and season is given at the lower left side, Swan et al., 2016), and the lower pie charts denote the corresponding community structure in the top 50 m in ROMS-BEC in the 5-PFT setup (middle row, same as in Fig. 2 in the main text) and in the 4-PFT setup (lowest row, no *Phaeocystis*, Nissen et al., 2018), respectively. Note that the categories in the CHEMTAX analysis are not 100% equivalent to the model PFTs, and here, "Hapto-8 reassigned" corresponds to the contribution of Hapto-6 where the temperature is $<2^\circ\text{C}$ (see also section 2.3.1 in the main text).

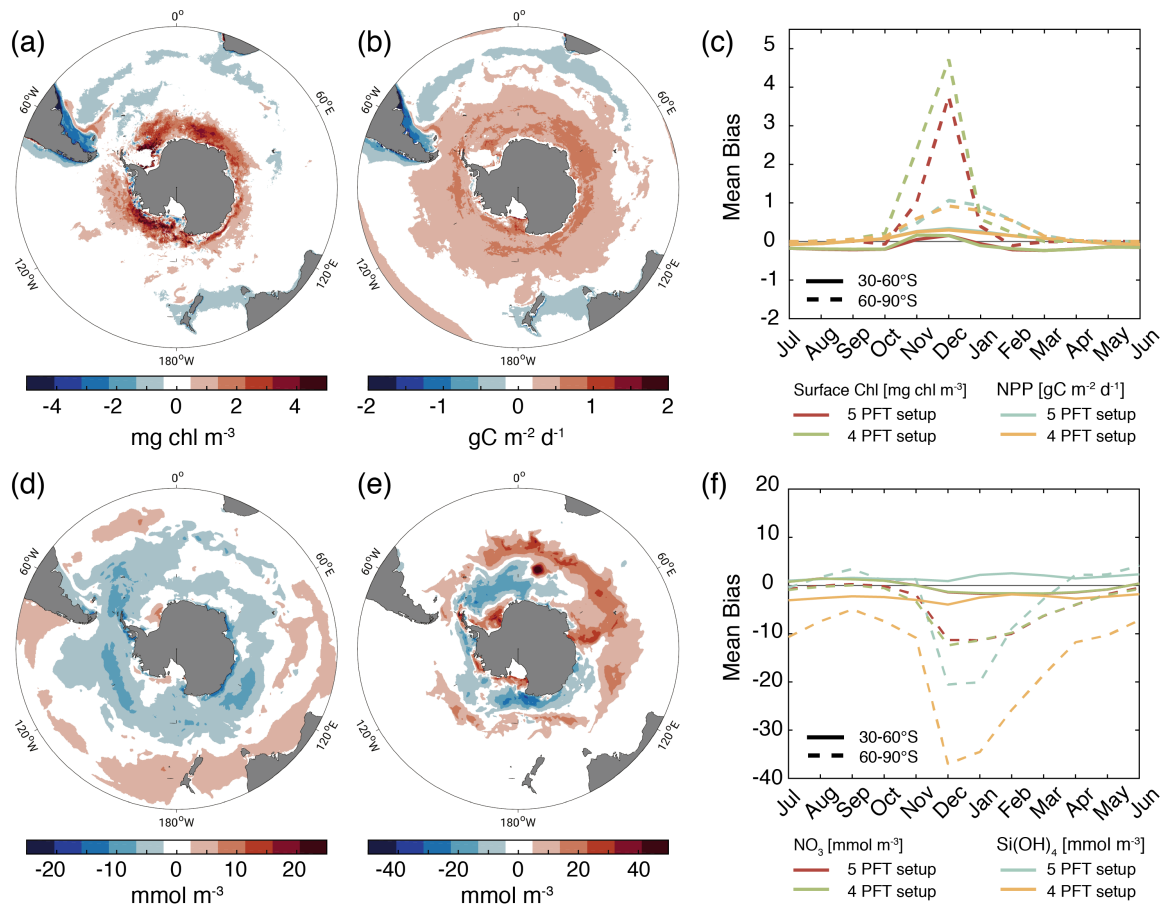


Figure S5S7: Annual mean bias (*Baseline* simulation minus observations) of a) total surface chlorophyll concentrations [g chl m⁻³], b) total vertically integrated NPP [mg C m⁻² d⁻¹], d) surface nitrate concentrations [mmol m⁻³], and e) surface silicic acid concentrations [mmol m⁻³]. The panels c) & f) denote the temporal evolution of the model bias of c) total surface chlorophyll concentration (red) and total NPP (blue), as well as f) surface nitrate concentrations (red), and silicic acid concentrations (blue) in the 5-PFT setup of ROMS-BEC between 30-60° S (solid) and 60-90° S (dashed), respectively. For comparison, the model bias obtained with the 4 PFT setup of ROMS-BEC is included in both panels in green (chlorophyll and nitrate) and yellow (NPP and silicic acid), respectively (see also supplement in Nissen et al., 2018).

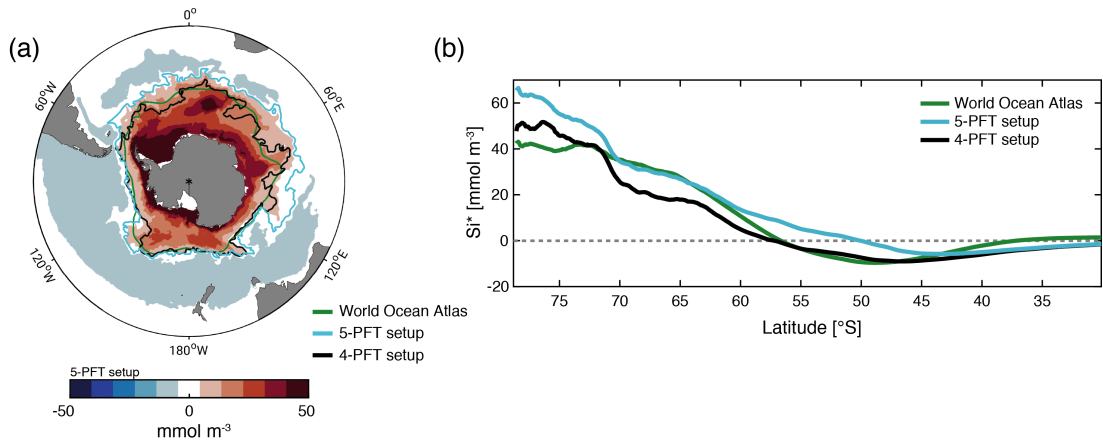


Figure S6S8: Annual mean top 100 m average a) Si^* [mmol m⁻³], which is defined as the difference in concentration between silicic acid and nitrate (Freeman et al., 2018), in the *Baseline* simulation of the 5-PFT setup of ROMS-BEC (colors). The contours denote the latitude of the silicate front, i.e. where $\text{Si}^*=0$, in data from the World Ocean Atlas (green, Garcia et al., 2014) and in the *Baseline* simulation of the 5-PFT setup (light blue) and the 4-PFT setup (black, Nissen et al., 2018) of ROMS-BEC, respectively. b) zonal average Si^* [mmol m⁻³], colors are the same as the contours in panel a).

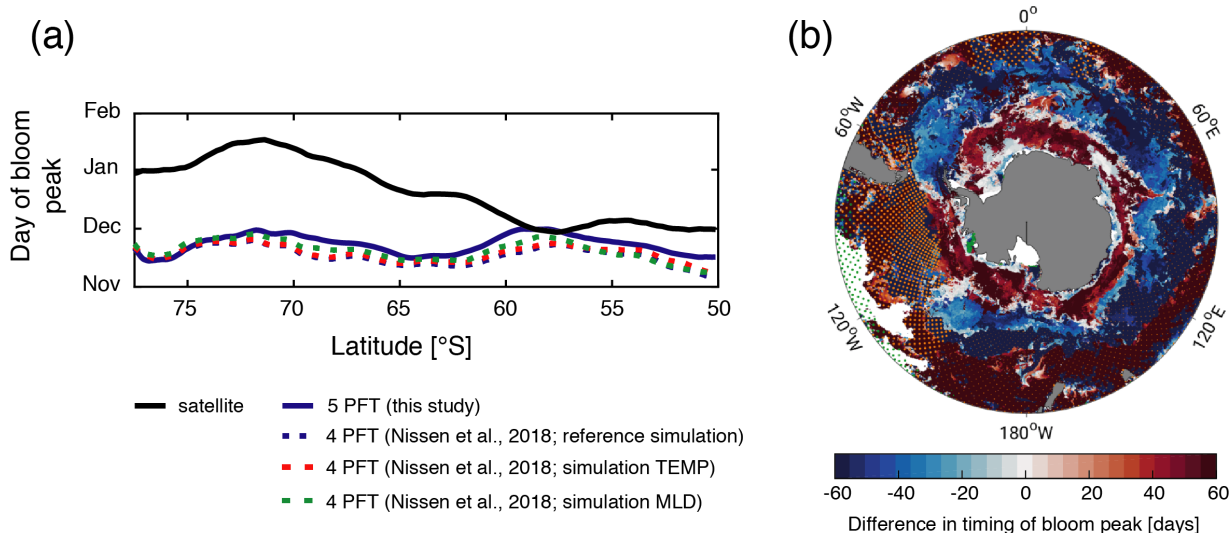


Figure S7S9: a) Same as Fig. 3 in the main text, Hovmöller plots south of 50° S of the day of maximum total chlorophyll concentrations in a satellite product (black line, Globcolor climatology from 1998-2018 based on the daily 25 km chlorophyll product, see Fanton d’Andon et al., 2009; Maritorena et al., 2010), the *Baseline* simulation of this study (solid blue line), the *Baseline* simulation of Nissen et al. (2018, dashed blue line; without *Phaeocystis*). Additionally, two sensitivity simulations in the 4 PFT setup from Nissen et al. (2018) are shown here to show the impact of biases in the simulated physical fields on phytoplankton phenology: The simulations TEMP (dashed red line) and MLD (dashed green line) correct for the simulated average temperature and MLD biases, respectively, within the biological subroutine of the model. b) Difference in day of bloom peak between *Phaeocystis* and diatoms, based on chlorophyll concentrations in the 5-PFT *Baseline* simulation. Stippling indicates locations where maximum chlorophyll concentrations never exceed 0.1 mg chl m⁻³ for *Phaeocystis* (orange) and diatoms (green), respectively. White areas correspond to areas where the peak total chlorophyll concentrations do not exceed 0.5 mg chl m⁻³.

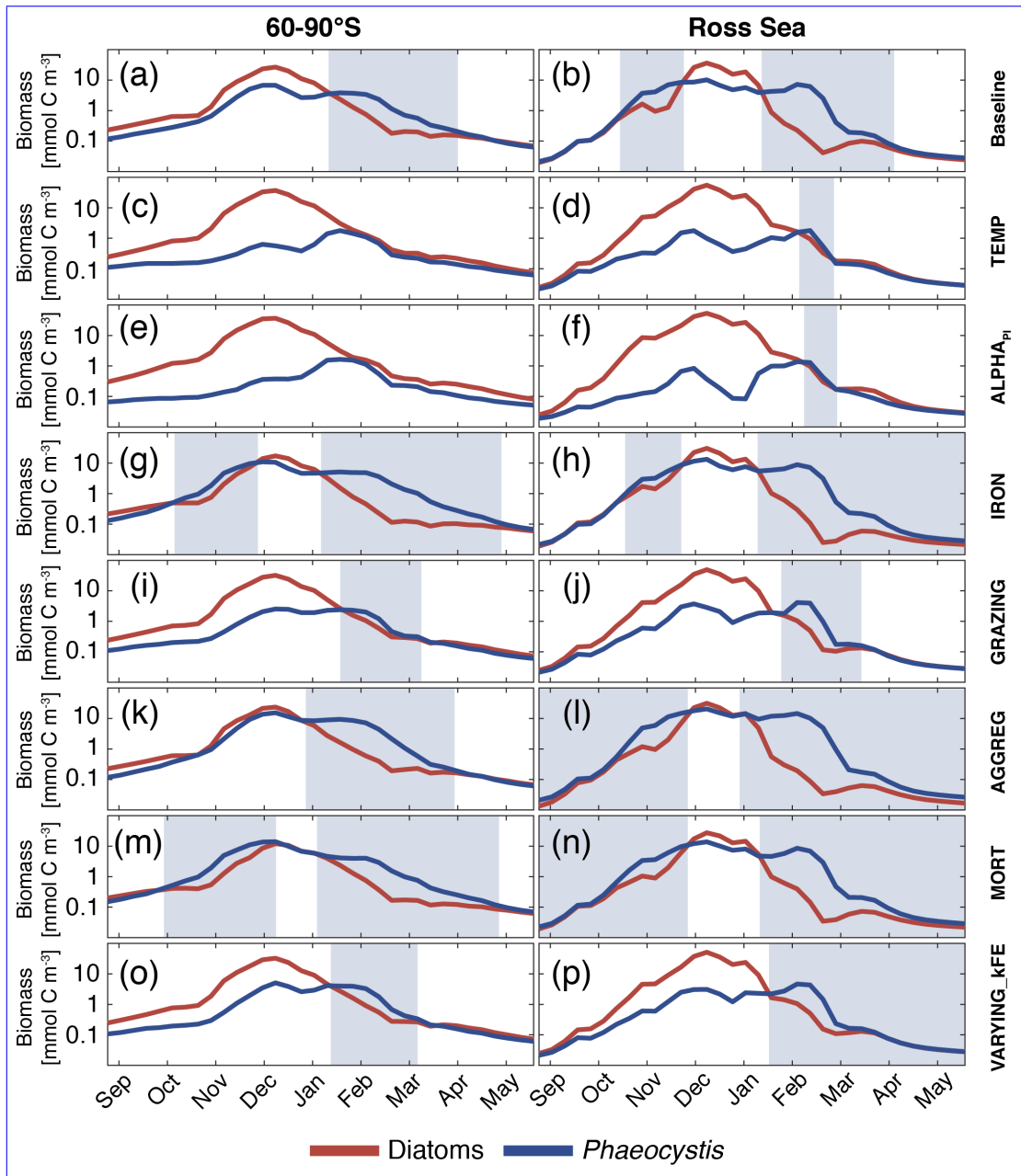


Figure S8S10: Simulated DJFM average top 50 m average coccolithophore *Diatom* (red) and *Phaeocystis* (blue) surface carbon biomass concentrations (mmol C m^{-3}) south of 40°S as a function of the simulated temperature ($^{\circ}\text{C}$) and a) nitrate concentrations (mmol N m^{-3}) and b) mixed layer PAR levels (W m^{-2}). Overlain are the observed ecological niche centers (median) and breadths (inter quartile ranges) for example taxa from Brun et al. (2015, circles and solid lines) and as simulated in ROMS-BEC (triangles and dashed lines; area and biomass weighted). The red bars on the axes indicate the simulated range of the respective environmental condition in ROMS-BEC between] in the different simulations performed in this study. See section 2.2. in the main text for details. The left panels are surface averages over $60\text{-}90^{\circ}\text{S}$ and averaged over DJFM and the top 50 m. S and those on the right for the Ross Sea. Light blue area indicate times of the year when *Phaeocystis* biomass is larger than diatom biomass.

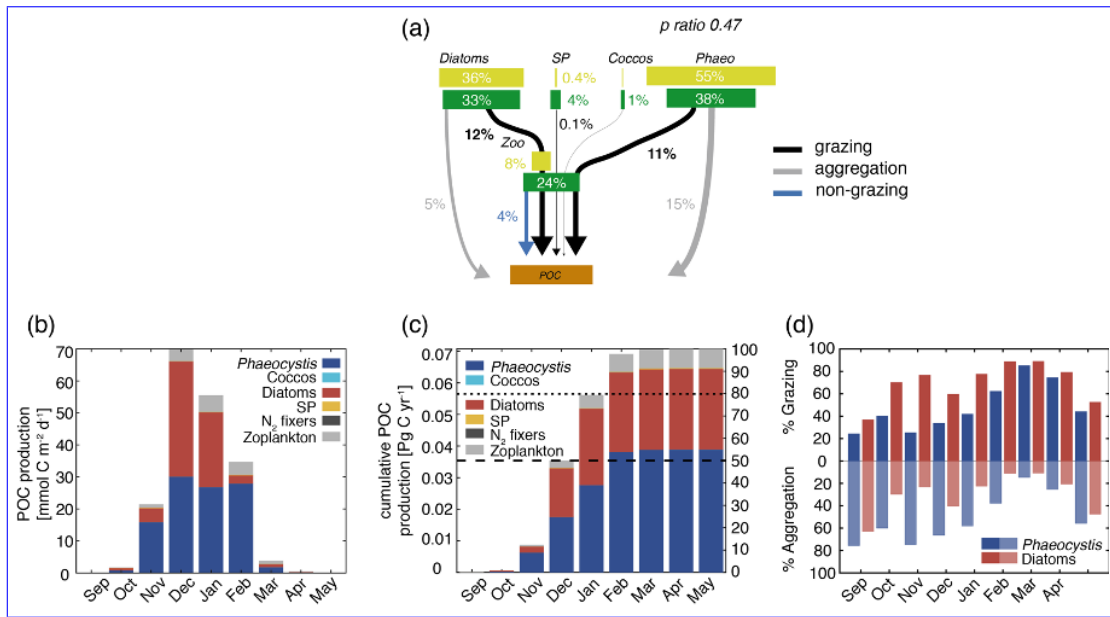


Figure S9: Simulated DJFM average top 50 m average a) **Figure S11:** Carbon cycling in the Ross Sea: a) Pathways of particulate organic carbon (POC) formation in the *Baseline* simulation of ROMS-BEC averaged annually over the Ross Sea. The green and yellow boxes show the relative contribution (%) of *Phaeocystis*, b) diatom, and c) coccolithophore carbon biomass concentrations (mmol C m^{-3}) south of 40°S , diatoms, coccolithophores, small phytoplankton (SP), and zooplankton (Zoo) to the combined phytoplankton and zooplankton biomass (green) and total POC production (yellow) in the top 100 m, respectively. The arrows denote the relative contribution of the different POC production pathways associated with each PFT (black = grazing by zooplankton, grey = aggregation, blue = non-grazing mortality), given as % of total NPP in the top 100 m. Numbers are printed if $\geq 0.1\%$ and rounded to the nearest integer if $> 1\%$. The sum of all arrows gives the POC production efficiency, i.e., the fraction of NPP which is converted into sinking POC upon biomass loss (p ratio). Note that diazotrophs are not included in this figure due to their minor contribution to NPP in the model domain. b-d) Simulated vertically integrated production of particulate organic carbon (POC) b) as a function of the simulated a) c) dissolved iron concentrations ($\mu\text{mol Fe m}^{-3}$) and mixed layer PAR levels (W m^{-2}) and d) f) temperature ($^\circ \text{C}$) and dissolved silicic acid concentrations time [$\text{mmol Si m}^{-3} \text{C m}^{-2} \text{d}^{-1}$] in the 5-PFT *Baseline* simulation of, c) cumulative over time (absolute production in Pg C yr^{-1} on the left axis and relative to annually integrated production on the right axis), and d) as a function of time via grazing and aggregation, respectively. The colors correspond to the different PFTs in ROMS-BEC. Overlain are the simulated area and biomass weighted ecological niche centers (median, triangle) and breadths (inter-quartile ranges, dashed lines) for the three functional types, and the panels correspond to averages or integrals over the Ross Sea.

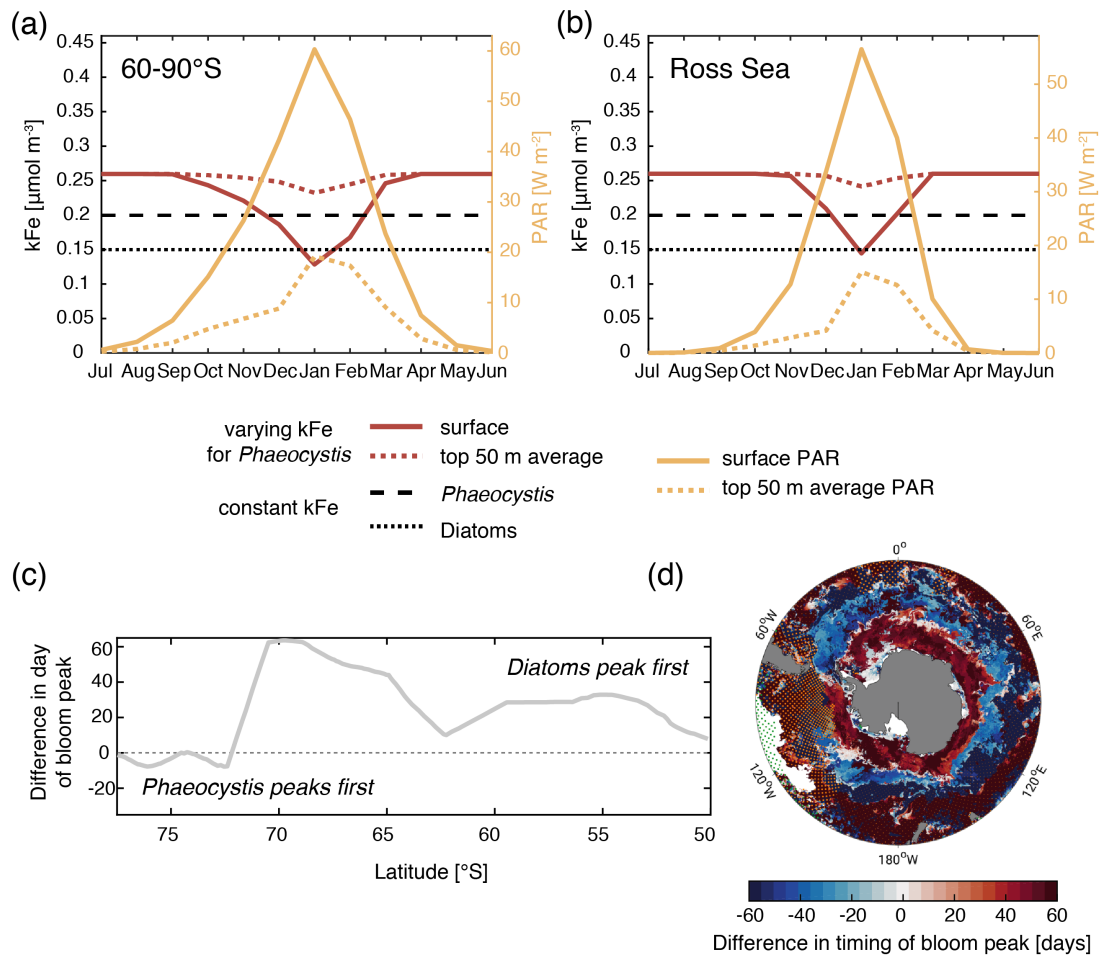


Figure S10S12: Results from the simulation VARYING k_{Fe} (see section 2.2 in the main text): Varying half-saturation constant of iron of *Phaeocystis* (k_{Fe} , red, left y axis) and PAR (yellow, right y axis) as a function of time (x axis) for the surface (solid) and averaged over the top 50 m (dashed) for a) between 60-90° S and b) in the Ross Sea. Black lines indicate the constant k_{Fe} of *Phaeocystis* (dashed) and diatoms (dotted) used in the *Baseline* simulation of this study. c) Difference in days in the timing of the bloom peak of diatoms and *Phaeocystis* for each latitude, with negative values denoting a succession from *Phaeocystis* to diatoms throughout the season. d) Difference in day of bloom peak between *Phaeocystis* and diatoms. Stippling indicates locations where maximum chlorophyll concentrations never exceeded $0.1 \text{ mg chl m}^{-3}$ for *Phaeocystis* (orange) and diatoms (green), respectively. White areas correspond to areas where the peak total chlorophyll concentrations do not exceed $0.5 \text{ mg chl m}^{-3}$.

S2: Parameter sensitivity experiments

Table S1: Overview of parameter sensitivity simulations, varying the respective parameter by $\pm 50\%$. PA=*Phaeocystis*, D=diatoms. See also Table 1 & Table 2 in the main text.

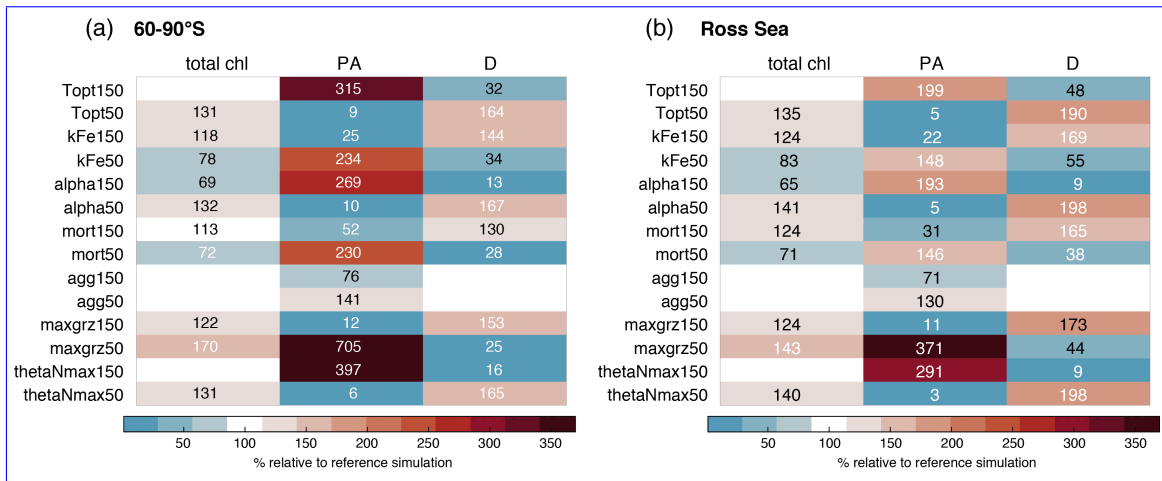
Figure S11: Run Name	Diatom (red)and	Description	
Topt150		Increase T_{opt}^{PA} by 50%	} Param_Topt
Topt50		Decrease T_{opt}^{PA} by 50%	
kFe150		Increase k_{Fe}^{PA} by 50%	} Param_kFe
kFe50		Decrease k_{Fe}^{PA} by 50%	
alphaPI150		Increase α_{PI}^{PA} by 50%	} Param_alphaPI
alphaPI50		Decrease α_{PI}^{PA} by 50%	
mortality150		Increase $\gamma_{m,0}^{PA}$ by 50%	} Param_mortality
mortality50		Decrease $\gamma_{m,0}^{PA}$ by 50%	
aggregation150		Increase $\gamma_{a,0}^{PA}$ by 50%	} Param_aggregation
aggregation50		Decrease $\gamma_{a,0}^{PA}$ by 50%	
grazing150		Increase $\gamma_{g,max}^{PA}$ by 50%	} Param_grazing
grazing50		Decrease $\gamma_{g,max}^{PA}$ by 50%	
thetaNmax50		Increase $\theta_{chl:N,max}^{PA}$ by 50%	} Param_thetaNmax
thetaNmax50		Decrease $\theta_{chl:N,max}^{PA}$ by 50%	

In order to more systematically quantify the sensitivity of simulated distributions of *Phaeocystis* and diatoms and integrated estimates of NPP and POC export in ROMS-BEC to *Phaeocystis* model parameter choices, we have performed a set of model parameter sensitivity experiments. To that aim, we have systematically increased/decreased all key *Phaeocystis* parameters by 50%, allowing for an objective ranking of model sensitivities. We varied the following seven parameters of *Phaeocystis*, resulting in a total of 14 simulations: the temperature optimum, the half-saturation constant of iron, α_{PI} , the maximum chl:N ratio $\theta_{chl:N,max}$, the linear mortality rate, the quadratic mortality rate (aggregation), and the maximum grazing rate of zooplankton on *Phaeocystis* (blue) surface carbon biomass concentrations mmol C m^{-3} in the different simulations performed in this study. See section 2.2. in the main text for details. The left panels are surface averages over see Table S1).

We then quantify the sensitivity S of any target variable A (here A being one of the following targets: total phytoplankton, *Phaeocystis*, and diatom chlorophyll concentrations, total NPP, and POC export across 100 m) to changes in the parameter X as follows, allowing for a ranking of the seven sets of simulations by the magnitude of the sensitivity (see Table S1):

$$S_X^A = 100 \cdot \frac{A_{X150} - A_{X50}}{A_{XBaseline}} \quad (1)$$

As expected (see also Nissen et al., 2018), we find that both total chlorophyll concentrations and chlorophyll levels of *Phaeocystis* and diatoms are highly sensitive to parameters describing the growth and loss of *Phaeocystis* biomass, with increases of up to 700% (grazing50) and declines of up to >90% (Topt50, thetaNmax50) in *Phaeocystis* biomass between 60-90° S for a 50% change in the associated parameters (see Fig. S13). In general, any decline/increase in *Phaeocystis* chlorophyll biomass is associated with an increase/decline in diatom chlorophyll biomass, pointing to the direct competition for resources of these two phytoplankton types at high SO latitudes. Yet, the biomass compensation is not always complete due to non-linearities in the model system (e.g. food web feedbacks), resulting in changes of up to 70% (grazing150) in total chlorophyll levels upon changes in *Phaeocystis* parameters. The ranking of model sensitivities between 60-90° S reveals the highest sensitivity of *Phaeocystis*



and diatom chlorophyll concentrations to the maximum grazing rate $\gamma_{g,max}^{PA}$, the maximum chl:N ratio $\theta_{chl:N,max}^{PA}$, the initial slope of the photosynthesis-irradiance curve (α_{PI}^{PA}), and the temperature optimum T_{opt} of *Phaeocystis* growth (Param_grazing, Param_thetaNmax, Param_alphaPI, Param_Topt in Table S1 & S2). In comparison, the opposed changes in *Phaeocystis* and diatom chloro- **Figure S13:** Annual mean surface chlorophyll concentrations of all phytoplankton (*total Chl*), *Phaeocystis* (*PA*), and diatoms (*D*) in the parameter sensitivity simulations (see Table S1) relative to the *Baseline* simulation. The model output is averaged over a) 60-90° S and those on the right for the Ross Sea. Light blue area indicate times of the year when b) the Ross Sea.

phyll levels (see Fig. S13) result in lower sensitivities of total chlorophyll levels to changes in *Phaeocystis* biomass is larger than diatom biomass. parameters in general and a lower ranking of the temperature optimum and thetaNmax experiments in particular (Param_Topt and Param_thetaNmax in Table S2).

In comparison to the ranking of model experiments for total chlorophyll, the model sensitivities for NPP and POC export across 100 m are similar in magnitude both between 60-90° S and in the Ross Sea (20-90%, compare Table S2 & Table S3). Additionally, the ranking of model experiments for NPP and POC export reveals only small differences to the ranking of model sensitivities for total chlorophyll: While the experiments Param_alphaPI and Param_grazing consistently rank amongst the top two most sensitive experiments for NPP and POC export and between 60-90° S for total chlorophyll concentrations, the experiments Param_mortality/Param_Topt are less/more important for NPP and POC than for total chlorophyll levels in ROMS-BEC (compare Table S2 & S3). In summary, this demonstrates the large model sensitivity of bulk biogeochemical quantities to parameter choices describing the temperature and light dependence of *Phaeocystis* growth and zooplankton grazing.

Table S2: Ranking of the parameter sensitivity experiments by the absolute sensitivity of annual mean total surface chlorophyll ($|S_X^{\text{Chl}}|$), *Phaeocystis* chlorophyll ($|S_X^{\text{Chl}^{\text{PA}}}|$), and diatom chlorophyll ($|S_X^{\text{Chl}^{\text{D}}}|$) to a $\pm 50\%$ change in the model parameter X relative to the *Baseline* setup of ROMS-BEC between 60-90°S and in the Ross Sea, respectively. The sensitivity S (%) is quantified using Eq. 1. See Table S1 for details on the experimental setup and Fig. S13 for details on the resulting chlorophyll fields in ROMS-BEC in each experiment. Note that the simulated changes in carbon biomass fields are qualitatively similar to those of chlorophyll (not shown) and that the ranking shown here is therefore insensitive to the choice of chlorophyll in the analysis.

	Ranking ($ S_X^{\text{Chl}} $ in %)	Ranking ($ S_X^{\text{Chl}^{\text{PA}}} $ in %)	Ranking ($ S_X^{\text{Chl}^{\text{D}}} $ in %)
60-90°S			
	1. Param_alphaPI (63.6)	1. Param_grazing (693.1)	1. Param_alphaPI (153.4)
	2. Param_grazing (48.3)	2. Param_thetaNmax (390.9)	2. Param_thetaNmax (149.6)
	3. Param_mortality (40.6)	3. Param_Topt (306.8)	3. Param_Topt (132.7)
	4. Param_kFe (39.8)	4. Param_alphaPI (259.4)	4. Param_grazing (128.3)
	5. Param_Topt (37.5)	5. Param_kFe (209.1)	5. Param_kFe (109.6)
	6. Param_thetaNmax (33.0)	6. Param_mortality (178.0)	6. Param_mortality (101.8)
	7. Param_aggregation (6.4)	7. Param_aggregation (65.1)	7. Param_aggregation (10.2)
Ross Sea			
	1. Param_alphaPI (76.3)	1. Param_grazing (360.3)	1. Param_thetaNmax (189.1)
	2. Param_mortality (53.3)	2. Param_thetaNmax (288.9)	2. Param_alphaPI (189.1)
	3. Param_thetaNmax (46.4)	3. Param_Topt (194.2)	3. Param_Topt (142.1)
	4. Param_Topt (41.6)	4. Param_alphaPI (188.3)	4. Param_grazing (129.8)
	5. Param_kFe (41.3)	5. Param_kFe (126.2)	5. Param_mortality (126.7)
	6. Param_grazing (19.2)	6. Param_mortality (114.8)	6. Param_kFe (114.3)
	7. Param_aggregation (12.3)	7. Param_aggregation (59.5)	7. Param_aggregation (9.0)

Table S3: Ranking of the parameter sensitivity experiments by the absolute sensitivity of annually integrated NPP ($|S_x^{\text{NPP}}|$) and POC export across 100 m ($|S_x^{\text{POC}_{100\text{m}}}|$) to a $\pm 50\%$ change in the model parameter X relative to the *Baseline* setup of ROMS-BEC between 60-90°S and in the Ross Sea, respectively. The sensitivity S (%) is quantified using Eq. 1. See Table S1 for the experimental setup.

	Ranking ($ S_x^{\text{NPP}} $ in %)	Ranking ($ S_x^{\text{POC}_{100\text{m}}} $ in %)
60-90°S	<ol style="list-style-type: none"> 1. Param_grazing (68.4) 2. Param_alphaPI (46.7) 3. Param_Topt (43.6) 4. Param_kFe (23.6) 5. Param_thetaNmax (23.4) 6. Param_mortality (11.6) 7. Param_aggregation (7.6) 	<ol style="list-style-type: none"> 1. Param_grazing (86.4) 2. Param_alphaPI (35.4) 3. Param_Topt (26.7) 4. Param_mortality (12.9) 5. Param_kFe (11.6) 6. Param_thetaNmax (10.7) 7. Param_aggregation (1.4)
Ross Sea	<ol style="list-style-type: none"> 1. Param_grazing (55.6) 2. Param_alphaPI (48.5) 3. Param_Topt (44.0) 4. Param_thetaNmax (24.7) 5. Param_kFe (20.4) 6. Param_aggregation (11.6) 7. Param_mortality (8.3) 	<ol style="list-style-type: none"> 1. Param_grazing (71.9) 2. Param_alphaPI (39.0) 3. Param_Topt (26.9) 4. Param_thetaNmax (11.9) 5. Param_kFe (10.5) 6. Param_mortality (10.2) 7. Param_aggregation (2.6)

References

- Balch, W. M., Bates, N. R., Lam, P. J., Twining, B. S., Rosengard, S. Z., Bowler, B. C., Drapeau, D. T., Garley, R., Lubelczyk, L. C., Mitchell, C., and Rauschenberg, S.: Factors regulating the Great Calcite Belt in the Southern Ocean and its biogeochemical significance, *Global Biogeochemical Cycles*, 30, 1199–1214, <https://doi.org/10.1002/2016GB005414>, 2016.
- Brun, P., Vogt, M., Payne, M. R., Gruber, N., O'Brien, C. J., Buitenhuis, E. T., Le Quéré, C., Leblanc, K., and Luo, Y.-W.: Ecological niches of open ocean phytoplankton taxa, *Limnology and Oceanography*, 60, 1020–1038, <https://doi.org/10.1002/lno.10074>, 2015.
- Cubillos, J. C., Wright, S. W., Nash, G., de Salas, M. F., Griffiths, B., Tilbrook, B., Poisson, A., and Hallegraeff, G. M.: Calcification morphotypes of the coccolithophorid *Emiliania huxleyi* in the Southern Ocean: changes in 2001 to 2006 compared to historical data, *Marine Ecology Progress Series*, 348, 47–54, <https://doi.org/10.3354/meps07058>, 2007.
- Fanton d'Andon, O., Mangin, A., Lavender, S., Antoine, D., Maritorea, S., Morel, A., Barrot, G., Demaria, J., and Pinnock, S.: GlobColour - the European Service for Ocean Colour, in: Proceedings of the 2009 IEEE International Geoscience & Remote Sensing Symposium, IEEE International Geoscience & Remote Sensing Symposium (IGARSS), ISBN: 9781424433957, 2009.
- Freeman, N. M., Lovenduski, N. S., Munro, D. R., Krumhardt, K. M., Lindsay, K., Long, M. C., and MacIennan, M.: The variable and changing Southern Ocean silicate front: Insights from the CESM large ensemble, *Global Biogeochemical Cycles*, 32, 752–768, <https://doi.org/10.1029/2017GB005816>, 2018.
- Garcia, H. E., Locarnini, R. A., Boyer, T. P., Antonov, J. I., Baranova, O. K., Zweng, M. M., Reagan, J. R., and Johnson, D. R.: World Ocean Atlas 2013, Volume 4 : Dissolved inorganic nutrients (phosphate, nitrate, silicate), NOAA Atlas NESDIS 76, 4, 25 pp, 2014.
- Gravalosa, J. M., Flores, J.-A., Sierro, F. J., and Gersonde, R.: Sea surface distribution of coccolithophores in the eastern Pacific sector of the Southern Ocean (Bellingshausen and Amundsen Seas) during the late austral summer of 2001, *Marine Micropaleontology*, 69, 16–25, <https://doi.org/10.1016/j.marmicro.2007.11.006>, 2008.
- Leblanc, K., Arístegui, J., Armand, L., Assmy, P., Beker, B., Bode, A., Breton, E., Cornet, V., Gibson, J., Gosselin, M.-P., Kopczynska, E., Marshall, H., Peloquin, J., Piontkovski, S., Poulton, A. J., Quéguiner, B., Schiebel, R., Shipe, R., Stefels, J., van Leeuwe, M. A., Varela, M., Widdicombe, C., and Yallop, M.: A global diatom database - abundance, biovolume and biomass in the world ocean, *Earth System Science Data*, 4, 149–165, <https://doi.org/10.5194/essd-4-149-2012>, 2012.
- Maritorea, S., Fanton D'Andon, O., Mangin, A., and Siegel, D. A.: Merged satellite ocean color data products using a bio-optical model: Characteristics, benefits and issues, *Remote Sensing of Environment*, 114, 1791–1804, <https://doi.org/10.1016/j.rse.2010.04.002>, 2010.
- Nissen, C., Vogt, M., Münnich, M., Gruber, N., and Haumann, F. A.: Factors controlling coccolithophore biogeography in the Southern Ocean, *Biogeosciences*, 15, 6997–7024, <https://doi.org/10.5194/bg-15-6997-2018>, 2018.
- O'Brien, C. J., Peloquin, J. A., Vogt, M., Heinle, M., Gruber, N., Ajani, P., Andrulleit, H., Arístegui, J., Beaufort, L., Estrada, M., Karentz, D., Kopczyńska, E., Lee, R., Poulton, A. J., Pritchard, T., and Widdicombe, C.: Global marine plankton functional type biomass distributions: coccolithophores, *Earth System Science Data*, 5, 259–276, <https://doi.org/10.5194/essd-5-259-2013>, 2013.
- Saavedra-Pellitero, M., Baumann, K.-H., Flores, J.-A., and Gersonde, R.: Biogeographic distribution of living coccolithophores in the Pacific sector of the Southern Ocean, *Marine Micropaleontology*, 109, 1–20, <https://doi.org/10.1016/j.marmicro.2014.03.003>, 2014.
- Swan, C. M., Vogt, M., Gruber, N., and Laufkötter, C.: A global seasonal surface ocean climatology of phytoplankton types based on CHEMTAX analysis of HPLC pigments, *Deep-Sea Research Part I*, 109, 137–156, <https://doi.org/10.1016/j.dsr.2015.12.002>, 2016.
- Tyrrell, T. and Charalampopoulou, A.: Coccolithophore size, abundance and calcification across Drake Passage (Southern Ocean), 2009, <https://doi.org/10.1594/PANGAEA.771715>, 2009.
- Vogt, M., O'Brien, C., Peloquin, J., Schoemann, V., Breton, E., Estrada, M., Gibson, J., Karentz, D., Van Leeuwe, M. A., Stefels, J., Widdicombe, C., and Peperzak, L.: Global marine plankton functional type biomass distributions: *Phaeocystis* spp., *Earth System Science Data*, 4, 107–120, <https://doi.org/10.5194/essd-4-107-2012>, 2012.